THE CHARACTERIZATION OF THE NOVEL CHLOROQUINE DERIVATIVE VR23 FOR ITS ANTICANCER PROPERTIES

by

SHEETAL PUNDIR

A thesis submitted to the Faculty of Graduate and Postdoctoral Studies in partial fulfillment of the requirements for the degree of

DOCTOR OF PHILOSOPHY

Department of Biochemistry, Microbiology and Immunology
University of Ottawa
Ottawa, Ontario, Canada

ABSTRACT

Since Bortezomib®, a proteasome inhibitor, was approved by US FDA for the treatment of multiple myeloma in 2003, proteasome is recognized as one of the most promising targets for cancer therapeutics. The proteasomes play a critical role in regulating the level of cellular proteins and recycling damaged and misfolded proteins. Although the activity of the proteasome is essential for normal cells, it is especially critical for the proliferation and survival of cancer cells. In an attempt to develop effective and safe proteasome inhibitor-based anticancer drugs, the Lee laboratory created a chemical library by a hybrid approach using a 4-piperazinylquinoline scaffold and a sulfonyl phamarcophore. It is known that the chloroquine scaffold possesses a weak proteasome inhibition activity, and chloroquine itself preferentially kills malignant cells over non-cancer cells, alone or in combination with other therapeutics. To identify compounds with desirable anticancer activities, I have screened the aforementioned chemical library. The screening yielded several hits with substantial efficacy and selectivity against malignant cells. In this thesis, I describe the functional mechanism of VR23, one of the most promising compounds identified from my screening, as it kills cancer cells up to 17 fold more effectively than non-cancer cells. Molecular docking and substrate competition studies revealed that VR23 binds to the β2 peptide of the 20S proteasome catalytic subunit. The IC_{50} value of VR23 in inhibiting trypsin-like proteasome activity is 1.0 nM. VR23 is also substantially effective in inhibiting chymotrypsin-like proteasome activity (IC_{50}, 50-100 nM). The inhibition of proteasome activity by VR23 led to the accumulation of ubiquitinated cyclin E at centrosomes. This, in turn, induces abnormal

centrosome amplification by a *de novo* centrosome synthesis pathway in cancer cells, but not in non-cancer cells. The presence of multiple centrosomes in single cancer cells results in cell cycle arrest at prometaphase and, eventually, cell death by apoptosis. Thus, VR23 possesses a very desirable property as a safe anticancer drug.

ACKNOWLEDGEMENTS

First and foremost I would like to thank my research supervisor, Dr. Hoyun Lee, for giving me this opportunity to work in his lab. I thank him for always taking me seriously and most importantly for respecting my opinions and ideas and giving me the freedom to make errors. His unbounded enthusiasm transformed the project into an exciting work. I have learned much more than I ever thought possible in the short time since I have known him. I thank him for his patience and for always keeping his “door open”. I learnt to always see the big picture and above all to enjoy working in the lab.

I would like to thank my co-supervisor, Dr. Seung-Hwan Lee, and my committee members Dr J.T. Arnason and Dr. Hoang-Tanh Le for always being truly supportive and for keeping me on track. Your guidance and suggestions throughout this work were invaluable. The positive feedback and encouragement that I received during my committee meetings helped me to see the impossible worthy to challenge.

I would like to thank Julia Romero for supporting me in the beginning stages of my project. I would like to thank Dr. Robert Lafrenie, he has been an extremely positive influence for me here at the cancer centre. There are many things that I have learnt from him that will always be a part of the way I do science. I learnt to never fear a piece of equipment from you.

I would like to thank Jane Vanderklift, especially for arranging my committee meetings, for everything that you do for students. Victoria Stewart, thank you for all your help at the department of BMI and for making the distance between Sudbury and Ottawa easier. You could solve all my issues over just a phone call.

I would also like to extend my sincere thanks to the people who work at research lab on the second floor for their friendship and support on all manners of day-to-day matters. Especial thanks to Shawn Hughes for helping me with docking software.

Lastly, my deepest gratitude to the Indian community in Toronto, Sudbury and Ottawa for support (most importantly Indian food) throughout my entire time in graduate school….and life.

TABLE OF CONTENTS

LIST OF ABBREVIATIONS

AMC	7-amino-4-methylcoumarin
APC	anaphase promoting complex
Ala	alanine
Arg	arginine
ATP	adenosine-triphosphate
BCA	bicinchoninic acid
BrdU	bromodeoxyuridine
BSA	bovine serum albumin
Cdk	cyclin-dependent kinase
CQ	chloroquine
Conc	concentration
°C	degree in celsius
DMSO	dimethyl sulfoxide
EdU	5-ethynyl-2'-deoxyuridine
Emi1	early mitotic inhibitor
ER	endoplasmic reticulum
FACS	fluorescence-activated cell sorting
FBS	fetal bovine serum
Gly	glycine
h	hour(s)
H-bond	hydrogen-bond
IC_{50}	50% inhibitory concentration
Ile	isoleucine
kDa	kilodalton
LLE	leu-leu-glu
LRR	leu-arg-arg
Lys	lysine
min	minute(s)
ml	milliliter
µM	micromolar
MOE	molecular operating environment
MTOC	microtubule organizing centre
Na_2VO_3	sodium orthovanadate
NaF	sodium fluoride
NEM	N-ethylmaleimide
NF-kB	nuclear factor-kB
ng	nanogram

PAGE	polyacrylamide gel electrophoresis
PBS	phosphate buffered saline
PDB	protein data bank
PI	propidium iodide
plk	polo like kinase
PMSF	phenylmethylsulfonyl fluoride
PVDF	Polyvinylidene fluoride
RMSD	root mean square deviation
RFU	relative fluorescence unit
S or Ser	serine
SAC	spindle assembly checkpoint
SCF	skp, cullin, F-box
SDS	sodium dodecyl sulphate
siRNA	small interfering ribonucleic acid
SRB	sulforhodhamine B
Suc-LLVY	suc-leu-leu-val-tyr
T or Thr	threonine
TBS	tris buffered saline
TUBEs	tandem ubiquitin binding entities
Ub	ubiquitin
Y or Tyr	tyrosine
Z-L_3VS	carboxybenzyl-leucyl-leucyl-leucine vinyl sulfone

LIST OF FIGURES

LIST OF TABLES

1.0 Introduction

1.1 BACKGROUND

The anti-malarial drug chloroquine (CQ) can induce cell death by inhibiting autophagy, or inducing apoptosis and necrosis. CQ inhibits autophagy by disrupting lysosome function. When CQ enters the lysosome, it gets protonated and accumulates in the lysosome disrupting its acidic environment. Inhibition of signalling pathways in cancer cells often activates autophagy as a part of the cytoprotective mechanism. Cancer cells use autophagy as a source of energy during unfavourable growth conditions (1). The survival advantage provided by autophagy can decrease the efficacy of chemotherapeutic agents. Therefore, the inhibition of autophagy in combination with various inhibitors (described below) is considered an attractive strategy against cancer (1).

Several studies have reported the synergistic effects of CQ in combination with radiation or chemotherapeutic agents (Table 1). CQ can sensitize cancer cell death by ionizing radiation or by chemotherapeutic agents. CQ destabilizes lysosomes, plasma membrane and induces necrosis in cells treated with irradiation (2). CQ potentiates colon cancer cell death when used in combination with 5-fluorouracil (3). CQ, in combination with other therapies, has shown very promising results in killing cancer cells, although it has not proven to be very effective when used alone (4). As a result, potential of CQ as a lead compound in anticancer drug discovery is being widely explored, rather than using it as a single regimen (5). The efficacy of CQ against cancer cells combined with its safe tolerance in humans as antimalarial drug suggests that the pharmacophore of CQ would be an attractive target for novel anticancer drug synthesis.

Table 1. Combinatorial effects of chloroquine with other anticancer agents on malignant cells

Chloroquine sensitizes the resistant and non-resistant cancer cells to increased cell death. The table lists some of the studies that have reported synergistic or additive effects of chloroquine when used in combination with radiation or various inhibitors.

CHLOROQUINE + Inhibitor	Chemosensitivity	Reference
Herceptin	Sensitizes HER2+ resistant cells to cell death	Cufi S. et al, 2013 (6)
PI3K inhibitor LY294002	Sensitizes breast cancer cells to cell death	Maycotte P. et al., 2012 (7), Hu C. et al., 2008 (4)
Metformin	Eliminates cancer stem cells in pre-malignant intraepithelial lesions.	Vazquez-Martin A. et al, 2013 (5)
mTOR inhibitor Rapamycin.	Sensitizes breast cancer cells to cell death	Maycotte P. et al., 2012 (7)
HDAC inhibitor Vorinostat	Sensitizes colon cancer cells to apoptosis.	Carew J.S. et al, 2011 (8)
Radiation	Sensitizes radioresistant stem-like glioma cells.	Firat E. et al, 2012 (9)
Topotecan	Sensitizes lung cancer cells to apoptosis.	Wang Y. et al, 2011 (10)
Flavinoid Luteolin	Sensitizes squanmous cell carcinoma to apoptosis.	Verschooten L. et al, 2012 (11)
Ubiquitin proteasome protein degradation inhibitor RAMB1	Sensitizes cervical cancer cells to apoptosis.	Anchoori R.K. et al, 2011 (12)
Imidazoacridinones	Sensitizes resistant lung cancer A549 cells to apoptosis.	Adar Y. et al, 2012 (13)
Tyrosine kinase inhibitor Imatinib	Sensitizes Chronic myeloid leukemia to cell death.	Bellodi. C. et al, 2009 (14)
5-fluorouracil	Sensitizes gallbladder carcinoma cells to apoptosis.	Liang X. et al, 2014 (15)
Src-kinase inhibitors	Sensitizes prostate cancer cells to apoptosis.	Wu. Z. et al, 2010 (16)
PI3K/mTOR inhibitor XL765	Sensitizes pripheral malignant nerve sheath tumors to apoptosis.	Ghadimi. M.P., et al., 2012 (17)
RAF inhibitor Vemurafenib	Sensitizes resistant and BRAF mutant brain tumor cells.	Levy J.M., et al. 2014 (18)
Akt inhibitor	Decreases ovarian cancer cell viability	Correa R.J. et al., 2014 (19)

CQ's chemical structure contains a 4-aminoquinilone scaffold, and 4-aminoquinoline derivatives are commonly used as anti-malarial, anti-bacterial and anti-inflammatory agents (20). Several groups have designed novel derivatives of 4-aminoquinoline as immunostimulatory agents and anti-tumor agents (21-23). 2-arylvinyl-4-aminoquinoline derivatives designed by introducing a halogen atom, aliphatic amines and arylvinyl on the CQ ring significantly improved the anticancer activity of CQ (24-26). This has led to intensive efforts to design novel derivatives from a 4-aminoquinoline moiety for improved anticancer activity (27). The strategy was directed toward substituting or designing a variety of chemical moieties with different chemical properties.

1.2 The objectives of the study

The specific aims of this thesis were to:

1. screen novel CQ derivatives for their selectivity and activity against a panel of cancer and non-cancer cells.
2. study the effect of the most promising leads (determined from aim 1) on the cell cycle progression to help characterize its functional mechanism.
3. to characterize the mechanism of action of the most effective drug candidate and find the target of the compound.

1.3 PROTEASOMES

1.3.1 Structure and function

Proteasomes are the machinery for protein degradation in the cell. The ubiquitin-proteasome system breaks down a variety of proteins that regulate cell cycle progression, centrosome duplication, cell and DNA segregation, and the regulators of gene expression, apoptosis, immune surveillance and protein quality control. The 26S proteasome is a 2.4 megadalton proteolytic complex. This complex contains six proteolytically active subunits with different substrate specificities. The 26S proteasome consists of a core particle, the 20S catalytic subunit which is capped by two 19S regulatory subunits. The 20S subunit is composed of four stacked rings (Fig. 1). Each inner ring comprises seven different β subunits and each outer ring is consisted of seven different α subunits. β rings are located inside the cylinder and contain chymotrypsin-like, trypsin-like, and caspase-like proteolytic activity sites. The chymotrypsin-like subunit cleaves proteins after hydrophobic residues and is located on β5 subunits. The trypsin-like subunit cleaves after basic residues and is located on β2 subunits. The caspase-like subunit cleaves after acidic residue and is located in β1 subunits (28). Caspase-like sites are named so as it was found that they are responsible for cleavage after aspartic acid very efficiently (29) (caspases are intracellular proteases, which cleaves proteins after aspartate). Substrates are presented to the β subunits through the narrow, gated channel of an α subunit. The α subunit unfolds polypeptides and allows the access of substrates to 20S proteasomes in an ATP dependent mechanism.

Figure 1. 26S proteasome structure and function

The 26S proteasome consists of two particles: the 20S core particle (CP) and 19S regulatory particle (RP). The 19S RP binds to one or both ends of the CP to make an active proteasome. CP is a barrel-shaped structure composed of two outer β rings and two inner α rings. Each of them are made up of seven structurally similar α and β subunits. β1, β2 and β5 subunits are associated with caspase-like, trypsin-like and chymotrypsin-like activities, respectively. The α subunits regulates the entry of substrates to the active sites. The RP recognizes the polyubiquitinated proteins, removes the ubiquitin chain, unfolds the substrate protein, opens the α ring which then transfers the unfolded proteins to the catalytic units for proteolysis.

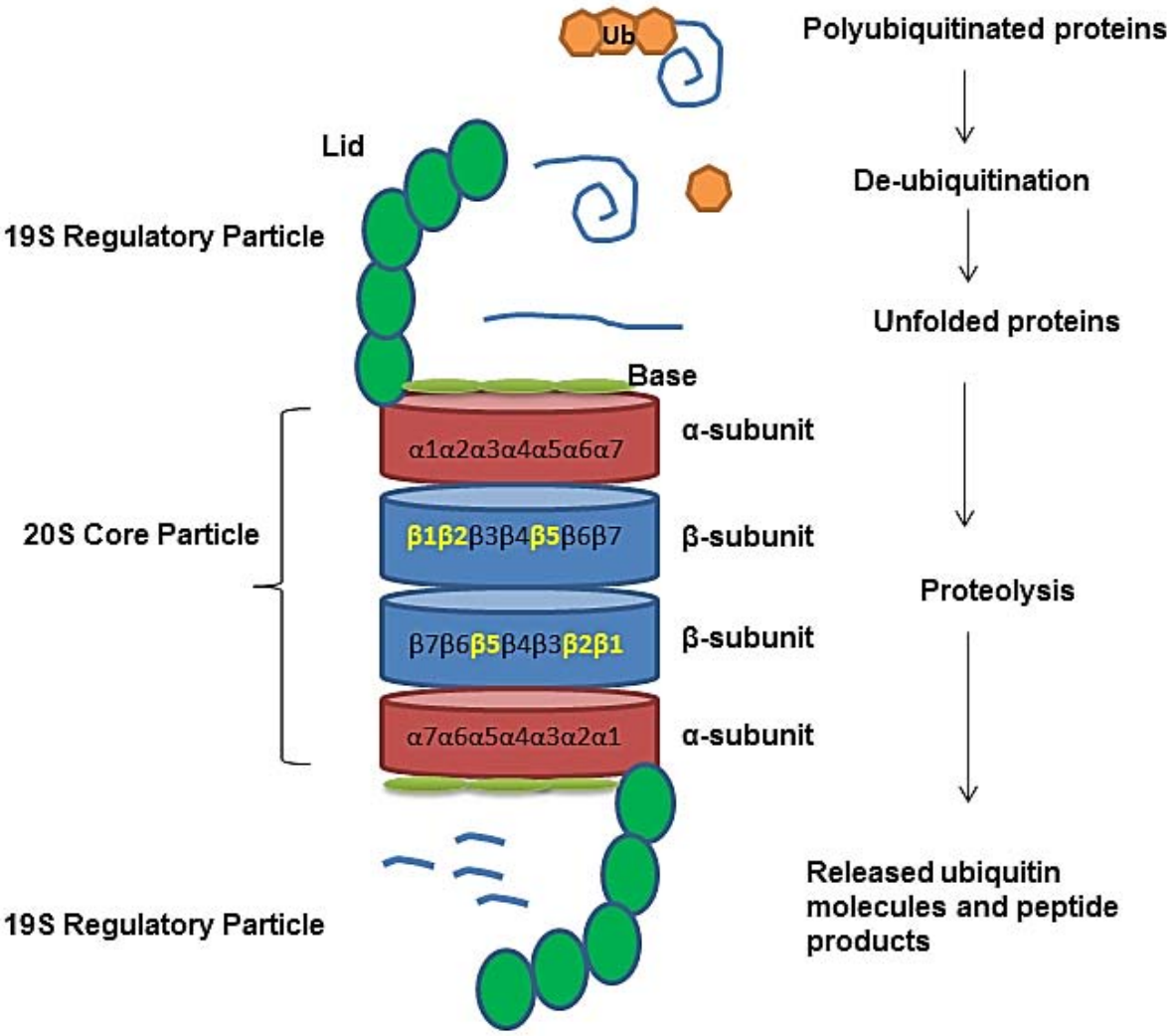
Ub
Polyubiquitinated proteins
Lid
De-ubiquitination
19S Regulatory Particle
Unfolded proteins
Base
α-subunit
α1α2α3α4α5α6α7
20S Core Particle
β1β2β3β4β5β6β7
β-subunit
Proteolysis
β7β6β5β4β3β2β1
β-subunit
α-subunit
α7α6α5α4α3α2α1
Released ubiquitin molecules and peptide products
19S Regulatory Particle

Proteins to be degraded are tagged by small ubiquitin molecules. Several ubiquitin molecule attaches to the free amino acid of the substrate, forming a polyubiquitinated substrate. This is achieved by E1, E2 and E3 enzymes. E1 activates ubiquitin molecule in an ATP-dependent manner and transfers it to E2, the ubiquitin carrier molecule. The ubiquitin is then transferred to the substrate protein by E3, a ubiquitin ligase. Eukaryotic cells contain different E3 enzymes which recognize different degradation signals on substrates. The polyubiquitinated substrates are then recognized by the 19S regulatory subunit of 26S proteasome which subsequently removes the ubiquitin. The substrates then pass through α subunits to the catalytic sites of 20S proteasomes. Polypeptides are cleaved at multiple sites and the cleaved products are released for recycling (30).

1.3.2 Types of proteasome inhibitors

There are four major classes of proteasome inhibitors (Table 2): peptide aldehydes, peptide-boronates, peptide-vinyl sulfones and natural compounds (β-lactones).

Peptide aldehydes: Peptide aldehydes interact preferentially with the β5 subunit and are cell-permeable, and reversible inhibitors. Besides proteasomes, peptide aldehydes also inhibit cysteine and serine proteases like lysosomal cathepsins.

Peptide boronates: These are much more potent, specific and reversible inhibitors of proteasomes. The dissociation rate of the proteasome-boronate adduct is very slow resulting in the inhibition lasting for a longer duration.

Table 2. Classification of known proteasome inhibitors and their activities

Type	Example	Activity
Peptide-aldehydes	MG132	β5>>β1>β2
Peptide-boronates	Bortezomib, MG262	β5>>β2
Peptide-vinyl sulfones	Z-L_3VS	β5>β2>β1
β-lactones	Lactacystin	β5>>β2>β1
Peptide-Epoxyketons	Epoxomycin	β5>>β2

Pedptide-vinyl sulfones: These are irreversible inhibitors. They covalently modify the γ-hydroxyl group of the proteasomal N-threonine group of the β5 subunit.

Natural compounds: Natural compound β-lactone modifies the γ-hydroxyl group of the N-threonine group of the β5 subunit. This group of compounds are not specific to proteasomes and also inhibits lysosomal cathepsins and cytosolic tripeptidyl peptidases. These are irreversible inhibitors but in the mammalian system they are not very stable as they become inactive by hydrolysis thus resulting in the recovery of proteasomal activity. Natural compound epoxyketone reacts with the γ-hydroxyl group and with the α-amino group of the proteasomal N-threonine group (30).

1.3.3 Inhibitors of proteasome activity in clinical trials

Bortezomib, a peptide-boronate, is the first proteasome inhibitor that has been approved by FDA for the treatment of human cancer (multiple myeloma). It binds to β5 subunit and inhibits the chymotrypsin-like activity of proteasomes. It is very effective for the treatment of myeloma and mantle cell lymphoma, but it has a very narrow therapeutic window. Clinical efficacy of bortezomib in the treatment of solid tumors remains low and the development of resistance to this drug is also frequent. Cells develop resistance to bortezomib either by overexpressing β5 subunits or by mutation in the binding site of bortezomib (31). MLN9074 and CEP-18770 are proteasome inhibitors with similar mechanism as bortezomib and are currently in clinical trials. These drugs are all reversible proteasome inhibitors.

One of the well-known irreversible inhibitors is carfilzomib, which can induce cell death in bortezomib resistant cells and is currently under clinical trials. However, because it has a peptidic structure, carfilzomib can easily be digested by endogenous proteases and peptidases. This can limit its efficacy. NPI-0052 is a very potent irreversible proteasome inhibitor (32) and, unlike bortezomib and other inhibitors mentioned above, it inhibits all three proteasome activities. Patients with relapsed myeloma have shown favourable responses in phase I clinical trials with this drug.

Most proteasome inhibitors bind to the active site of proteasomes (competitive inhibition). Several compounds however bind outside the active site. CQ inhibits the proteasome activity via non-competitive inhibition and it binds between α and β subunits. However, the concentration of CQ required for inhibiting the proteasome activity is very high, and cannot be achieved in the clinical setting. Therefore, lysosome inhibition appears to be the more relevant mechanism resulting in cancer cell death by CQ. A structurally similar compound 5AHQ (5-amino hydroxyl quinoline) also inhibits proteasomes via non-competitive inhibition. It has been shown that 5AHQ binds to α subunits of 20S proteasomes. The combination of bortezomib and 5AHQ has shown synergistic effects on tumor cell killing (33).

CQ and 5AHQ are the only reported proteasome inhibitors that do not bind directly to the active sites (β subunits) of the proteasome. CQ also leads to G2/M arrest and mitotic spindle abnormalities in breast cancer cells (34). However, the mechanism causing spindle abnormalities by CQ is unknown.

1.3.4 Cell death by proteasome inhibition

Proteasomes are responsible for ~80% of protein degradation in a cell (35). The inhibition of the cellular proteasomes leads to the accumulation of abnormal or misfolded proteins and proteins targeted for degradation.

Proteasome inhibition can affect the regulation of various signalling pathways (Fig. 2). The three most studied effects are: (a) inhibiting the activation of NF-kB, (b) the activation of unfolded protein response, and (c) the activation of endoplasmic reticulum (ER) stress (35, 36). NF-kB is a transcription factor which is frequently up-regulated in cancer cells. Its activation may lead to cyclin D up-regulation, which facilitates the next round of the cell cycle. The inhibition of proteasomes stabilizes IkB, an inhibitor of NF-kB (37). Several proteasome inhibitors have been shown to inhibit NF-kB activity (38). Although proteasome inhibition by bortezomib (PS-341) inhibits NF-kB activity and activates p53 and p21, the induction of cell death by bortezomib is independent of the NF-kB and p53 pathways (39). Sensitivity to bortezomib was reported to be more dependent on its ability to cause mitotic catastrophe.

The majority of mitotic proteins are regulated by proteasome activity (40). Regulated proteolysis is an engine that leads to forward mitotic progression (41). Accumulation of non-degradable mitotic proteins (e.g., cyclins) arrests the cells in mitosis. Therefore, proteasome inhibitors lead to G2/M arrest (42).

Proteolysis of cyclins by the ubiquitin-proteasome pathway provides directionality to the orderly cell cycle progression. In many cancer cells, cyclins and their binding partners, cdks (cell dependent kinases), are up-regulated (43).

Figure 2. Effects of proteasome inhibition

Inhibition of proteasome activity can activate apoptosis by disrupting multiple signalling pathways and by impairing the turnover of multiple proteins. Accumulation of these proteins (cdk inhibitors p21, p27, p53) can cause cell cycle arrest and disrupt mitosis. Accumulation of misfolded proteins can activate endoplasmic reticulum stress. Consequently, the inhibition of proteasome activity can disrupt cell cycle progression and activate apoptosis.
ER and ROS denotes endoplasmic reticulum and reactive oxygen species, respectively.

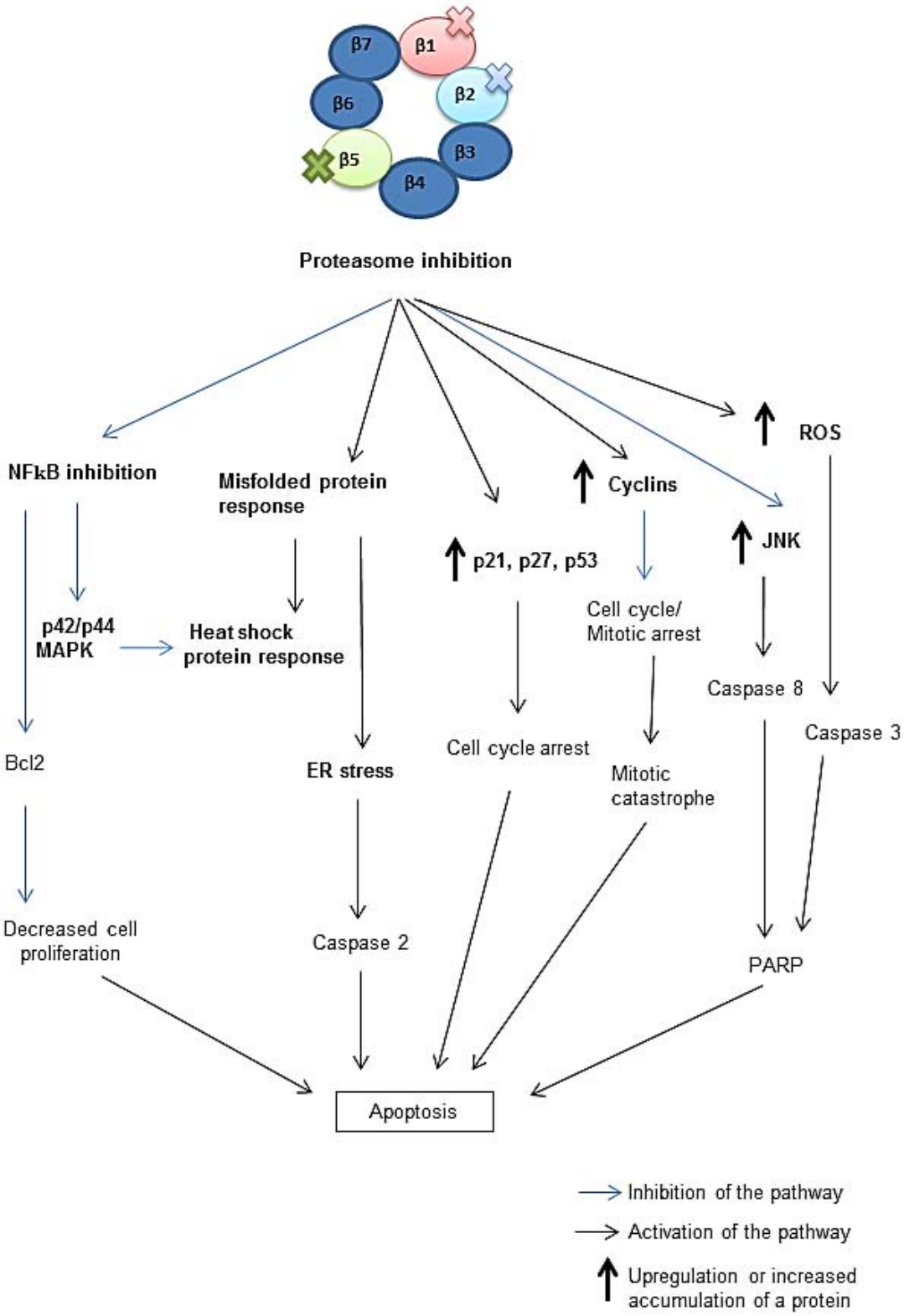
β7
β1
β6
β2
β5
β3
β4
Proteasome inhibition
NFkB inhibition
Misfolded protein response
Cyclins
ROS
p21, p27, p53
JNK
p42/p44 MAPK
Heat shock protein response
Cell cycle/ Mitotic arrest
Caspase 8
Caspase 3
Bcl2
ER stress
Cell cycle arrest
Mitotic catastrophe
Decreased cell proliferation
Caspase 2
PARP
Apoptosis
Inhibition of the pathway
Activation of the pathway
Upregulation or increased accumulation of a protein

Cdks are inhibited by several cdk inhibitors (CKI), including p21 and p27. CKIs can arrest cell cycle progression in response to DNA damage or other genotoxic stresses. There is increased degradation of p27 and p21 in cancer cells by the high levels of proteasome activity (44), preventing cell cycle arrest in response to stress. Up-regulation of cyclins and rapid degradation of CKIs can contribute to continuous cell proliferation in cancer cells. When proteasomes are inhibited, CKIs may accumulate in the cell (45, 46) which, in turn, arrests cell cycle and prevents cell proliferation.

Proteasome inhibition also abrogates ERK, Akt, mTOR pathways (47, 48), all of which are often constitutively active in cancer cells and drive cell cycle progression.

1.3.5 Proteasomes: a target for anticancer therapy

The activity of proteasomes was shown to be increased by >90% in primary breast cancer tissue (49). This increase in proteasome activity was related to the increased expression of proteasome subunits. In the same study, authors also noted that there were elevated levels of polyubiquitinated proteins in breast cancer cells. Interestingly, MCF10A cells (non-malignant epithelial breast cell line) do not show an increased proteasome activity. Abnormally high expression of proteasomes was also seen in acute lymphocytic leukemia, T-cell Leukemia and acute myelocytic leukemia cells, when compared to normal blood cells (50). The proteasome content of malignant hematopoietic cells is also found to be ten-fold higher than normal hematopoietic cells. It is hypothesized that, since cancer cells are continuously under stress of division, the increased level of proteasome activity

may provide them with an advantage of rapid turnover of proteins, degrading misfolded proteins faster (cancer cells have high turnover of misfolded proteins) and stress response (cancer cells have elevated cellular stress). Adaptation to stress (proteotoxic, oxidative, replicative, metabolic stress) is required for the survival of cancer cells.

Two properties of proteasome inhibitors make them a promising target for anticancer therapy: First, malignant cells have higher dependency on proteasome activity. Malignant cells, or rapidly proliferating, cells have been shown to be more sensitive to proteasome inhibition than quiescent or non-malignant cells (51). For example: myeloma cells are more sensitive than peripheral blood mononuclear cells (52); chronic leukocyte leukemia cells are more sensitive than normal lymphocyte cells (53); and transformed fibroblast/lymphoblasts cells are more sensitive than their normal fibroblasts/lymhoblasts counterparts (54, 55). Second, proteasome inhibition affects multiple pathways, as it regulates the stability of many proteins that participate in cell cycle regulation, cell signalling pathways, DNA repair and apoptosis.

Despite being an enticing anticancer target, primary and secondary resistance to proteasome inhibitor bortezomib is common in clinics (56). Formation of *de novo* proteasomes and an increase in expression of the proteasome subunits was reported in response to proteasome inhibitors lactacystin and MG132 in rat vascular smooth muscle cells (VSMCs). In a separate study, the treatment of bortezomib in lymphoma cells resulted in an increased chymotrypsin-like activity (57). The increase in proteasomal subunit expression could be the compensatory mechanism for cells to survive, which may result in the resistance to proteasome inhibitors.

It has also been shown that cells can depend on non-proteasomal systems to compensate for the loss of proteasome functions (58). A large protease complex known as tricorn protease has been reported in *Thermoplasma acidophilum.* Tricorn proteases are resistant to proteasome inhibitors. Similar complexes have been suggested to exist in mammalian cells. Cells that survive in the presence of proteasome inhibitors have been shown to depend on other proteases present in the cell for proteasomal functions (59).

Given the therapeutic potential of proteasome inhibitors against malignant cells, the development of novel proteasome inhibitors with less toxicity and increased sensitivity or inhibitors that can overcome bortezomib resistance is an attractive field to explore for future cancer therapy. Irreversible inhibitors NPI-0052 and carfilzomib have shown increased potency and can also overcome bortezomib induced resistance (60, 61).

1.4 MITOSIS

Timely degradation and activation of kinases and phosphatases is essential for the forward progression of mitosis. The majority of mitotic proteins are degraded by the ubiquitin-proteasome pathway (62). An unbalance caused by proteasome inhibition may make this phase most sensitive to apoptosis (39).

Mitosis is a tightly controlled mechanism driven by the cdk1-cyclin B complex (also known as maturation promoting factor or MPF). The orderly activation and inactivation of MPF drives several steps of morphological and biochemical changes essential for a cell to traverse through the different stages of mitosis: prophase, metaphase, anaphase and telophase (63). The exit from mitosis

(metaphase to anaphase transition) requires the degradation of cyclin B by APC/cdc20 thus inactivating cdk1. APC (anaphase promoting complex) is kept inactive by Emi1 (early mitotic inhibitor). Cdk1 (and plk1) phosphorylates Emi1 in prometaphase releasing APC (64). APC then binds to cdc20 and degrades cyclin B via the proteasome pathway. A low threshold level of cdk1-cyclin B activity has been shown to activate APC and initiates the negative feedback loop (65).

Cells have surveillance mechanism known as checkpoints throughout the cell cycle. Checkpoints are involved in regulating the timely and accurate cell cycle progression. Activation of cell cycle checkpoints slows or arrests the cell cycle in response to DNA damage or other genotoxic stress. There are 3 major checkpoints in mitosis: DNA damage, spindle assembly and antephase checkpoint. In response to DNA damage, checkpoint kinases, chk1 and chk2, are activated and ensure that cdc25 phosphatases remain in an inactive state until DNA damage has been repaired. Cdc25 phosphatases are the major players in G1/S and G2/M cell cycle transitions. Activation of checkpoint(s) prevents the activation of cdk1-cyclin B by cdc25 phosphatases.

Spindle assembly checkpoint (SAC) prevents mitotic progression if chromosomes are not correctly attached to spindles (66, 67). Activation of SAC inhibits APC activation. In fission yeast, p38 (p38α) has been reported as part of SAC. The p38 stress kinase can be activated by a variety of stress stimuli and can delay cell cycle progression or lead to cell cycle arrest in mitosis (68-70).

The antephase checkpoint prevents the cells from completing prophase in response to stress (71). This checkpoint is primarily mediated by p38. This checkpoint requires ubiquitination of chfr, a downstream target of p38, but does not

rely on proteasome activity (72). If the antephase checkpoint is activated, cells will decondense the chromosome in prophase and will return to G2. Prophase is defined as the stage when nuclear membrane is still intact. Breakdown of the nuclear envelope marks the beginning of mitosis and cells cannot return to interphase without completing mitosis. However, in cells such as the Ptk1 cell line in which the antephase checkpoint is functional, cells return to G2 after treatment with either nocodazole or colcemid. HeLa and U2OS cells lack this checkpoint mechanism and do not return to G2 but arrest in mitosis. pp38 kinase activates chfr, a ubiquitin ligase, which then prevents entry into metaphase after the cdk1-cyclin B complex is activated. However, other studies report that chfr activates antephase checkpoint before nuclear envelope breaks down (before cdk1-cyclin B is activated above a certain threshold level) (73).

1.5 CENTROSOME

1.5.1 Centrosome structure

A centrosome is a non-membranous organelle located in proximity to the nucleus that serves as a microtubule organizing centre (MTOC) (74). A centrosome is made up of two elements: centriole and pericentriolar material (PCM) (Fig. 3). Centriole is a cylindrical structure which is surrounded by PCM. Centriole is composed of microtubules arranged radially in a nine-fold triplet pattern. The primary role of centrioles is to provide a structural scaffold to facilitate the organization and recruitment of PCM (75) and the centriole is unstable in the absence of PCM (76). PCM serves as the principle site for a MTOC. γ-tubulin, localized to the edges of PCM, has been shown to be the core component of the

centriole (77). γ-tubulin ring complexes that are present in PCM interact with γ-tubulin binding proteins including (but not limited to) percentrin, CG-NAP, polo kinases, CPAP (78, 79). Initially PCM was considered as an amorphous material. However, recent studies using subdiffraction and super resolution microscopy imaging methods have shown that PCM is well-organized into different structural domains and has a distinct molecular organization (80-82).

A mitotic cell contains two centrosomes, and each centrosome is consisted of one ‘mother’ and one ‘daughter’ centriole. The ‘mother’ centriole has distinct anchoring capability but not the ‘daughter’ centriole. Structurally, a mother centriole has external appendages attached to its wall and, functionally, it can nucleate microtubules. As a cell progressed towards G2/M, centrosomes accumulate PCM in the process termed ‘maturation’. During G2/M transition, separation of duplicated centrosomes into two distinct MTOCs takes place. As a cell exits mitosis and enters G1 phase, the ‘mother’ and ‘daughter’ centrioles detach and are no longer arranged perpendicular to each other (83).

1.5.2 Centrosome duplication

New centrosomes form in the cell by the duplication of pre-existing centrioles. Similar to DNA replication, centrosome replication occurs only once per cell cycle and therefore is tightly regulated throughout the cell cycle. In the G1 phase, a centrosome contains two centrioles. Cdk2 activity (together with its partners cyclin E or cyclin A) drives the initiation of centrosome duplication (84-86). Recent studies show that plk4 is also required for the initiation of centrosome duplication (87).

Figure 3. Basic structure of a centrosome

The centrosome consists of two barrel-like centrioles surrounded by pericentriolar material. The two centrioles are oriented perpendicular to each other. The daughter centriole is attached to the mother centriole. The mother centriole differs from daughter centriole in having distal and sub-distal appendages.

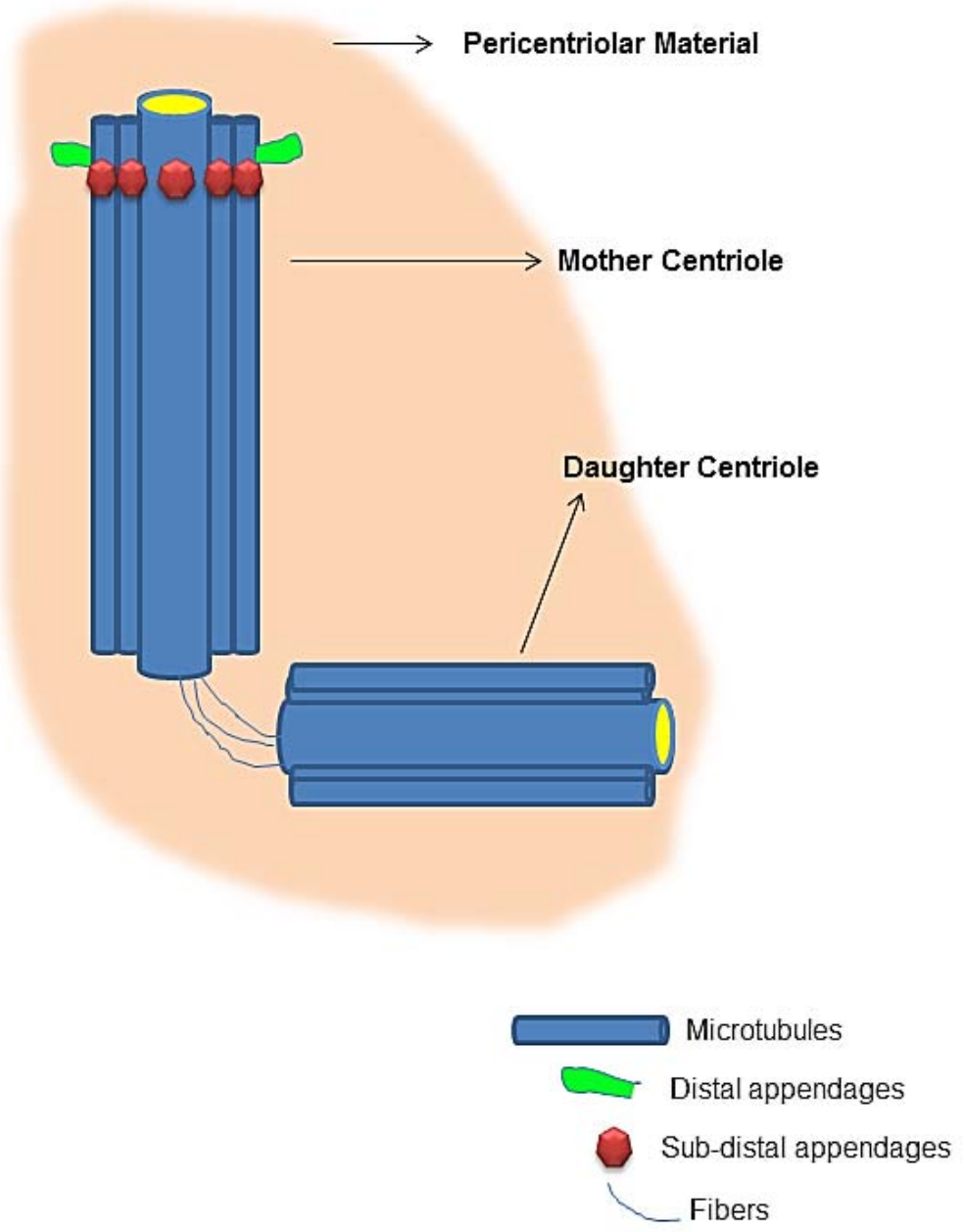
Pericentriolar Material
Mother Centriole
Daughter Centriole
Microtubules
Distal appendages
Sub-distal appendages
Fibers

plk4 localizes on the walls of parental centrioles, leading to further recruitment of hSaS-6, γ-tubulin, CPAP and other centrosomal proteins to the nascent procentriole. Plk4 then autophosphorylates and is removed from centrosomes to prevent the initiation of a second round of duplication until next cell cycle. Centrosome maturation occurs in G2 phase where additional proteins are recruited to PCM.

Activity of cdk2 is required for the centrosomal cycle initiation. In *Xenopus* egg extracts, cdk2-cyclin E can drive centrosome duplication in the presence of cyclohexamide, an inhibitor of DNA replication (88). However, results obtained from somatic cells are different from the one obtained from *Xenopus* egg extracts. Data from mouse embryonic cells (MEF) indicates that primary MEFs cells, in which cdk2 is deleted, can still initiate centrosome duplication, although it cannot initiate subsequent reduplication within the same cell cycle (89). This suggests that certain other proteins can compensate the requirement of cdk2 in the initiation of duplication, possibly from cdk family (cdk1, cdk4).

Mps1 and nucleophosmin are the two substrates of cdk2-cyclin E that function in centrosome duplication. Nucleophosmin associates with unduplicated centrosomes. Cdk2-cyclin E phosphorylates nucleophosmin, which leads to the dissociation of nucleophosmin from centrosomes, initiating the centrosome duplication. Mps1 is a protein kinase that regulates mitotic progression and the centrosome duplication process. Overexpression of Mps1 can cause centrosome amplification in NIH 3T3 and U2OS cells (90-92). However, in U2OS cells, the inhibition of Mps1 either by siRNA or a monoclonal antibody specific for Mps1 did not block centrosome reduplication (91, 92).

Overexpression of cyclin E in cells arrested in G0/G1 cannot initiate centrosome duplication. Conversely, when cyclin A is overexpressed in Rb mutant cells, it can override G1 arrest and can initiate centrosome duplication (93). This suggests that, for cyclin E to function in the centrosome duplication cycle, cells have to progress through G0/G1. In the absence of cyclin E, cdk2 can bind to cyclin A and can drive centrosome duplication (94).

During S-phase, a new procentriole begins to grow at an angle next to the proximal end of a pre-existing centriole. The parent and progeny centrioles are tightly connected to each other. At the onset of procentriole formation (in S phase), hSAS-6 localizes next to the centriole (95). During anaphase hSAS-6 is degraded by 26S proteasomes. Overexpression of hSAS-6 can cause the formation of multiple procentrioles next to one centriole (96). Similar to hSAS-6, CPAP (centrosomal associated protein) also increases during early S phase and is then degraded during mitosis by APC-cdh1 which targets it for degradation by proteasomes. CPAP controls the length of procentrioles and regulates the assembly of centriolar microtubules during centriolar elongation, and its depletion can prevent normal procentriole formation. CPAP and hSAS-6 are reported to be substrates of plk4. Furthermore, constitutively active plk4 can induce *de novo* centrosome amplification (97).

During G2/M phase, the daughter centriole remains attached to the mother centriole until mitosis is completed. Activation of plk1 facilitates centrosome separation during mitosis. Plk1 substrates include β-tubulin and kinesis-like motor proteins, which are required for spindle formation. Together with plk1, separase has also been implicated in centriole disengagement at the onset of mitosis. Plk1

initiates the disengagement process at early mitosis and separase performs disengagement at the start of anaphase (98, 99). Ablation of both plk1 and separase inhibits the centrosome disengagement at telophase. Plk1 also activates APC by binding to its inhibitor Emi1 and phosphorylating it during mitosis.

1.5.3 Mechanisms that control centrosome duplication

There are several mechanisms and protein kinases involved in maintaining the centrosome number in the cell. Some of these control mechanisms are regulated by the centrosome itself and some by the recruitment of certain inhibitors or removal of activators from the centrosomes.

Intrinsic block: Physical engagement between mother and daughter centrioles blocks the further round of centrosome duplication. Data from *in vitro* studies using *Xenopus* eggs have shown that centriole growth does not take place if the two centrosomes are engaged. Separase, a protease and target of APC in mitosis, is responsible for the disengagement of centrioles. A premature activation of separase can cause premature disengagement of centrioles. Disenegaged centrioles then continue to form new centrioles and this was inhibited as long as they are engaged. Thus, it can be concluded that in the normal cell cycle when the two centrioles are attached, it inhibits the formation of new centrioles. This physical attachment could prevent the recruitment, activity of kinases or regulatory proteins required for centriole duplication thus preventing re-duplication (100, 101).

Extrinsic block: Centrosome cycle is controlled by the activation of centrosome specific proteins at specific time in cell cycle. Centrosome cycle in somatic cells is coordinated with nuclear cycle, requiring phosphorylation of Rb and E2F

transcription activity. The Rb/E2F pathway regulates the progression of cells through G1. When cells are arrested in G1 in CHO Rb-mutant cells, centrosome duplication do not take place (102). This suggests that centrosome duplication can only be initiated when cells progress through G1/S. Thus, Rb/E2F may not be the direct regulator of centrosome cycle, but may provide favourable environment for its duplication by promoting cell cycle progression through G1 to S phase.

Coordination of a centrosome cycle with a cell cycle is due to the sequential activation or inhibition of various kinases, as cells traverse through cell cycle and their differential localization at centrosomes throughout the cell cycle (Fig. 4).

Plk4 is a short lived kinase and its localization to centrosomes has been shown to be essential for centrosome duplication. Plk4 appears on the asymmetrically positioned centriole during interphase in certain population of cells (103). Components of SCF ubiquitin ligase localize on centrioles and degrade the plk4. Active plk4 phosphorylates itself, the phosphorylated plk4 is then recognized by SCF ubiquitin ligase, which targets it for degradation by the ubiquitin-proteasome pathway (104). Overexpression of plk4 can either form multiple centrosomes which are scattered in a cell or produce daughter centrosomes which are arranged in a ‘flower-like’ structure. This ‘flower-like’ arrangement of daughter centrioles was only seen in cyclin A positive cells (105). Overexpression of plk4 in *Drosophila* embryos promoted accelerated duplication of centrosomes. Within 60 min of plk4 overexpression, a minimum of 3,700 centrosomes were formed (106). Plk4 has been shown to be sufficient in forming multiple centrosomes via both *de novo* and canonical duplication pathways (Fig. 5). p53, a transcription factor and tumor suppressor, also regulates centrosome amplification. p53-induced cell cycle

Figure 4. Centrosome duplication cycle

Centrosome duplication and maturation occurs during discrete phases of cell cycle. During G1, the two centrioles are linked. During Late G1, procentriole nucleation occurs at both the centrioles. Procentriole elongation and maturation takes place as cells progress from S to G2 phase. During late G2, dissolution of linkers between centrioles take place and the two centrioles separate yet they are still close to each other. During prophase and prometaphase the two centrosomes move to opposite poles. During anaphase and telophase the two centrioles in each centrosome disengage and are linked by linker fibers. Thus, at the end of mitosis and early G1 each daughter cell has one centrosomes consisting of two centrioles joined by linker fibre.

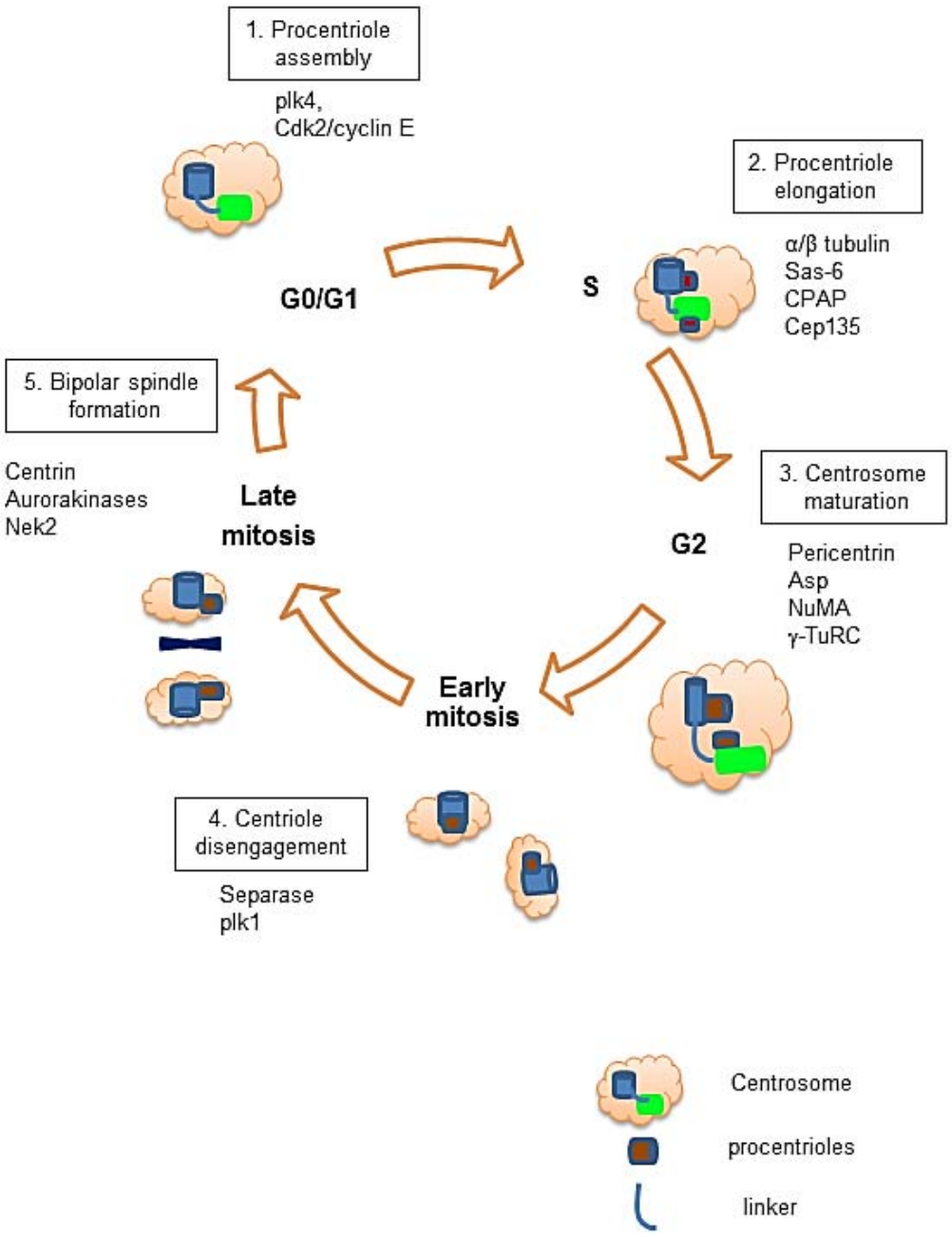
1. Procentriole assembly
plk4,
Cdk2/cyclin E
2. Procentriole elongation
α/β tubulin
Sas-6
CPAP
Cep135
G0/G1
S
3. Centrosome maturation
Pericentrin
Asp
NuMA
γ-TuRC
G2
Early mitosis
Late mitosis
4. Centriole disengagement
Separase
plk1
5. Bipolar spindle formation
Centrin
Aurorakinases
Nek2
Centrosome
procentrioles
linker

arrest can limit the centrosome amplification. p53 directly binds to centrosomes and mutant p53 which does not bind to centrosomes in MEFs undergo repeated duplication of centrosomes (107, 108).

A downstream target of p53 is p21. The cdk inhibitor p21 can inhibit the centrosome duplication when accumulated or overexpressed in cells. Chemical inhibitors of cdk2 have also been shown to inhibit centrosome duplication (108).

1.5.4 The regulation of cyclin E in the context of centrosome duplication/amplification and cell cycle progression

In somatic cells, the centrosome cycle is coupled with the nuclear cycle. The abrogation of the coordination between DNA replication cycle and centrosome duplication cycle can lead to centrosome hyperamplification (109, 110). In animal cells, one of the links between DNA replication and centrosome duplication is cyclin E and cdk2. (111). Cyclin E activation in G1 phase triggers both DNA synthesis and centrosome replication. Cyclin E has a centrosomal localization signal (CLS) which is necessary for both centrosome localization and accelerated entry into S phase. A mutation in the CLS domain of cyclin E prevents its localization to centrosomes and cyclin E mediated accelerated entry into S phase (112). Cyclin E appears to be the common link between nuclear and centrosome cycles. Many proteins involved in DNA replication also localize to centrosomes and regulate cyclin E. For instance, the CLS binding domain of cyclin E binds to MCM5, a DNA licensing factor (113) and recruits it to the centrosomes. Expression and localization of MCM5 to centrosomes inhibits centrosome over-duplication in CHO cells arrested in S phase. Centrosome amplification is commonly studied in cells

arrested in S phase either by hydroxyurea or by aphidicolin, because S-phase inhibition uncouples the DNA replication cycle with centrosome duplication cycle, supporting the idea that regulators of the DNA replication cycle also coordinate the centrosome duplication cycle. Orc1, a DNA replication factor, localizes to centrosomes and removes cyclin E from centrosomes, thus preventing further rounds of duplication. When cyclin E is not localized to centrosomes, it prevents DNA synthesis in S phase (113, 114). CHO cells, in which cyclin E was not localized to centrosomes, could not synthesize DNA. These cells were also defective in formation of the pre-initiation complex on DNA, the first step to initiating DNA replication (113, 114).

The second mechanism, by which the coordination between the nuclear and centrosome cycles is maintained, is the proteolysis pathway (115, 116). For example, the levels of cyclin E and plk4 are regulated by the ubiquitin-proteasome pathway. These proteins are targeted for destruction by the attachment of ubiquitin proteins by ubiquitin ligase complexes. Components of ubiquitin ligases (skp and cullin) and 20S proteosomes are localized to centrosomes as well as to the nucleus (117). Inhibition of proteasomes can lead to the accumulation of cdk2-cyclin E and plk4 on the centrosomes. The inhibition of plk4 autophosphorylation and subsequent degradation by the ubiquitin-proteasome pathway can lead to centrosome over-amplification and inhibition of cell proliferation (118).

Several studies have shown that the cdk2-cyclin E complex is required for the initiation of centrosome duplication (119), while other studies have shown that plk4 is required for the initiation of centrosome duplication. Overexpression of both plk4 and cdk2-cyclin E can cause the formation of multiple centrosomes from a

single mother centrosome. One proposed mechanism of centrosome over-duplication is that plk4 stimulates centrosome duplication and cdk2-cyclin E can enhance it. Neither plk4 nor cyclin E can initiate the centrosome duplication in the absence of the other (120).

Cyclin E also has dual effects on the cell cycle. Cyclin E is required for G1/S transition, but its overexpression can also activate apoptosis. For example, radiation treatment to hematopoietic cells increases the cyclin E level, which activates apoptosis (121). Thus, the presence of non-degradable plk4 and cyclin E in cells can inhibit cell proliferation. Because of its role in both centrosome duplication and G1/S progression, cyclin E overexpression can also cause chromosome instability and polyploidy.

1.5.5 Regulation of cyclin E protein levels

Many breast tumors that show multiple centrosomes deregulate the expression of cyclin E (122). Cyclin E exists in two states inside a cell: a free state which is unbound and bound to cdk2. The latter is to form an active kinase complex (123). Cyclin E is degraded by the ubiquitin-proteasome pathway. The half-life of cyclin E can be increased from 30 min to 2 hours by inhibiting proteasomes (124). Ubiquitination of cyclin E is governed by two distinct ubiquitin ligases, SCF and cul-3. The SCF pathway requires the phosphorylation of cyclin E for ubiquitination, whereas the cul-3 pathway is independent of phosphorylation status of cyclin E, but dependent upon whether it is bound to cdk2 or not (125).

Phosphorylation of substrates is one of the mechanisms by which they can be targeted for ubiquitination. Cdk2 and GSK3 kinases regulate the assembly of

cdk2-cyclin E complex by phosphorylation at five different sites: T62, S372, T380, and S384 (126). Cdk2 can phosphorylate cyclin E on S384 while GSK3 phosphorylates cyclin E on T380. The cdk2-cyclin E complex can also be autophosphorylated at an appropriate site. Thus, multiple pathways can affect the turnover of cyclin E (127, 128).

Binding of cyclin E to cdk2 protects it from proteasome-mediated degradation, and unbound cyclin E gets rapidly degraded. When cdk2 was knocked down in cells treated with a proteasome inhibitor, it resulted in excess accumulation of cyclin E protein levels (129). The protection of bound-cyclin E from ubiquitination can be reversed in the process that involves phosphorylation of cyclin E at T380. This phosphorylation is required for targeting cyclin E bound to cdk2 (but not unbound cyclin E) for ubiquitination. Therefore, cyclin E can be targeted for ubiquitination either by its dissociation from cdk2 (cul-3 dependent) or by its phosphorylation at T62 and T380 (skp1 dependent) (130, 131).

1.5.6 Consequences of centrosome abnormalities

The most commonly reported consequences of having abnormal numbers of centrosomes is multipolar mitosis and cell death. However, cancer cells and mouse embryonic cells containing an abnormal number of centrosomes can continue to survive. It has been reported that multiple centrosomes can cluster. As many as 16 centrioles can cluster and can prevent the formation of multiple spindles (132). Actin-dependent forces and spindle intrinsic pole forces contribute to the clustering of the centrosomes that prevents the formation of multipolar mitosis. Bundling of centrosomes has been observed in different cell lines, including BSC-1 and NIH

3T3 cells (133). The bundling of centrosomes will allow cells to divide in a bipolar fashion and avoid cell death by multipolar mitosis. However, the resulting daughter cells may not necessarily contain equal number of chromosomes. Cells with an abnormal number of chromosomes may end up with selective advantage of survival (134).

Novel drugs that inhibit centrosome clustering have been shown to have selective inhibition on the growth of cancer cells (135, 136). However, it is also likely that cells with multiple centrosomes will eventually die due to abnormal mitosis or abnormal complements of chromosomes during successive rounds of the cell cycle. A structural study from high-grade tumor cells revealed that these cells have an abnormal number of centrioles and excessive amounts of PCM. Invasive breast tumor cells contain 1 to 9 centrioles with excessive PCM. These invasive breast tumor cells show high grade aneuploidy and multiple centrosomes (137). However, centrosome amplification in itself is not sufficient to contribute to the tumor formation. These cells also lack intact cell cycle checkpoints (p53, p21, and mutations in BRCA genes). This was shown in RPE1 cells which activate G1 arrest in response to the overexpression of plk4 that causes centrosome amplification (138).

Radiation can induce centrosome over-duplication (139). Exposure to radiation in 10 tumor cell lines revealed a 15-fold increase in multiple centrosomes, which was directly proportional to mitotic cell death (140). Glioma cell death induced by radiation was proportional to the formation of multiple centrosomes

Figure 5. Canonical *vs de novo* pathway

A. In the canonical pathway centrosomes duplicate only once per cycle from the pre-existing centrosome (template dependent).
B. Formation of multiple daughter centrioles simultaneously is by a *de novo* pathway. The daughter centrioles are either organised radially around the mother centrosome (**i**) or dispersed in the cytoplasm (**ii**). These multiple centrioles can then 'mature' and lead to numerical abnormality in cell. In *de novo* pathway, centrosomes can also form in the absence of template or pre-existing centrioles (template independent).

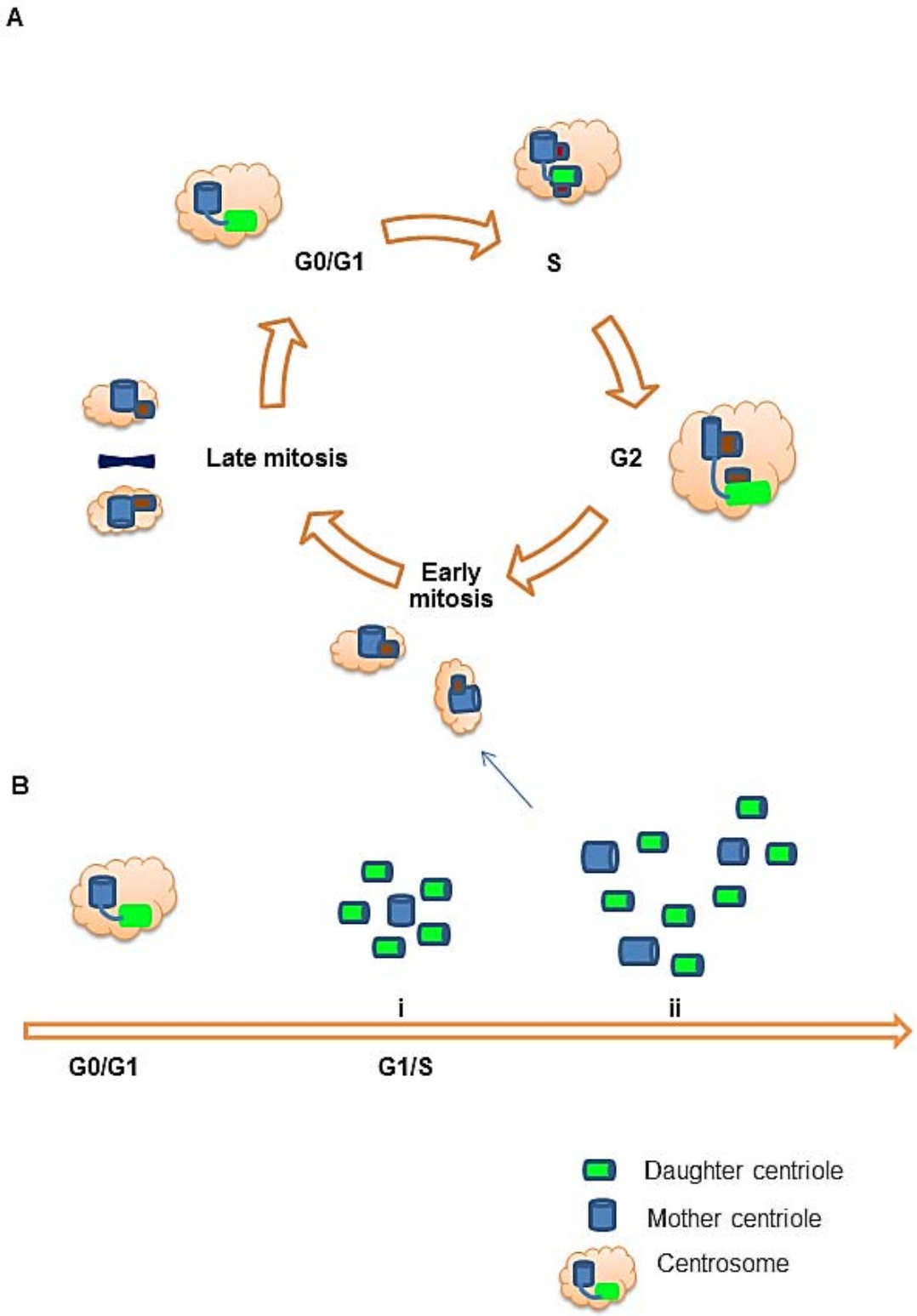
A
G0/G1
S
G2
Early mitosis
Late mitosis
B
i
ii
G0/G1
G1/S
Daughter centriole
Mother centriole
Centrosome

and the degree of chromosome instability (CIN) (141). The chemically synthesized tubulin binding compound EM011 has been shown to cause centrosome amplification, mitotic arrest and mitotic catastrophe (142). Lidamycin, an antibiotic and an anti-tumor agent, also causes the formation of multiple centrosomes, mitotic catastrophe and G2/M arrest (143). Centrosomes formed by this drug contained mature centrioles and were capable of forming spindle poles in mitosis.

1.5.7. Proteasomes on centrosomes

1% of the cell's total proteasomes assemble on the centrosome (144). Centrosomes expand and recruit an increasing pool of proteasome components in response to proteasome inhibition (145, 146). Proteasome activity is required for maintaining the size of PCM. Interestingly, the size of PCM has been shown to restrict the number of centriole formation. The formation of a large PCM cloud can lead to the formation of a variable number of centrioles (147). In support of this, multiple centrosomes concurrently formed from a single maternal centriole when proteasome activity was inhibited with Z-L_3VS (148). Nevertheless, not all proteasome inhibitors cause centrosome amplification (e.g., lactacystin) (149).

The ubiquitin ligase SCF complex (Skp1, Cul1 and F-box-Fbw7) and the 20S proteasome catalytic subunit are assembled at centrosomes, suggesting that proteolysis takes place at the centrosome to regulate centrosome duplication and mitosis. Given the role of centrosomes as a hub for many cell cycle regulatory proteins (e.g., p53, cdc25), it makes sense that centrosomes would have their own exclusive proteolytic machinery.

1.6 Summary of work presented in this thesis

The work described in this thesis is to investigate the biological functions and mechanisms of a novel anticancer compound derived from a CQ pharmacophore. This thesis comprises three parts. The first part describes the screening of the CQ-derivatives against malignant and non-malignant cell lines to determine their selectivity and efficacy. This led to the identification of VR23 as a potentially effective anticancer drug with good selectivity for malignant cells. I initially determined the effect of VR23 on cell cycle progression. A prediction on the mechanism of action can be based on the information derived from cell cycle studies. This initial work led me to the identification of the potential target of the drug, which proved to be the proteasome. CQ is only a weak proteasome inhibitor, whereas VR23 the novel derivative has substantially improved proteasome inhibition activity.

It was shown previously that the inhibition of proteasome activity leads to the formation of multiple centrosomes and spindle fragmentation (150). Using the novel VR23 CQ-derivative as a tool, data presented in this thesis shed new light on the mechanism of how proteasome inhibition can lead to the phenomenon of centrosome amplification by a *de novo* mechanism. Proteolysis machinery is localized to centrosomes and the inhibition of this machinery increases the number of centrosomes, perhaps due to the accumulation of certain proteins involved in centrosome biogenesis.

This study further sought to explore 2 questions: why are mitotic cells hypersensitive to VR23, and how does VR23 disrupt the once-per-cell cycle rule of

the centrosome cycle? The answer to both can be explained by the inhibition of proteasome activity by VR23.

Together, data presented in this thesis establishes the accumulation of ubiquitinated cyclin E by VR23-mediated inhibition of cellular proteasome activity. This, in turn, leads to centrosome amplification and, eventually, mitotic abnormalities including lack of coordinated microtubule attachment to the kinetochore, mono-, tri- and multi-polar mitosis, and prolonged cell cycle arrest at mitosis. These abnormalities eventually lead to cell death by apoptosis. Since these abnormalities are not observed in non-malignant cells, VR23 has a very desirable property as a potential anticancer drug.

2.0 Materials & Methods

2.1 Cell culture

HeLa S3, MCF7, MDA-MB231, MCF10A and 184B5 cell lines were purchased from ATCC (Manassas, VA). HeLa S3 cells were grown in RPMI 1640 medium (Hyclone), supplemented with 10% (v/v) fetal bovine serum (FBS). MCF7 and MDA-MB231 cells were grown in DMEM (Hyclone) supplemented with 10% (v/v) FBS. MCF10A and 184B5 cells were grown in DMEM F-12 (Hyclone) supplemented with FBS (10% v/v), 10 µg/ml insulin, 20 ng/ml EGF (epidermal growth factor) and 0.5 µg/ml hydrocortisone. Cells were routinely cultured and maintained under standard culture conditions in a humidified atmosphere at 37°C, and 5% CO_2. Cells were not used past 18 passages or continuously subcultured for longer than 1.5 months (whichever comes first). HeLa S3 is a subclone of HeLa cell line (Human cervix carcinoma). MCF7 and MDA-MB231 are human breast adenocarcinoma cell lines. MCF10A and 184B5 are human mammary epithelial cell lines.

2.2 Clonogenic assay

Exponentially growing cells were trypsinized, counted, and a pre-determined number of cells (10,000/ml) were plated on T25 flasks in 5 ml medium for 24 h. After 24 h, cells in each of the T25 flask were exposed to increasing concentrations of a compound for 24 h, nontreated control samples were included with each set of experiment. After 24 h exposure, cells were washed in 1X PBS, trypsanized, and resuspended in 1 ml of medium. Cells were suspended in pre-made 0.4% agarose (kept in water bath at 37°C), and were mixed thoroughly using a 3 cc syringe equipped with a 16 gauge needle. 1 ml of each sample was dispensed into each

well of a six-well plate. Once agarose was solidified, 500 µl of complete medium was gently added on the top of agar, followed by incubation at 37ºC and 5% CO_2. After 12 days of incubation, numbers of colonies were counted in 10 random fields for each sample as described previously by Franken *et al.* (151). Average number of colonies per field was plotted against the concentration of the cytotoxic agent being tested. Only those colonies containing more than 50 cells per colony were counted as viable colonies.

2.3 Sulforhodhamine B (SRB) assay

A fixed number of cells (10,000/ml for MCF7 cells, 8,000/ml for MCF10A cells, 5,000/ml for MDA-MB231 cells) were plated in each of the 96-well plate and incubated for 24 h. The growth medium was replaced with medium containing different dilutions of the drug, or left not treated or treated with 50% TCA (trichloro acetic acid), and incubated for additional 48 h. Culture medium was then removed from plates and cells were fixed in ice-cold 50% TCA and incubated at 4ºC for 1 h. Cells were repeatedly washed in running water, and then air dried. Cells were stained with 0.1 % (w/v) SRB solution for 30 min at room temperature, followed by washing in running water and air-drying. Cells were resuspended in 200 µl of 10 mM Tris buffer (pH10.5) and absorbance was read on an automated plate reader (Molecular devices, Spectra max 340 PC) at a wavelength of 530 nm, as described previously by Vichai *et al* (152).

Non-treated cells were taken as a positive control, and cells treated with 50% TCA were taken as a negative control. IC_{50} values were calculated using a sigmoidal dose-response curve (variable slope) in Graphpad Prism V 4.02 (Graph

Pad Software, Inc.). Data was normalised using the following formula: (Mean O.D. sample – Tn)/Tp -Tn (where, Tp is mean O.D. of positive control and Tn is mean O.D. of negative control).

2.4 Cell synchronization

For G1/S synchronization, exponentially growing HeLa S3 cells were exposed to 2 mM thymidine for 18 h followed by release in complete medium for 11 h. A second block was with 2 mM thymidine for 14 h. For G2/M synchronization cells were exposed to 50 ng of nocodazole for 18 h.

2.5 Analysis of cell cycle distribution

Cells were trypsanized after exposure to drug(s) at different timepoints. Cells were washed twice in 1X PBS and fixed overnight in 75% ice-cold ethanol at -20ºC. Cells were centrifuged, washed twice in PBS, and resuspended in PI (propidium iodide) staining solution (0.1% sodium citrate, 0.3% Nonidet P-40, 100 µg/ml RNase A, 100 µg/ml propidium iodide) for 1 h.

For BrdU labelling, cells were incubated in the dark at 37°C for 45 min with 10 µM BrdU, and were then trypsanized, fixed in 75% ice-cold ethanol overnight at 4ºC. Cells were washed twice with 1X PBS and nucleic acids were denatured with 2M HCl for 20 min, washed once with 1X PBS, and once with PBST (1X PBS with 1% Tween 20), cells were then incubated with BrdU-FITC antibody (BD biosciences) for 30 min at room temperature in dark. Finally, unbound antibodies were washed off in 1X PBS, and DNA was stained with PI staining solution for 30 min before analyzing by flow cytometry. Samples were analyzed by flow cytometry using an Epics Elite Flow Cytometer (Beckman Coulter), using a protocol adapted

from Dolbeare *et al*. (153). Ten thousand events were gated on PI intensity. PI fluoresces at 623 nm and FITC at 520 nm when excited at 488 nm. Dual parameter and single parameter displays were created with flow cytometery data acquisition software. FL1 and FL3 fluorescence signals were recorded. Cell doublets and debris were excluded using an FL3-A *vs* FL3-w gate. Analysis of DNA fragmentation was performed using an FL3-A *vs* FL1-H cytogram. FL1 and FL3 fluorescence signals were, respectively, recorded on logarithmic and linear scale, using a protocol adapted from Nunez *et al.* (154).

2.6 Immunofluorescence experiment

Cells were plated on sterile glass coverslips (Fisher Scientific) that had been placed in sterile 6-well plates. Cells were allowed to adhere overnight. After indicated treatments and specific timepoints, coverslips were fixed in ice cold methanol for 10 min at -20°C (for all centrosomal stainings methanol fixation was used). For single antibody staining: Coverslips were washed in 1X PBS and permeabilized and “blocked” for 30 min at room temperature by adding 1X PBST with 1% BSA (1X PBS buffer with 0.1% Triton X-100 and 1% (w/v) bovine serum albumin), followed by washing with 1X PBS. The primary antibodies were diluted (1:100) in 1x PBST buffer, followed by incubation overnight (or for a minimum of 4 h) with primary antibodies at 4°C with gentle shaking. After washing with 1X PBS, secondary antibodies (1:1000) were added for 1 h in dark with gentle shaking. Secondary antibodies were diluted in 1X PBST buffer. All primary and secondary antibodies were titrated to optimize the optimal concentrations. Appropriate controls with secondary antibodies were included to ensure and minimize the

bleedthrough different channels in microscopy. Experiments also included primary antibody omission controls to exclude non-specific staining. (Fig. A1). Coverslips were mounted onto slides containing 4 µl of 50% glycerol/1X PBS. A minimum of 20 fields/per sample/per coverslip were captured for each and all experiments.

For double labelling with two different antibodies, cells on the coverslips were processed according to the single antibody staining protocol. This process was then repeated for the second probe. Additional washing and blocking in PBST buffer was included, followed by staining with second primary antibody by incubating at 4°C for 2-4 h. Hence, the staining was done in two steps (instead of adding all different primary antibodies or secondary antibodies at the same time).

When immunostaining was performed with three different antibodies, the coverslips were processed in the same manner as the double antibody staining, except an additional washing and an additional blocking step (with PBST+BSA buffer) and third antibody. A list of antibodies used in the experiments is shown in appendix table A1.

TUBEs (tandem ubiquitin binding entities) staining: For the staining of ubiquitin, TUBEs (Life Sensors) tagged with a fluorescent moiety (Fluorescent-TUBE-FITC. FLR-TUBE2 excitation 490 nm, emission 520 nm) was used. 1:250 dilution of FLR-TUBE2 diluted in PBST (1X PBS with 0.1% Triton X) buffer was used. Cells were stained for 2 h in dark.

2.7 EdU labelling

Cells ability to proliferate was also checked using an EdU-alexa fluor kit (Invitrogen). EdU labelling was carried out after exposing cells to a compound for 3

h after double thymidine block. Cells were grown on coverslips treated with siRNA, followed by exposing cells to 10 µM EdU and then incubated at 37°C for 45 min in dark. Cells were then washed with 3% BSA in PBS and fixed in 3.75% formaldehyde in PBS, followed by permeabilization with 0.5% triton X-100 for 15 min at room temperature. Finally, EdU was detected by exposing cells to reaction buffer containing alexafluor azide, ascorbic acid and CuSO4. The coverslips were then mounted and immediately analyzed by confocal microscope. Protocol was adapted from Salic *et al.* (155).

2.8 Confocal Microscopy

All Immunofluorescence experiments were visualized using a Zeiss 510 Meta laser scanning microscope (Carl Zeiss) equipped with a 63x objective lens. Three laser lines were utilized for excitation with the following band pass filter settings: Argon 488 nm (band pass 505-530), HeNe 543 nm (long pass 560), and 633 nm (long pass 650). Images were captured and analyzed using LSM 510 software equipped with the microscope (LSM Image examiner, Carl Zeiss).

2.9 Protein extraction and Quantification

Proteins were extracted from samples by removing culture medium, plates were then placed on ice, and cells were scraped using a scraper. Floating cells were also collected in a 15 ml tube and centrifuging at 1,000 g for 5 min. Cells were then pooled and washed three times with ice cold 1X PBS. 500 µl of cell Lysis buffer (20 mM Tris-HCl, pH 7.5, 150 mM NaCl, 1 mM EDTA, 1mM EGTA, 1% (v/v) Triton X-100) supplemented with 1mM PMSF, 1x protease inhibitor cocktail

(Roche), 2 mM sodium orthovanadate and 10 mM sodium fluoride. Cells were sheared with a 21-gauge needle, incubated at 4°C with shaking for 30 min, and were then cleared by centrifugation at 10,000g for 15 min at 4°C. The supernatant was collected and proteins were quantified by a BCA assay (Pierce). The concentrations of unknown protein samples were determined by interpolating the values from the standard curve against a known amount of BSA (25-2,000 µg/ml) using a linear regression curve analysis on GraphPad Prism version 4.03.

2.10 SDS-PAGE

Protein extracts were diluted in 5X Laemmli sample buffer (0.1 M Tris.HCl, pH 6.8, 10% (w/v) SDS, 40% (v/v) glycerol, 2%(w/v) DTT, 10% (w/v) bromophenol blue). 25 µg of proteins were loaded onto 4-20% polyacrylamide gels (acrylamide:N,N-methylene bisacrylamide, 29:1). Proteins were resolved by electrophoresis in Running buffer (25 mM Tris, 192 mM Glycine, 0.1% (w/v) SDS) at 90-120 volts for 2-2.5 h.

2.11 Western Blot

Proteins were transferred using a semi-dry apparatus at 10 volts for 1-2 h onto PVDF membranes (GE Health care) which were soaked in Transfer buffer (48 mM Tris, 39mM Glycine, 20% (v/v) methanol, 0.037% (w/v) SDS). Membranes were ‘blocked’ for 1 h in Blocking buffer (1X TBS with 0.1% tween, 50 mM Tris-HCl, pH 7.4, 150 M NaCl, 0.1 % (v/v) Tween 20 with 5% carnation non-fat skim milk), incubated overnight in primary antibodies (diluted in 5% BSA in 0.1% TBST solution) at 4ºC. Membranes were washed three times in 0.1% TBST, and incubated in a secondary antibody (diluted in 0.1% TBST with 5% non-fat skim

milk) for 1 h at room temperature. The membranes were then washed twice with 0.1% TBST, and once with 0.1% TBS. The blots were visualized using ECL (Enhanced Chemiluminescence, GE Health care). List of antibodies used in the experiments is compiled in table A1.

2.12 Immunoprecipitation

Cell lysate was precleared by incubating for 4 h with agarose beads. The lysate is centrifuged, and the primary antibody is added onto the precleared lysate, which was then incubated overnight at 4ºC with agitation. After overnight incubation with an antibody, prewashed agarose beads were added and incubated for 6 h with agitation at 4ºC. After the incubation, protein samples are centrifuged and supernatant is removed, denatured in 2X loading buffer, and boiled for 5 min, followed by PAGE and Western blotting.

The immunoprecipitation of ubiquitinated proteins using agarose-TUBEs was carried out according to the manufacturer's protocol (Life sensors, UM401). The sample preparation protocol was the same as above, except that cells were lysed in slightly modified Lysis buffer (50 mM Tris-HCl, pH7.5, 0.15 M NaCl, 1 mM EDTA, 1% NP-40, 10% glycerol). 1X protease inhibitor cocktail and 50 µM of PR-619 (reversible inhibitor of ubiquitin proteases) was added in the Lysis buffer. Na_3VO_4 and PMSF were not included in the Lysis buffer.

For the immunoprecipitation of ubiquitinated cyclin E: A similar protocol for TUBEs study was used, except that 2 mM of fresh NEM (N-ethylmaleimide) was added in Lysis buffer. High molecular weight transfer buffer was used for

transferring higher molecular weight proteins (48 mM Tris, 39 mM Glycine, 10% (v/v) methanol, 0.075% (w/v) SDS).

2.13 Proteasome activity assay in cells

Exponentially growing cells were plated on 96 well plates. Following overnight incubation, cells were treated with different concentrations of drugs or left not treated. Cells were exposed to drugs for another 6 h. At the end of 6 h, proteasomes were extracted in 0.5% NP40 Lysis buffer (50 mM Tris-HCl, 150 mM NaCl, 5 mM EDTA, 0.5% NP40, 2 mM DTT). 100 µl of Lysis buffer was added in each well, and cells were incubated in the Lysis buffer, at room temperature for 45 min with shaking. Cell lysates were cleared by centrifuging at 10,000g for 5 min, and supernatant (lysates) was collected. Protein concentration was determined by BCA assay. An equal amount of sample lysates (equal concentration of proteins) was transferred in a black-bottom 96 well plates. 25 µM of substrate from Boston Biochem (LRR- specific for trypsin-like activity, LLE-specific for caspase-like activity and Suc-LLVY-specific for chymotrypisin like activity) were added to each sample in proteasome assay buffer (20 mM HEPES, 0.5 mM EDTA, pH 8.0 with a final SDS concentration of 0.035%). The final volume in each well was 100 µl. Hydrolysis reaction was allowed to proceed at 37°C. If proteasomes are active in the sample, it would cleave the peptide which will release the fluorogenic substrate. Fluorescence was measured at the wavelength of 380 (excitation) and 460 nm (emission). The fluorescence was measured every 5 min for 50 min. (In some experiments fluorescence was measured at 30 min only). Relative fluorescence units were plotted to determine the IC_{50}. Bortezomib and MG132 were used as

controls. IC_{50} was calculated using GraphPad prismV software by sigmoidal dose-response curve (variable slope). All experiments were carried out using fresh sample lysates. The protocol was adapted from Lightcap *et al*. (156).

2.14 *In vitro* flurogenic substrate activity assay

In a typical assay, 2 nM of purified h20S proteasomes (human) (E-360 Bos. Biochem, MA) was added to black-bottom plates containing VR23 (final concentration of VR23 used was 1 to 0.01 µM) in a total volume of 100 µl in Assay buffer ((20 mM HEPES, 0.5 mM EDTA, pH 8.0 with a final SDS concentration of 0.035%). Samples were pre-incubated for 1 h at 37°C. After the incubation, substrates were added to a final concentration of 25 µM (for catalytic kinetics of proteasomes different concentrations of substrate were added: 0, 25, 50, 100 and 200 µM). The hydrolysis reaction was allowed to proceed for 30 min (for chymotrypsin-like substrate) and 1 h for (trypsin-like substrate) at 37°C. Fluorescence was measured at 30 min (for some experiments at 15, 30, 45 and 60 min). The florescence was measured at 380 nm (excitation) and measurement of emission at 460 nm. Data was analyzed in GraphPad PrismV using double-reciprocal Lineweaver-Burk plot or by nonlinear regression curve analysis (Michaelis-Menten kinetics). The protocol was adapted from Li *et al*. (157).

2.15 siRNA experiments

siRNA transfections were performed in 6-well plates. Cells were plated 24 h prior to transfection. Cells were exposed to 100 nM of siRNA in Opti-MEM I reduced serum media (Gibco) and Lipofectamine 2000 (Invitrogen). The Lipofectamine 2000 and siRNA or scrambled RNA were pre-incubated for 20 min

at room temperature prior to additing Opti-MEM I media. 1.5 ml of total transfection media was added to each well. The plates were incubated for 12 h, after which transfection medium was replaced with complete fresh medium (RPMI 1640 with 10% FBS). The plates were then placed back in the incubator at 37°C and processed for further experiments (double thymidine block, immunostaining or protein extraction etc.). Scrambled RNA control (santa cruz. sc-37007) was included in each experiment.

The sequence of cyclin E siRNA (h) (santa cruz. sc-29288) is:

• Sense: 5’ UGGAAAAUCAUGUUAAACAAGG 3’

• Antisense: 5’ CCUUGUUUAACAUGAUUUUCCA 3’

plk4 (SAK) siRNA (h) (santa cruz. sc-61491) is a pool of 3 different siRNA:

sc-61491A:

• Sense: 5’ CUUCUAUCUUGGAGCUUUAtt 3’

• Antisense: 5’ UAAAGCUCCAAGAUAGAAGtt 3’

sc-61491B:

• Sense: 5’ CAGGGAUGUUGUAUCUUCAtt 3’

• Antisense: 5’ UGAAGAUACAACAUCCCUGtt 3’

sc-61491C:

• Sense: 5’ GAACAGACAUCUCUUCUAAtt 3’

• Antisense: 5’ UUAGAAGAGAUGUCUGUUCtt 3’

2.16 In-silico docking

Energy minimizations, Binding pocket analysis and ligand docking were carried out using MOE (Molecular Operating Environment) software (Chemical Computing Group, Montreal, QC, Canada). The subunits of 20S proteasome crystal structure (PDB 2F16) (158) were used for protein modeling (ligand (bortezomib) was deleted). The protocols for molecular modelling was adapted from the Chemical Computing Group website (http://www.chemcomp.com/MOE-Structure_Based_Design.htm).

Crystal structures were obtained from the Protein Data Bank (PDB). The active site was defined using Sitefinder in the MOE software. The induced-fit docking protocol was used. Poses were selected from the lowest RMSD values and S-scores. Low docking energy indicates high binding ability. All the calculations were carried out using the force field MMFF94.

2.17 Statistical analyses

All statistics were performed on GraphPad PrismV (GraphPad Software, Inc.). Univariante analysis of variance (ANOVA) was performed to determine the differences between samples and in the proteasome activity assay. A student's t-test was used to determine the statistical differences between treated and control groups and $p<0.05$ was considered as statistically significant. Lineweaver–Burk plot was performed for enzyme kinetics assays. Non Linear regression plots (variable slope) were used for IC_{50} determination. Linear regression plots were used for determining unknown values against a given standard curve.

3.0 RESULTS

3.1 Screening and identification of a compound that preferentially kills cancer cells

To develop highly specific anticancer agents, Dr. Solomon in Lee's lab designed and synthesized 31 novel 4-piperazinyl/amino quinoline derived sulfonyl compounds (Fig. 6 and Fig. A2) using a hybrid pharmacophore approach. The IC_{50} of these compounds are summarized in Table A1. The purified compound VR23 was confirmed by NMR (Fig. A3. Data obtained from Dr. V.R. Solomon).

The screening of the CQ derivative compounds library revealed several hits. Among these, VR23 (Figs. 6 and 7) was recognized as a compound that kills cells in a cancer-specific manner (Table 3). The IC_{50} of VR23, determined by clonogenic and SRB assays, showed preferential killing of cancer cells over non-cancer cells more than eight-fold. The IC_{50} of VR23 by SRB assay on the MCF7 cell line was 1.5 μM and by clonogenic assay was 0.78 μM. VR23 showed no notable effect on the cell cycle profile of the MCF10A non-malignant cells, up to 8 μM concentration (Fig. 7). Following 48 h treatment, MCF7 and Jurkat cells showed significant sub-G1 DNA content, indicating that cells may die by apoptosis. The mode of cell death by apoptosis was confirmed by PARP1 cleavage (Fig. 7), a hallmark for apoptosis. VR23 was then chosen for further study to characterize its mechanism of action in more detail.

3.2 VR23 severely impedes cell cycle progression in each phase of the cell cycle

To study how VR23 affects the cell cycle, experiments were performed using synchronized cells. VR23 prevented the progression of cells through mitosis.

Figure 6. Synthesis of chloroquine based compounds

The structures of chloroquine and the VR23 derivative contain a quinoline moiety (PubChem. http://pubchem.ncbi.nlm.nih.gov/summary/). The derivative was designed by Dr. V. R. Solomon in the Lee laboratory. The figure shows the design scheme of 31 quinoline derived sulfonyl analogs synthesized using a hybrid pharmacophore approach (Figure obtained from Dr. V.R. Solomon).

Chloroquine

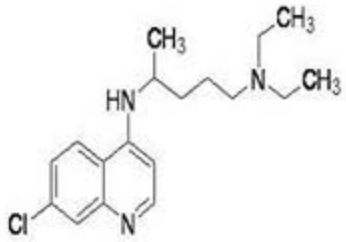

VR23

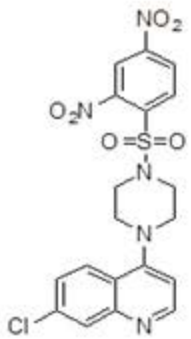

Design scheme of chloroquine derivatives

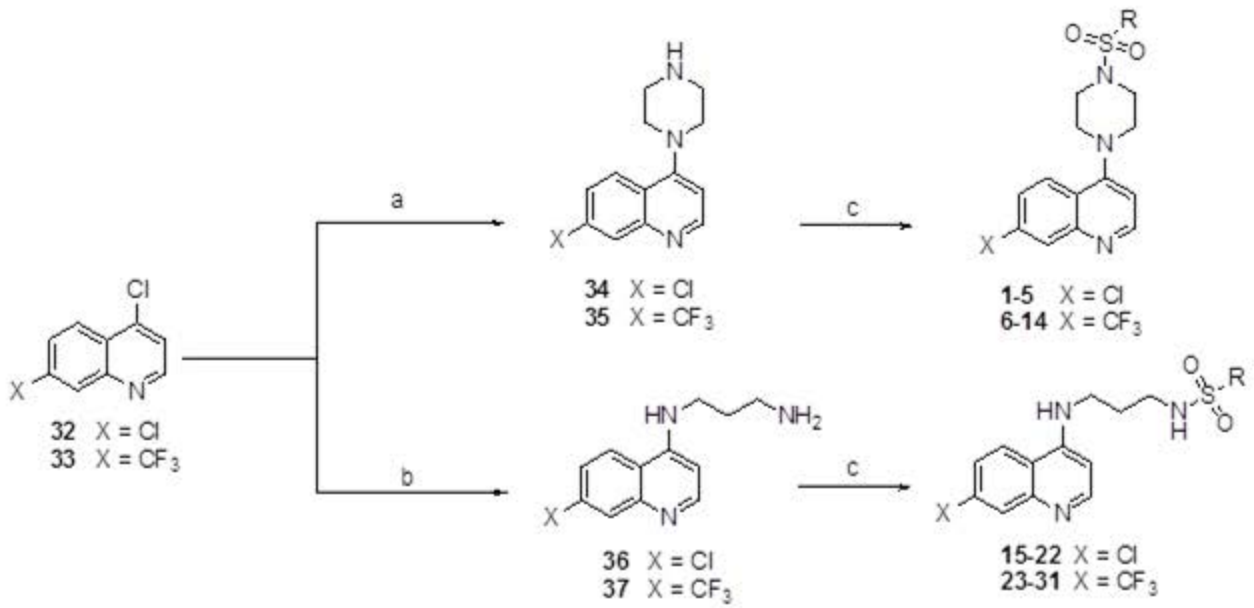

Figure 7: Determination of IC_{50} by clonogenic assay and differential effect of VR23 on malignant and non-malignant cells

A. IC_{50} was determined by a clonogenic assay on MCF7 cells and on MCF10A cells. As compared to sham-treated control, no colony was formed in the MCF7 cells treated with 1.5 µM of VR23. Colony formation was seen both in sham-treated and VR23-treated (8 µM) MCF10A cells. The experiment was performed three times with internal duplicates. Representative figures of MCF7 and MCF10A from clonogenic assay are shown.

B. Cell cycle profile of asynchronous cells treated with VR23 for 48 h. Unlike MCF10A cells, MCF7 and Jurkat cells undergo apoptosis as indicated by increased sub-G1 cell population. Sub-G1 peak in sham-treated MCF7 cells is 4.8%; VR23, 2.7 µM is 23.7%; and in VR23, 8 µM is 38.1%. Sub-G1 peak in sham-treated Jurkat cells is 7%; in VR23, 0.7 µM is 18.4%; and in VR23-1.7 µM is 32.2%. Sub-G1 peak was not significantly different in sham-treated MCF10A cells or in cells treated with VR23, 2.7 µM and 8 µM.

C. VR23 activates apoptosis in HeLa S3 cells in different cell cycle phases. G1/S cells were synchronized by the double thymidine block and released into the cell cycle for 24 h in the presence or absence of VR23 (20 µM). G2/M. Cells synchronized at G2/M by nocodazole and released into the cell cycle for 6 h in the presence or absence of VR23 (5 µM). G1 cells were defined for those cells that were synchronized by nocodazole were released into complete medium for 6 h. At the end of 6 h, when cells reached G1 (confirmed by their cell cycle flow profile), VR23 was added and these cells were incubated for another 6 h. Cleaved PARP-1 is a marker for apoptosis. Gapdh is the loading control.

A

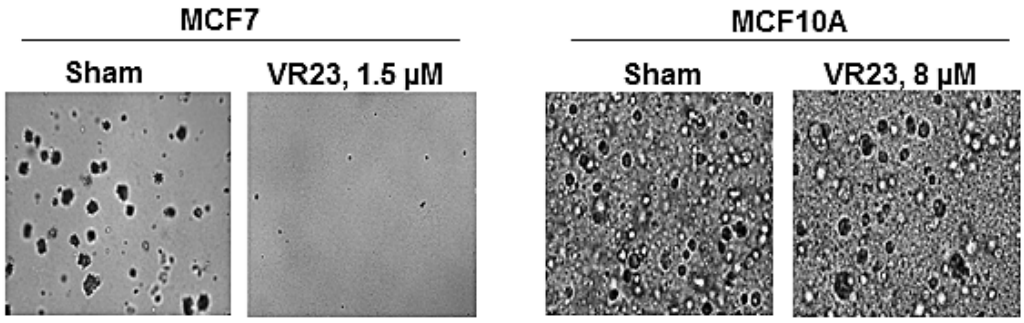
MCF7
MCF10A
Sham
VR23, 1.5 μM
Sham
VR23, 8 μM

B

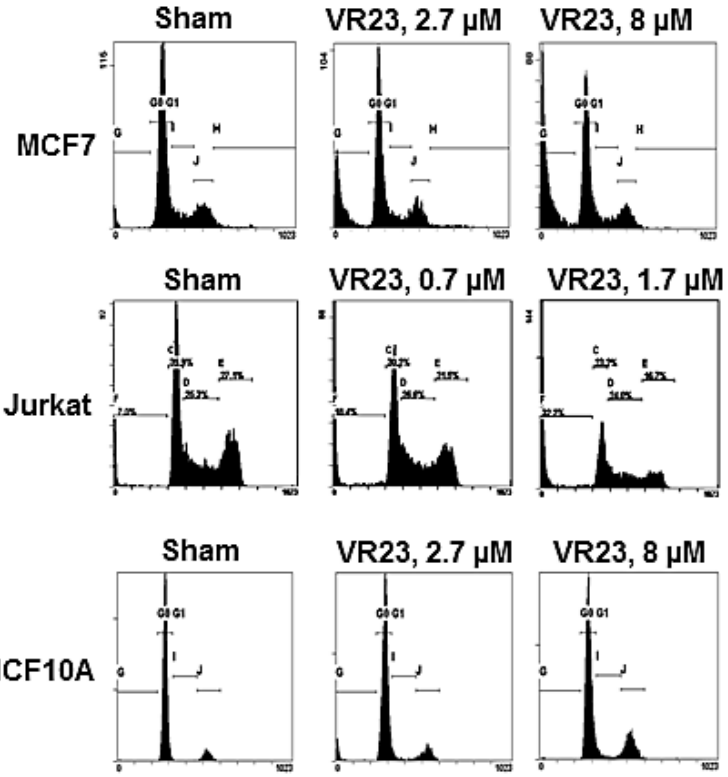
Sham
VR23, 2.7 μM
VR23, 8 μM
MCF7
Sham
VR23, 0.7 μM
VR23, 1.7 μM
Jurkat
Sham
VR23, 2.7 μM
VR23, 8 μM
MCF10A

C

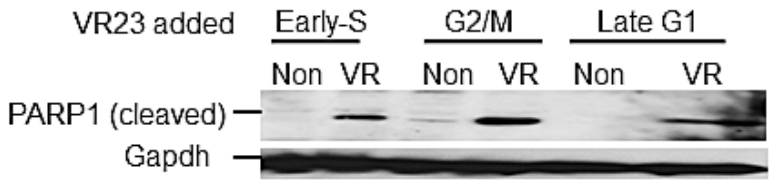
VR23 added
Early-S
G2/M
Late G1
Non
VR
Non
VR
Non
VR
PARP1 (cleaved)
Gapdh

Table 3: IC_{50} of VR23 on different cell lines

This table shows the IC_{50} of VR23 for different cell lines as determined either by SRB assay or by clonogenic assay for the cell lines that form colonies (MCF7, U87MG and MCF10A). Cell seeding numbers were determined for each cell line as outlined in Materials and Methods. The IC_{50} was determined by a sigmoidal dose response curve (four parameters) on Graphpad prism V.

Cells	IC_{50} (μM)
MDA-MB231	3.4 ± 0.1
MDA-MB468	0.7 ± 0.1
MCF7	1.0 ± 0.8
HeLa S3	4.4 ± 3.0
Jurkat	0.8 ± 0.1
U87MG	0.8 ± 0.5
184B5	9.0 ± 0.1
MCF10A	12.3 ± 1.0

Figure 8: Mitotic cell cycle arrest in response to VR23

A. HeLa S3 cells were synchronized by nocodazole (5 ng/ml for 18 h). At the end of 18 h, cells were collected and released into fresh medium in the absence (non-treated) or presence of VR23 (5 μM). Cells were placed back into the incubator at time 0 h (37°C/5%CO_2). Cells were collected at different timepoints (2-24 h) post-release. Unlike non-treated cells, VR23- treated cells remain arrested in mitosis. Cells in non-treated samples reach G1 by 2 h. Cells in VR23-treated samples remain arrested in G2/M and began undergoing apoptosis (as indicated by a sub-G1 peak). Representative flow cytometry profiles from three independent experiments are shown.

B. HeLa S3 cells treated with VR23 show high levels of cdk1 Y15 phosphorylation and cyclin B. Cells released in the presence or absence of VR23 from G2/M arrest were collected at different timepoints: 0.5, 0.75, 1, 2, 3 and 4 h. Figure shows Western blots with antibodies specific for cyclin B and cdk1. Equal quantity of each protein sample was loaded. Cyclin B was found to be degraded in non-treated cells at 0.5 and 0.75 min but did not degrade in VR23-treated cells. Inhibitory phosphorylation of cdk1 was decreased at 0.5 h in non-treated cells, facilitating the entry of cells into metaphase. Conversely, high levels of inhibitory phosphorylation (Y15) were found in VR23-treated cells at this same timepoint.

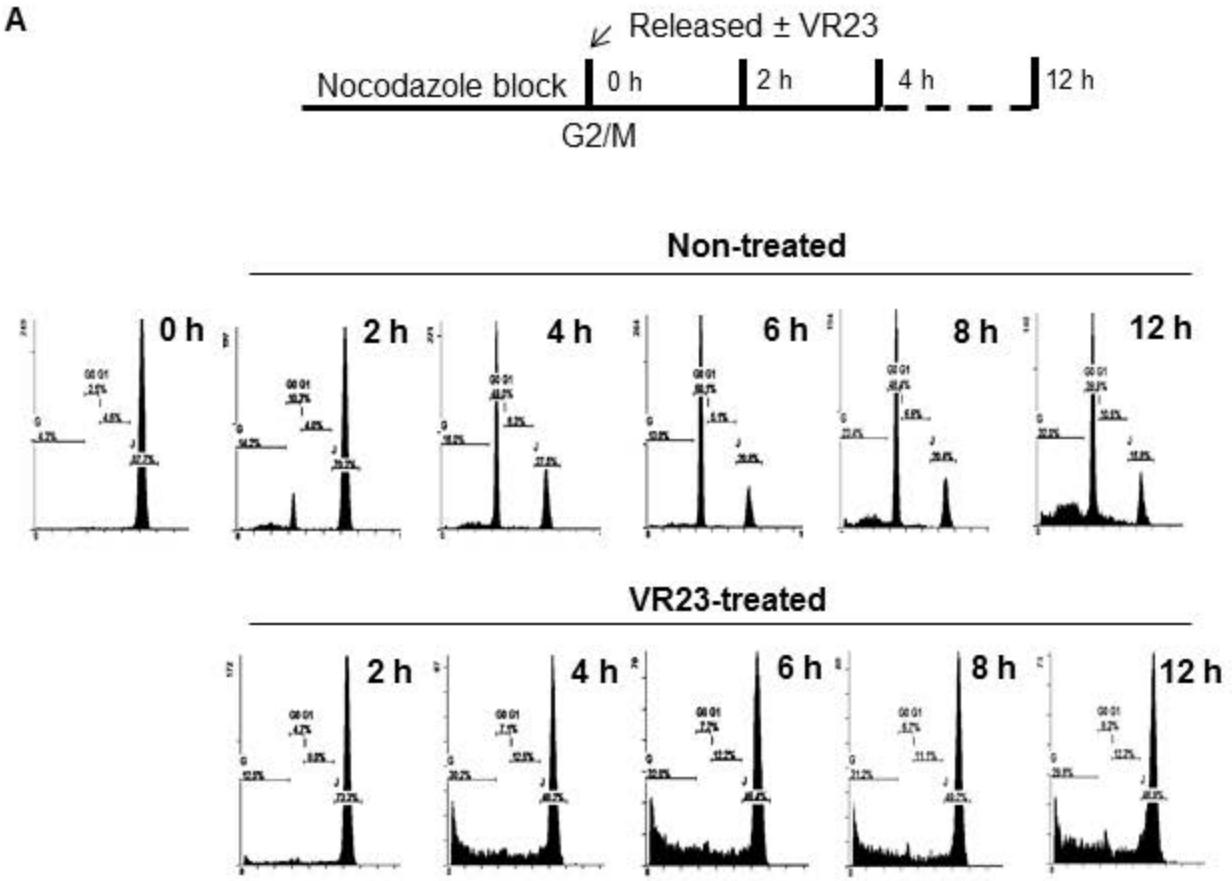
A
Released ± VR23
Nocodazole block
0 h
2 h
4 h
12 h
G2/M
Non-treated
0 h
2 h
4 h
6 h
8 h
12 h
VR23-treated
2 h
4 h
6 h
8 h
12 h

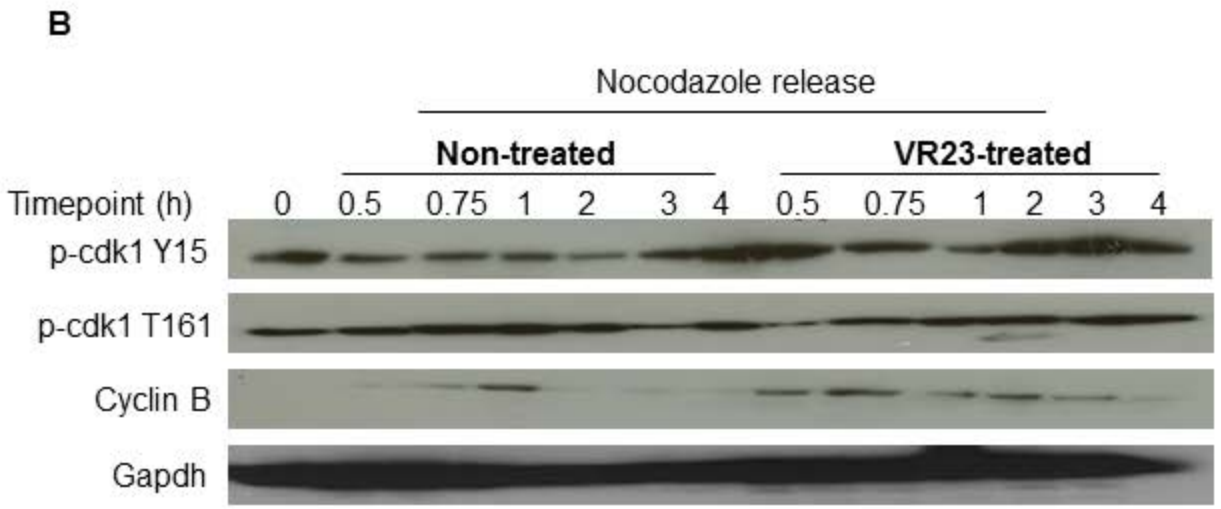
B
Nocodazole release
Non-treated
VR23-treated
Timepoint (h)
0 0.5 0.75 1 2 3 4 0.5 0.75 1 2 3 4
p-cdk1 Y15
p-cdk1 T161
Cyclin B
Gapdh

In HeLa S3 cell line, an increased accumulation of G2/M cells was seen by 24 h post-treatment (Fig. A4). The more sensitive cells such as MCF7, MDA-MB231 and Jurkat underwent apoptosis by 24 h post-treatment without showing an obvious G2/M arrest. When HeLa S3 cells were synchronized in prophase by nocodazole and released into the cell cycle, VR23-treated cells underwent cell death within 4 h (Fig. 8).

To examine if cells are less sensitive to cell cycle arrest when adding VR23 at different points in the cell cycle, cells were synchronized in G2/M and released into the cell cycle with VR23 added at different timepoints ranging from 2-6 h (Fig. A5). This approach allows for the cells to progress into different points of cell cycle phases when the drug is introduced. In this case, while non-treated cells progressed through the cell cycle normally, VR23-treated cells remain arrested at the point in the cell cycle where the drug was added.

Cells were then synchronized in G1/S by double thymidine block and released into cell cycle (Fig. 9). The progression of the cell cycle was delayed in the presence of VR23. Non-treated cells progressed through G1/S to G2/M within 4-6 h; in contrast, VR23-treated cells progressed to G2/M by 8-11 h. This suggests that G1/S to G2/M progression of these cells is impeded. Multiple foci of γ-tubulin were also seen in VR23-treated cells (Fig. 9), suggesting that the formation of multiple centrosomes occurred in the presence of VR23.

I hypothesized that this delay in transition between cell cycle phases can be used as an anticancer treatment by combining VR23 with other cell cycle specific agents like paclitaxel (a mitotic poison). Indeed, combination of paclitaxel and VR23 significantly increases cell death (Fig. A6).

Figure 9: Cell cycle progression from G1/S to G2/M is slowed down in response to VR23

Cells were synchronized by double thymidine block as shown in **A**. Synchronized cells were released in complete medium in the presence or absence of VR23 (20 μM). Cells were fixed at different timepoints. In non-treated samples, the majority of cells reach mitosis by 4-6 h. Unlike non-treated cells, VR23-treated cells reach mitosis by 8-11 h. Figure shows images taken by confocal microscopy. Cells were immunostained with primary antibody specific for γ-tubulin (green) and α-tubulin (red), followed by secondary immunostain corresponding to these antibodies. γ-tubulin were immunostained by secondary antibody that is fluorescent at 488 nm and α- tubulin that fluorescent at 546 nm. DNA was stained with DRAQ5 (blue). Multiple foci of γ-tubulin suggests the presence of multiple centrosomes in these cells.

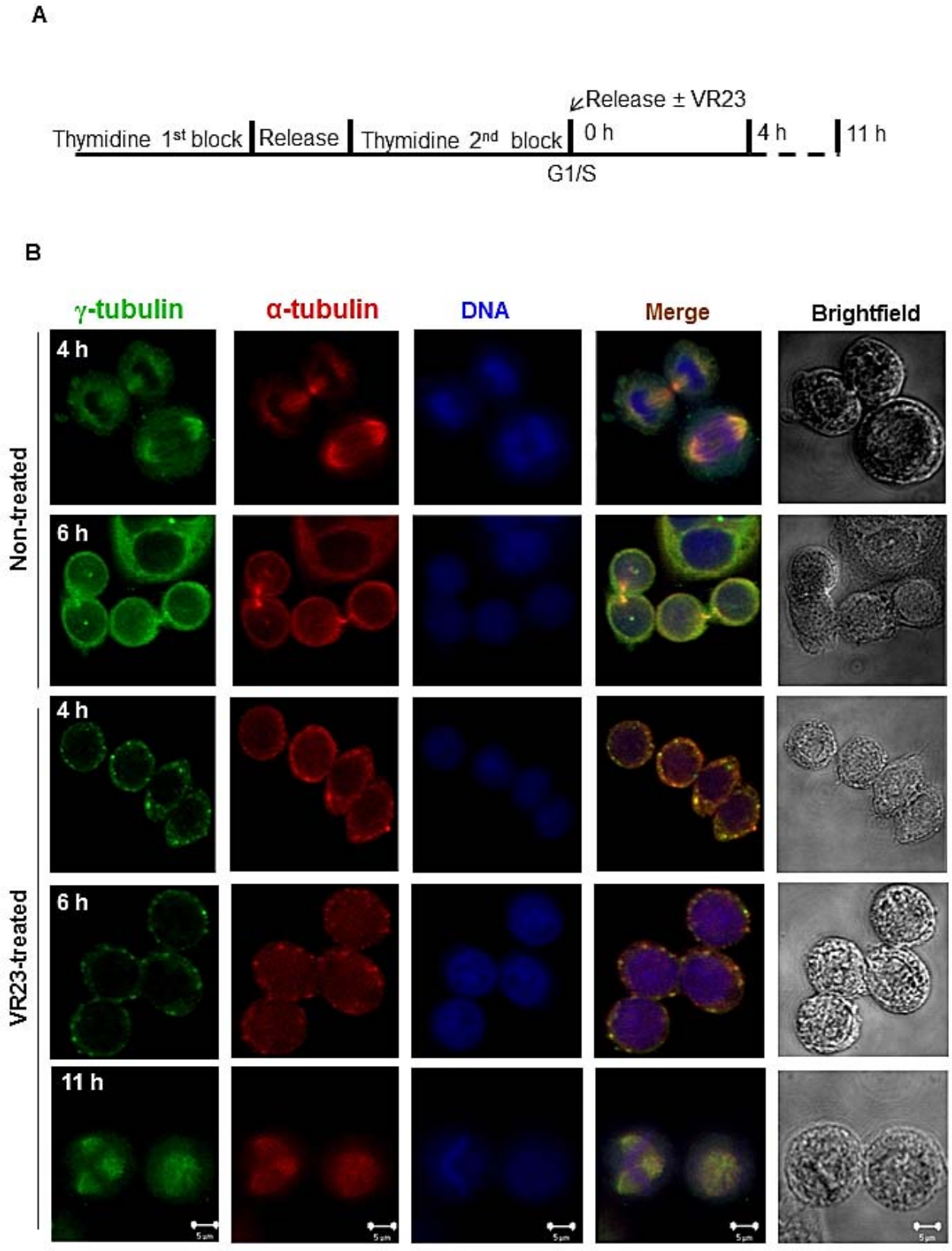
A
Release ± VR23
Thymidine 1st block
Release
Thymidine 2nd block
0 h
4 h
11 h
G1/S
B
γ-tubulin
α-tubulin
DNA
Merge
Brightfield
Non-treated
VR23-treated
4 h
6 h
4 h
6 h
11 h

Figure 10: VR23-treated cells arrest in prophase

A. Mitotic cells were released in the presence or absence of VR23 (5 μM) for 2, 6 and 10 h.

B. Cyclins are not degraded in VR23-treated cells.

Proteins were extracted from samples and subjected to SDS-PAGE. Western blotting was done for specific proteins. As compared to non-treated cells, VR23-treated cells did not degrade cyclin A, B and E. phosphorylated chk2 on T68 was also increased. A significant increase in pp38 (T180 and Y182) was found. Cdc25A S123 levels were reduced in VR23-treated cells. Representative blots are shown. Tubulin is shown as loading control.

C. Inhibition of p38 kinase delays apoptosis in VR23-treated cells.

Mitotic cells were treated with a p38 inhibitor (SB203580, 10 μM) for 6 h. VR23-treated cells underwent apoptosis by 6 h, whereas the inhibition of p38 in VR23-treated cells resulted in cell cycle arrest at M phase at the same timepoint. SB is SB203580.

D. Western blot of proteins extracted from samples shown in **C**. Drugs were added at 0 h in synchronized mitotic cells for 6 h. At the end of 6 h, proteins were extracted, followed by Western blotting for total p38 or pp38 (T180 and Y182). SB is SB203580 (10 μM) and Non is Non-treated.

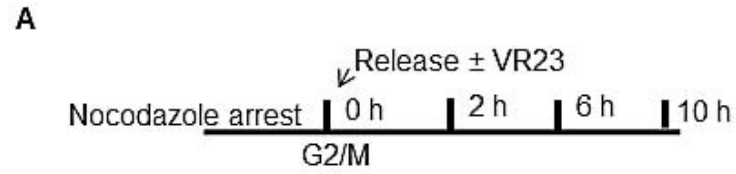
A
Release ± VR23
Nocodazole arrest
0 h
2 h
6 h
10 h
G2/M

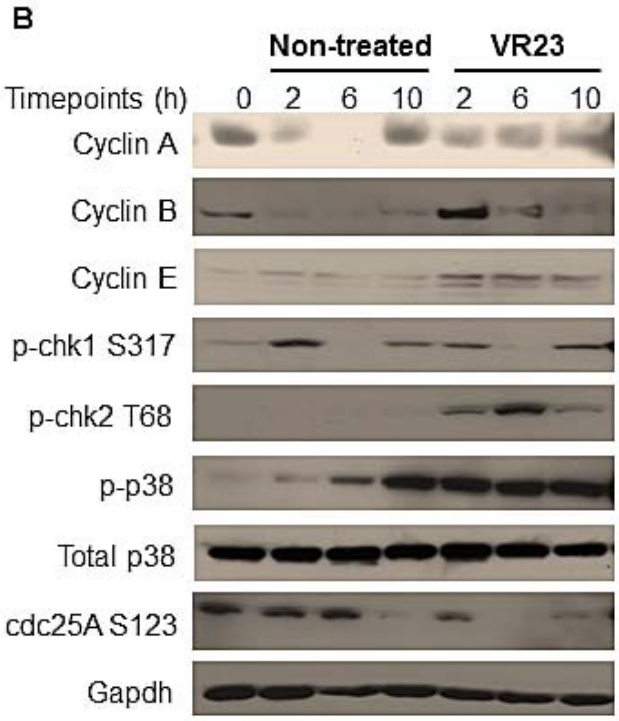
B
Non-treated
VR23
Timepoints (h)
0 2 6 10 2 6 10
Cyclin A
Cyclin B
Cyclin E
p-chk1 S317
p-chk2 T68
p-p38
Total p38
cdc25A S123
Gapdh

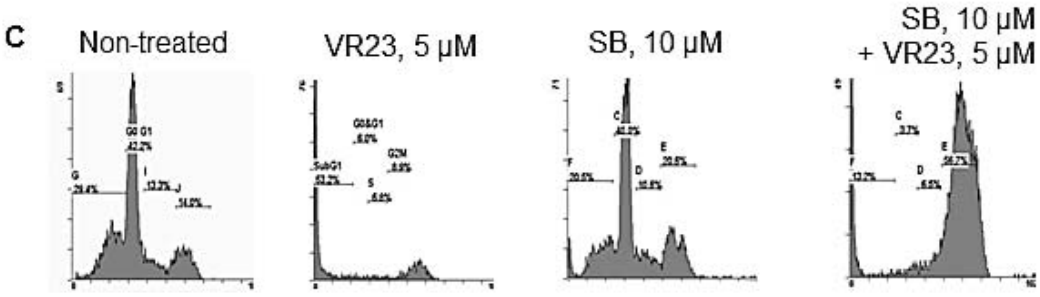
C
Non-treated
VR23, 5 μM
SB, 10 μM
SB, 10 μM
+ VR23, 5 μM

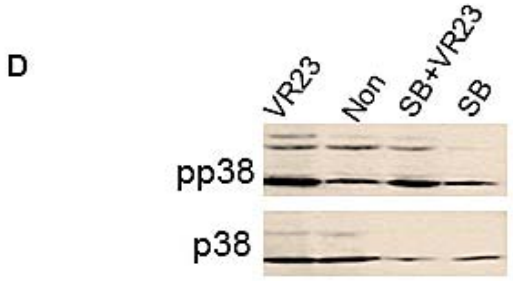
D
VR23
Non
SB+VR23
SB
pp38
p38

3.3 VR23 activates p38 stress kinase at mitosis

Progression through mitosis is driven by cdk1-cyclin B activity, which is below threshold levels during early prophase and reaches a maximum during metaphase (159).

Recently, it has been shown (160) that cells commit to progress forward into the prometaphase when cdk1 activity is the highest, and ablation of cdk1 prevents cells from the passage through prometaphase to metaphase. As non-treated cells progress from prophase to metaphase (0.5 to 2 h), cdk1 phosphorylation on T161 (activating) increases and phosphorylation on Y15 (inhibitory) decreases (Fig. 8). In contrast, in VR23-treated cells, cdk1 remain phosphorylated at the inhibitory phosphorylation (Y15) even at 2-3 h post-release. Cyclin B is not degraded in VR23-treated cells (Figs. 8, 10). It should be noted that presence of non-degradable cyclin B can prevent mitotic exit in cells (62, 63).

Prolonged activation of p38 in mitosis activates apoptosis (161). Mitotic cells exposed to VR23 undergo cell death through the activation of p38 stress kinase (Fig. 10), as indicated by an increase in the protein level of pp38 (phospho-p38). While VR23-treated mitotic cells underwent apoptosis within 4-6 h, pp38 inhibition resulted in prolonged cell cycle arrest in mitosis, although they eventually underwent apoptosis.

One of the well-studied mechanisms for mitotic arrest is the activation of the spindle assembly checkpoint (SAC). At first, an assumption was that VR23 might prevent the degradation of the SAC complex, hence preventing cyclin B degradation leading to prometaphase arrest. However, in the presence of VR23,

Figure 11: APC is not activated in VR23-treated mitotic cells

When cells are released after a G2/M block, APC (anaphase-promoting complex) is not activated as cdc27 (subunit of APC) is not bound to cdc20.
A. Nocodazole-based cell synchronization scheme is shown. Cells arrested in G2/M were released at 0 h in the presence or absence of VR23.
B. Cdc27 was immunoprecipitated at 0.5, 1, 2, and 4 h with anti-cdc27 antibody followed by Western blotting with antibodies specific for proteins indicated. Cdc20 was bound to cdc27 at 1 h post-release in non-treated cells but not in VR23-treated cells. BubR1 is not bound to cdc20 either, suggesting that cells do not activate the spindle assembly checkpoint and remain arrested in prophase. BubR1 was immunoprecipitated followed by Western blotting with anti-cdc20 antibody. Emi1 (early mitotic inhibitor) was bound to APC at the start of mitosis (0 and 0.5 h), but then at later timepoint (1-4 h) it is not bound to cdc20. In contrast, Emi1 in VR23-treated cells is not bound to cdc20 at 0.5 or 1 h.
C. Morphology of cells shown in **B**. Unlike non-treated cells, formation of the metaphase plate was not seen by 1 h in VR23-treated cells.

A

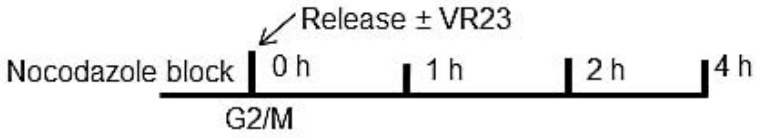
Release ± VR23
Nocodazole block
0 h
1 h
2 h
4 h
G2/M

B

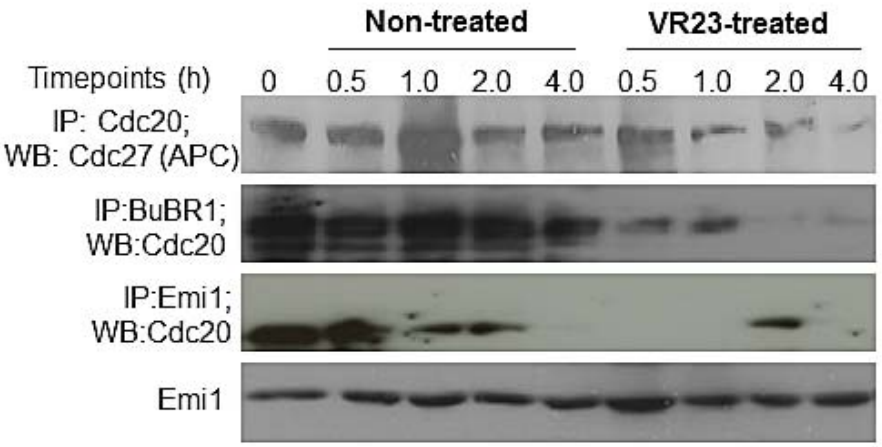
Non-treated
VR23-treated
Timepoints (h)
0
0.5
1.0
2.0
4.0
0.5
1.0
2.0
4.0
IP: Cdc20;
WB: Cdc27 (APC)
IP:BuBR1;
WB:Cdc20
IP:Emi1;
WB:Cdc20
Emi1

C

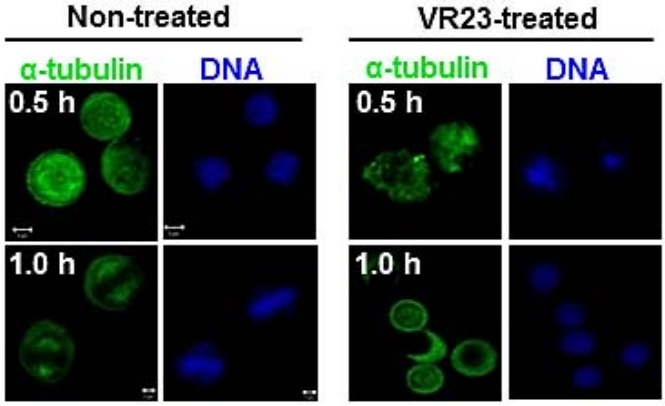
Non-treated
VR23-treated
α-tubulin
DNA
α-tubulin
DNA
0.5 h
0.5 h
1.0 h
1.0 h

Figure 12: Summary of the proteins examined for cells undergoing mitosis in the presence of VR23

Cyclin B is not degraded; APC/cdc20 is not activated; and levels of pp38 were elevated in VR23-treated cells. These results are consistent with notion that cells undergo apoptosis in the presence of VR23. Furthermore, the apoptosis is pp38 mediated, as the inhibition of p38 caused cells to stall at mitosis for an increased duration.

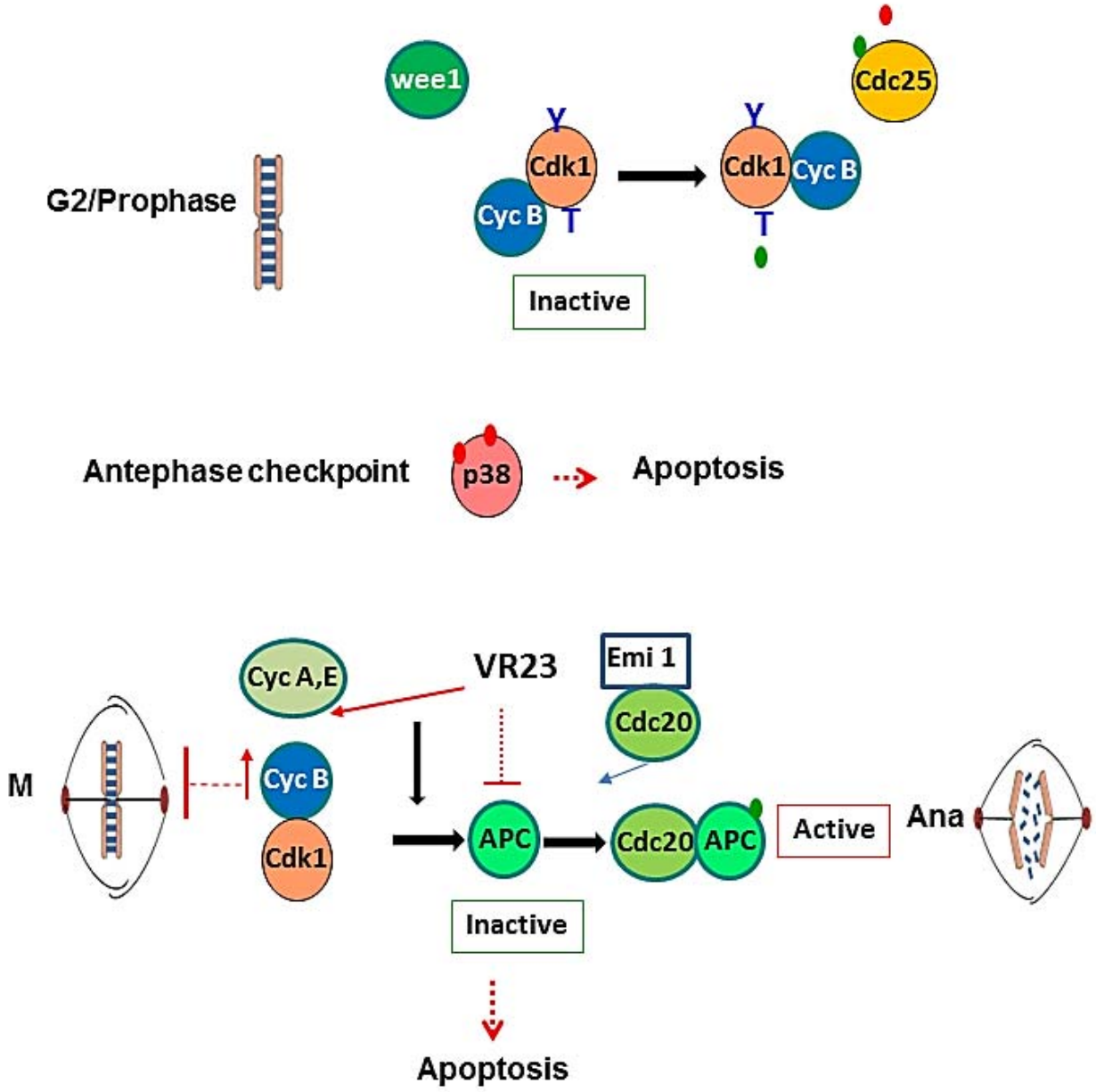
wee1
Cdc25
Y
Cdk1
Cyc B
T
Y
Cdk1
Cyc B
T
G2/Prophase
Inactive
Antephase checkpoint
p38
Apoptosis
Cyc A,E
VR23
Emi 1
Cdc20
M
Cyc B
Cdk1
APC
Cdc20
APC
Active
Ana
Inactive
Apoptosis

the BubR1 complex is not found to be activated (Fig. 11), suggesting that VR23 arrest cells is in prometaphase and cells don't even reach the point of the activation of SAC, further supporting the pp38-mediated activation of apoptosis in prophase.

Cells can be arrested in mitosis due to the activation of checkpoints that inhibits APC (anaphase-promoting complex). I then checked if APC is activated in VR23-treated cells. APC/cdc20 was not found to be active in the presence of VR23 (Fig. 11). This conclusion was further confirmed by the presence of increased levels of cyclins A and B (as shown previously in Fig. 10). Since APC/cdc20 is not active in these cells, this data suggests that cells are not progressing towards anaphase. Emi1 (Early Mitotic Inhibitor) binds to cdc20 and prevents the activation of the APC complex when cells are not ready to progress through the next mitotic stage. In VR23-treated cells, cdc20 was not bound to Emi1 (Fig. 11). Hence, these cells were completely arrested in prophase.

In the presence of VR23, even though chk2 is activated in response to DNA damage it still does not inhibit its downstream target cdc25C (S216) (Fig. A7). chk1-dependent phosphorylation of cdc25A (S123) was also not observed either (as shown previously in Fig. 10). This suggests that VR23-mediated cell cycle arrest is independent of ATM/ATR-dependent DNA damage response.

3.4 Formation of multiple spindle poles in VR23-treated cells

Further study by microscopy showed the presence of abnormal spindles with extra centrosomes in VR23-treated cells (Fig. 13). Cells were arrested by double thymidine block in G1/S, and VR23 was added as they were released into

Figure 13: Cells undergo mitotic catastrophe when treated with VR23

A. Cells synchronized by double thymidine block were released into the cell cycle at 0 h and incubated for 11 h in the presence or absence of VR23 (20 µM).
B. Cells were fixed for staining when they reached mitosis. Cells show multi-polar (**a, b**), tri-polar segregation **(c**) and eventually undergo apoptosis (**d**). Green, red and blue panels show γ-tubulin, α-tubulin and DNA respectively. Representative pictures from three independent experiments are shown.
C. Cells were quantified for each phenotype. Mitotic index in VR23-treated cells was 20%. 27% of mitotic cells showed multi-polar phenotype, 48% of mitotic cells showed tri-polar phenotype, and 5% showed apoptotic phenotype by 11 h post-G1/S arrest.

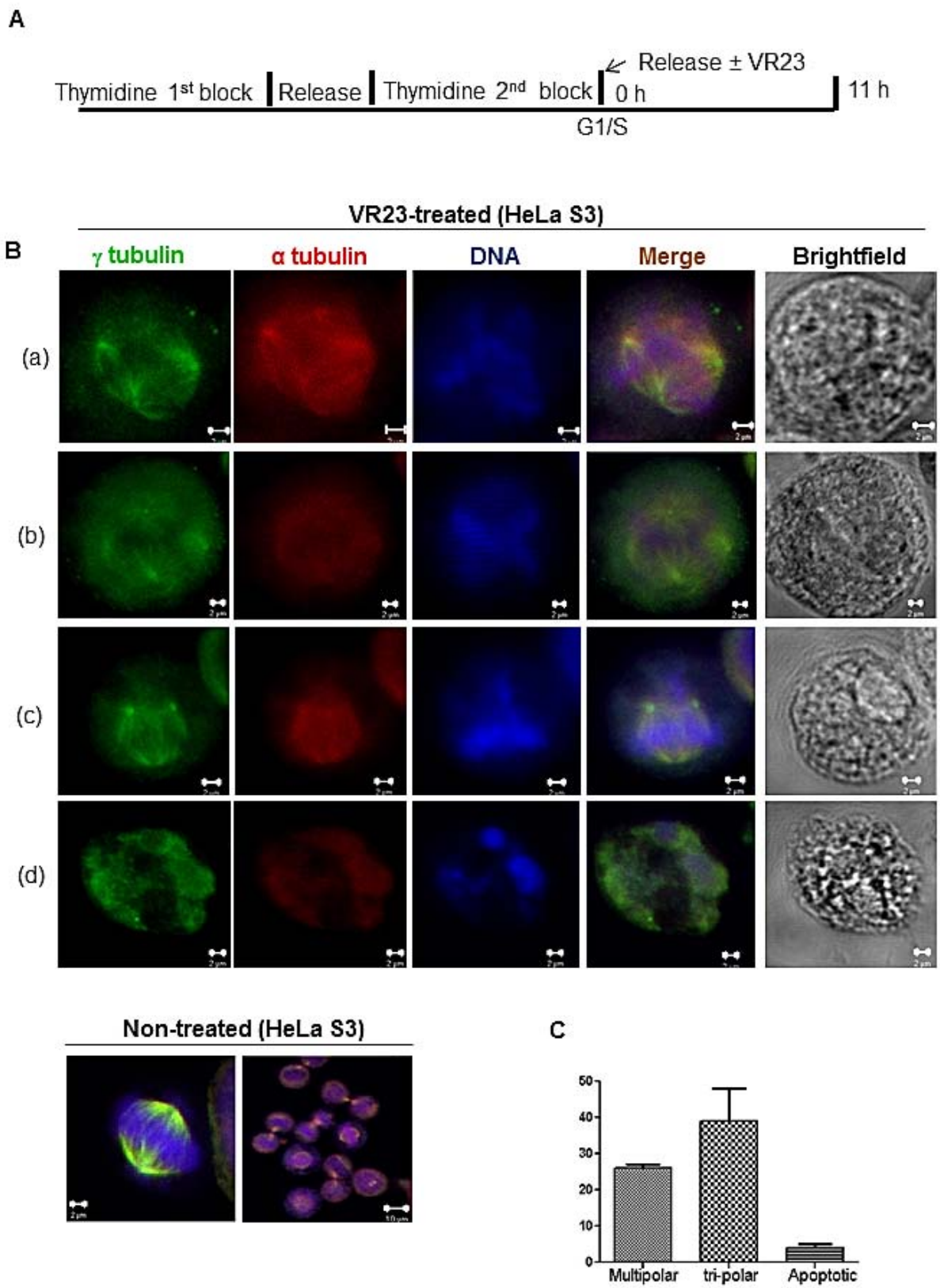
A
Thymidine 1st block
Release
Thymidine 2nd block
Release ± VR23
0 h
11 h
G1/S
B
VR23-treated (HeLa S3)
γ tubulin
α tubulin
DNA
Merge
Brightfield
(a)
(b)
(c)
(d)
Non-treated (HeLa S3)
C
50
40
30
20
10
0
Multipolar
tri-polar
Apoptotic

complete medium (time 0 h). Cells were then fixed at 11 h post-release (Fig. 13) because VR23-treated cells take longer to reach mitosis as discussed previously in Fig. 9. In non-treated cells, all of the mitotic phases appeared normal with bipolar spindle formation. In contrast various spindle abnormalities and chromosome missegregation were observed in VR23-treated cells. Among 55.5% of total cells in mitosis 44.4% out of the 55.5% showed multiple spindle abnormalities in VR23 treated cells. Uni- (10%), tri- (48%), and multi- (12%) polar spindles were quantified (Fig. 13). The cells with aberrant multiple spindles eventually underwent mitotic catastrophe.

Alternatively, cells were synchronized by double thymidine block and released into fresh medium for 6 h, at which point the majority of the cells reached G2/M (Fig. 14). VR23 was added to mitotic cells and cell cycle progression was examined by flow cytometry and microscopy. In VR23-treated cells, 52% of cells remain arrested in G2/M (Fig. 14), and 78% of them showed abnormal spindles. Cell were synchronized by double thymidine block instead of nocodazole block because double thymidine block was less toxic to cells and, unlike nocodazole, had no effect on the tubulin of cells.

3.5 VR23 inhibits proteasome activity

Previously, three observations were made with VR23: (a) cyclins were not degraded in the presence of VR23, and there is a delay in cell cycle progression; (b) an irreversible mitotic arrest which could not be rescued by using cdc25C, wee1 or cdk1 inhibitor (Fig. A8); and (c) multiple spindle poles were formed. It is known

Figure 14: Multiple spindles observed in VR23-treated cells after G1/S synchronization

VR23-treated cells form aberrant spindles and undergo mitotic catastrophe.
The synchronization scheme is shown. Asynchronous population of HeLa S3 cells (**a**) were synchronized by double thymidine block (**b**), and released into the cell cycle for 6 h (**c**). At the end of 6 h when cells reached G2/M phase, VR23 was added and cells were exposed for another 6 h. Hence, the total duration would be 12 h (**d**), of which exposing to VR23 is 6 h (**e**). Cells were immunostained with antibodies specific for α-tubulin (green) DNA was stained with DRAQ5 (blue). Panels (**f** and **g**) show DNA segregation defects in VR23 treated cells. Mitotic cells were examined from at least 20 different fields. Out of 38% of total mitotic cells, 78% showed spindle abnormalities. Due to DNA missegregation, these cells undergo mitotic catastrophe in anaphase. Representative pictures from three independent experiments are shown.

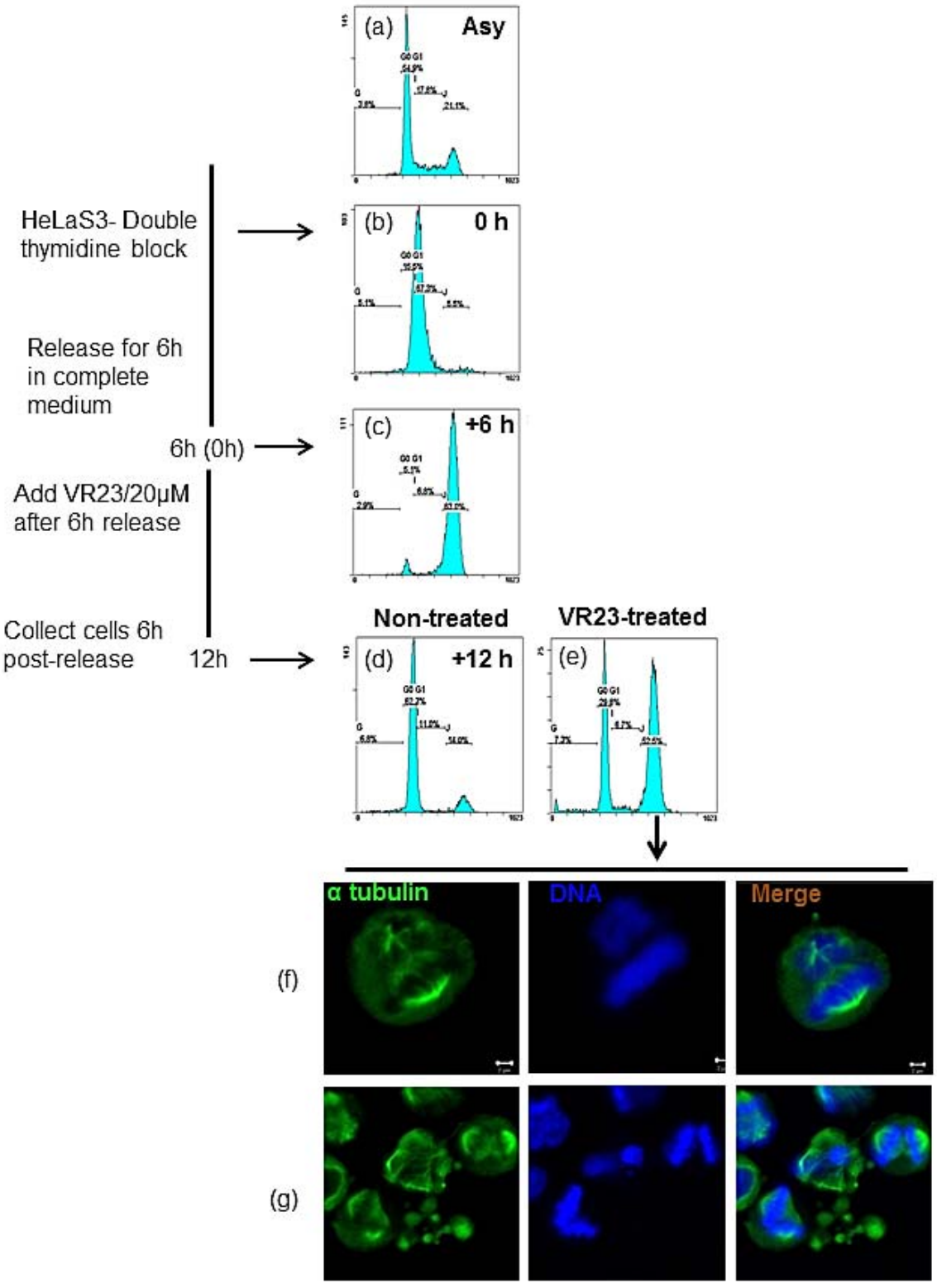
(a) Asy
HeLaS3- Double thymidine block
(b) 0 h
Release for 6h in complete medium
6h (0h)
(c) +6 h
Add VR23/20μM after 6h release
Collect cells 6h post-release
12h
Non-treated
VR23-treated
(d) +12 h
(e)
α tubulin
DNA
Merge
(f)
(g)

that the inhibition of proteasomes causes irreversible mitotic arrest and proteasome activity is required for maintaining spindle pole integrity (40, 62, 146). Therefore, I looked into the proteasome activity in the presence of VR23 because protein degradation is essential for properly regulating the cell cycle progression.

The ability of VR23 to inhibit proteolysis in proteasomes was determined with fluorogenic peptides as substrates using the proteasomes extracted from VR23-treated and non-treated cells. Hydrolysis of the fluorogenic substrate SUC-LLVY-AMC was measured in VR23-treated samples in a time and dose-dependent manner. The chymotrypsin-like activity was measured every 5 min. The activity started to decrease by 10 min incubation with fluorogenic substrate and remain inhibited until 30 min (the last timepoint in the experiment). Inhibition of the activity of each of the subunit (β1, β2, and β5) was then measured at a fixed timepoint (30 min reactions) at different doses of the drug (Fig. 15). The strongest inhibition was observed for trypsin-like activity (1 nM), with somewhat less inhibition for chymotrypsin-like activity (50-100 nM) in HeLa S3, MCF7 and MDA-MB231 cell lines (Table 4). Caspase-like (peptidylglutamyl peptidase) activity was the most resistant to inhibition as the IC_{50} of VR23 is 3 µM in HeLa S3 and 5 µM in MDA-MB231. The inhibition of proteasome activity by CQ was much weaker than VR23 (Table 4). The activity of VR23 was compared with different concentrations of bortezomib®. VR23 showed enhanced inhibition of trypsin-like activity when compared with bortezomib®.

When different concentrations of substrate (25, 50 and 100 µM) were used to measure trypsin-like activity on non-treated samples, a concentration dependent increase in fluorescence was seen (Fig. A9). Substrate conc. 25 µM of was used to

measure the trypsin-like activity with different concentrations of VR23. The trypsin-like activity was also measured after 50 min of incubation with substrate, instead of 30 min. After 50 min incubation, the decrease in relative fluorescence was similar to that observed at 30 min.

Since proteasome inhibition leads to the accumulation of ubiquitinated proteins, I examined the ubiquitination status of proteins. Ubiquitinated proteins were pulled down using TUBEs (Tandem ubiquitin binding entities). Subsequent blotting with an anti-ubiquitin antibody showed that ubiquitinated proteins were accumulated in a dose-dependent manner in the presence of VR23 (Fig. 16).

3.6 Inhibition of proteasome activity *in vitro*

Inhibition of proteasome activity was measured *in vitro* using purified human 20S proteasome catalytic subunit. VR23 inhibits the chymotrypsin-like activity noncompetitively. For trypsin-like activity, it gives a plot for mixed inhibition (Fig. 17), suggesting that it binds directly to the catalytically active β2 subunits as well as to an outside of the substrate binding site. VR23 caused the inhibition of trypsin-like activity better than bortezomib® (Fig. 15). This indicates that VR23 binds to a subunit or a binding site in trypsin-like (β2) site more effectively.

3.7 Molecular modelling of VR23 to the active sites of the β2 subunit

A molecular docking experiment was performed on all of the β subunits to identify potential interactions between β subunits and VR23. The crystal structure of proteasomes 2F16 and 1IRU obtained from protein data bank were used for the docking study (158, 162). The crystal structure of proteasomes (PDB: 2F16 and

Figure 15: Inhibition of trypsin-like, chymotrypsin-like and caspase-like activities by VR23 in HeLa S3 cells

Release of fluorescence (AMC) was measured using a spectrofluorometer using an excitation at 360 nm and an emission at 480 nm. Proteasome activity was evaluated in relative fluorescence unit (RFU). The trypsin (**a**), chymotrypsin (**b**), and caspase-like (**c**) activities were determined by the measurement of fluorescence generated by the cleavage of the fluorogenic substrate LRR-AMC, SUC-LLVY-AMC, and LLE-AMC, respectively. The hydrolysis reaction was allowed to proceed for 30 min at 37°C. Relative proteasome activity represented the percentage of fluorescence compared with the non-treated control. The graphs were plotted in GraphPad prism V.

(a)

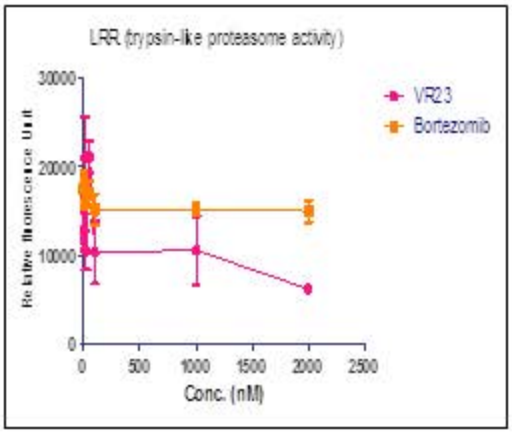
LRR (trypsin-like proteasome activity)
Relative fluorescence Unit
30000
20000
10000
0
0
500
1000
1500
2000
2500
Conc. (nM)
VR23
Bortezomib

(b)

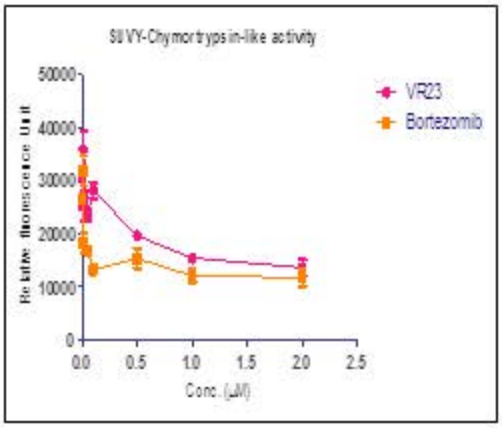
SUVY-Chymotrypsin-like activity
Relative fluorescence Unit
50000
40000
30000
20000
10000
0
0.0
0.5
1.0
1.5
2.0
2.5
Conc. (uM)
VR23
Bortezomib

(c)

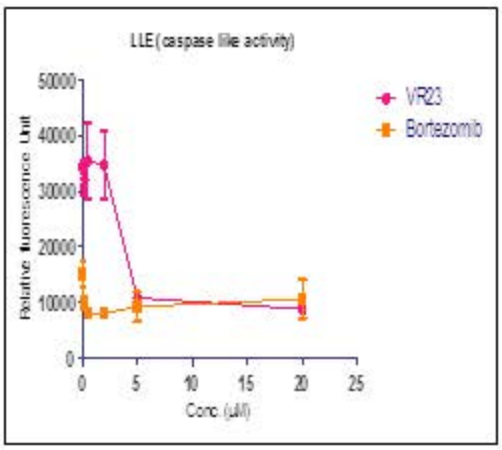
LLE (caspase like activity)
Relative fluorescence Unit
50000
40000
30000
20000
10000
0
0
5
10
15
20
25
Conc. (uM)
VR23
Bortezomib

Table 4: IC_{50} of VR23 for trypsin-like, chymotrypsin-like and caspase-like activities

IC_{50} was determined by the nonlinear regression analysis of the dose-response curve using GraphPad prism V. Relative fluorescence unit (measurement of activity) was plotted against the different concentrations of VR23.

VR23	HeLa	MCF7	MDA-MB231
Trypsin-like	1 nM	1 nM	1 nM
Chymotrypsin-like	100 nM	50 nM	50 nM
Caspase-like	3μM	>5 μM	~5μM

Figure 16: Accumulation of ubiquitinated proteins in VR23-treated cells

A. VR23-treated asynchronous HeLa S3 cells showed accumulation of ubiquitinated proteins. Ubiquitinated proteins were immunoprecipitated with TUBEs subsequently blotted with an anti-ubiquitin antibody. (**i**) Non-treated, (**ii**) MG132 (20 µM), and (**iii**) VR23 (20 µM). Input is total protein loaded (Gapdh).
B. Accumulation of ubiquitinated cyclin E in VR23-treated asynchronous HeLa S3 cells. Cyclin E was pulled down with an anti-cyclin E antibody, followed by Western blotting with an anti-ubiquitin antibody. (**i**) Non-treated, (**ii**) VR23 (20 µM), and (**iii**) bortezomib® (20 nM). Input is total protein loaded (cyclin E).
C. MCF10A cells were treated similarly as HeLa S3 cells. In contrast to HeLa S3 cells, the accumulation of ubiquitinated cyclin E was not observed in VR23-treated MCF10A cells. (**i**) Non-treated, (**ii**) VR23 (20 µM), (**iii**) VR23 (40 µM), (**iv**) bortezomib® (5 µM), and (**v**) MG132 (20 µM).

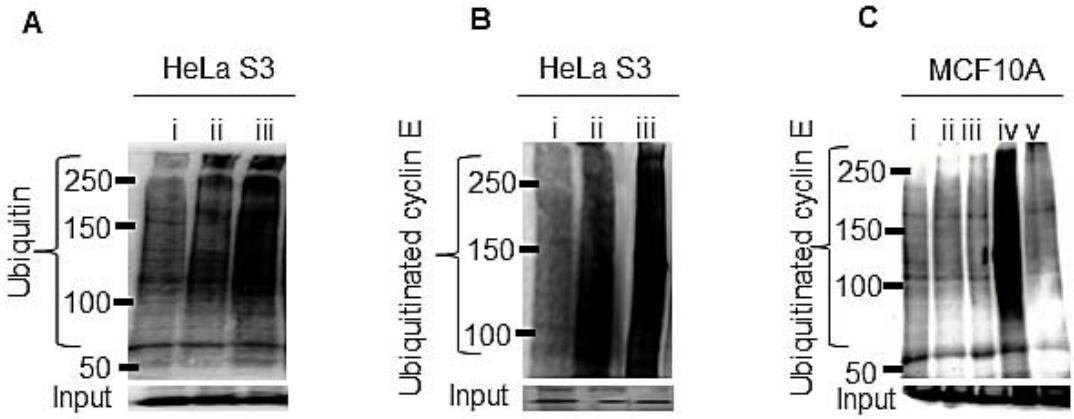
A
HeLa S3
i ii iii
Ubiquitin
250
150
100
50
Input
B
HeLa S3
i ii iii
Ubiquitinated cyclin E
250
150
100
Input
C
MCF10A
i ii iii iv v
Ubiquitinated cyclin E
250
150
100
50
Input

Figure 17: Inhibition of proteasome activity *in vitro*

This figure shows a Lineweaver-Burk plot for trypsin-like activity (mixed inhibition) (**a**) and noncompetitive inhibition for chymotrypsin-like activity (**b**). Purified human 20S proteasomes (Boston Biochem, MA) were incubated with 1 µM VR23. All samples were preincubated for 45 min at 37°C with assay buffer prior to the addition of different concentration of substrates (0-200 µM). Hydrolysis of substrates corresponding to trypsin-like and chymotrypsin-like activity was measured as relative fluorescent units after 1 h (for trypsin-like) and 30 min (for chymotrypsin-like) using a fluorescent spectrophotometer at 380 nm excitation and 480 nm emission. The plot was generated using GraphPad Prism V.

(a)

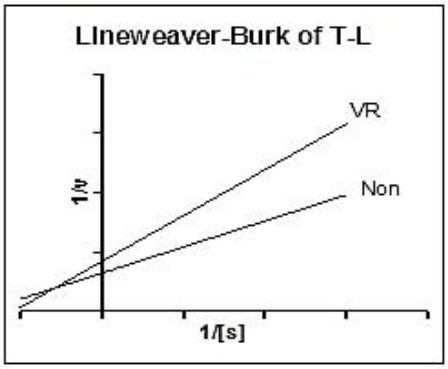
LIneweaver-Burk of T-L
VR
Non
1/v
1/[s]

(b)

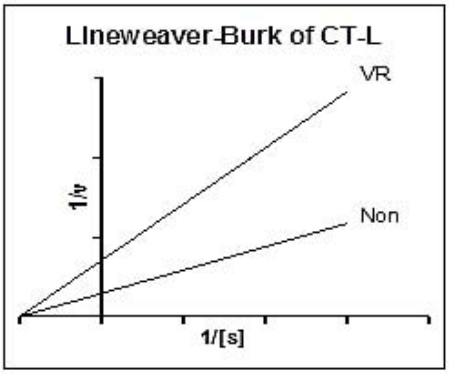
LIneweaver-Burk of CT-L
VR
Non
1/v
1/[s]

PDB: 1IRU) was first docked with bortezomib® to test the credibility of the procedure in MOE software. In order to validate the docking studies, the ligand of bortezomib® was removed from the 20S proteasome (PDB: 2F16) and bortezomib® was redocked within the catalytic subunits using MOE software. The binding mode of bortezomib® and inter-molecular interaction energies within the β1, β2 and β5 subunits were evaluated. This is consistent with the previous report on the interaction between bortezomib® and 20S proteasome (158).

Upon successfully reproducing the bortezomib interactions within the cavity of 20S proteasome, VR23 was then docked in the bortezomib pockets. The interactions with the lowest docking energy (S-score) and RMSD (root mean square deviation) values were selected. The docking results revealed that VR23 binds to the active site of the β2 subunit (PDB: 2F16.H and F216.V).The free energy for docking (final score to indicate binding free energy) was in the range of -5.6 to -6.5 kcal/mol and the lowest RMSD values were 0.6715 and 0.9363 Å in the F216, H (2F16, H-chain- β2 subunit) and 0.0035 Å in F216, V (2F16, V chain- β2 subunit), respectively (Figs. 18, 19). The data suggests that the sulfone group of VR23 forms hydrogen bond interactions with the threonine 1 and threonine 21. The average bond interaction between the sulfone group and threonine 21 group is predicted to be less than 3.2 Å, suggesting that it is the most stable interaction. The CQ moiety of VR23 mostly interacted with the lysine 33 group (pi-H) of the β2 subunit (Figs. 18, 19). The chlorine group in the CQ moiety showed hydrogen bonding with isoleucine 119 from the neighbouring subunit (β3). Besides the threonine 1 cluster, the glycine 47 cluster has also been shown to play a key role in

Figure 18: Interactions between VR23 and the β2 subunit of 20S proteasome

A and **B**. (**a**) Molecular modelling of VR23 (green molecule) with the β2 subunit (PDB: 2F16.H). The ligand is shown as a stick and a protein surface is displayed as a ribbon. (**b**) Ligand interactions between receptor (proteosome) and ligand (VR23) shown in (**a**). The hydrogen bonds formed are indicated by arrows. Hydrogen bonds formed between VR23 and the receptor via threonine 1, threonine 21, arginine 19, histidine 35. The arene group of CQ is forming pi-bonds (noncovalent binding) with lysine 33 (cation-pi interactions) RMSD values are in Å and S-scores are in kcal/mol. (**c**) Summary of ligand interactions, the average distance between the interacting sites, and type of bonds formed by VR23 in the pocket shown in (**a**).

Ligand interaction color scheme: hydrophobic residues are all colored with a green interior, whereas polar residues are colored in light purple. Basic residues are further annotated by a blue interior ring, and acidic residues with a red ring. Water molecules are drawn without interior color, and metals are colored grey. Hydrogen bonding interactions between the receptor and the ligand are drawn with an arrowhead to denote the direction of the hydrogen bond (i.e. the donor is at the base of the arrow and the acceptor is at the head). In cases where there could be a hydrogen bond in either direction, the arrow is two-headed. When the hydrogen bond is formed with the residue's side-chain, the arrow is drawn in green. Hydrogen bonds to the residue's backbone are drawn in blue, with an additional dot drawn at the residue attachment point.

A

(a)

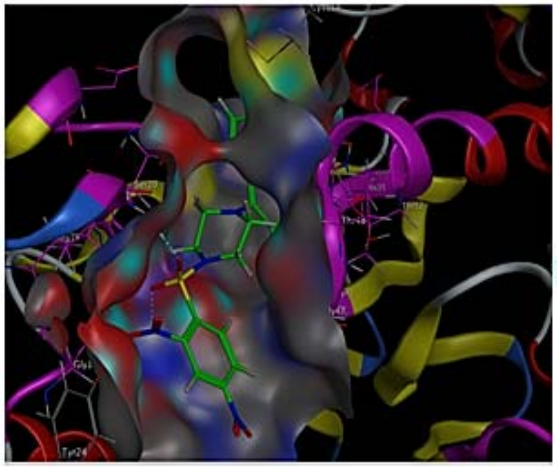

RMSD: 0.6715
S-score: -5.6288

(b)

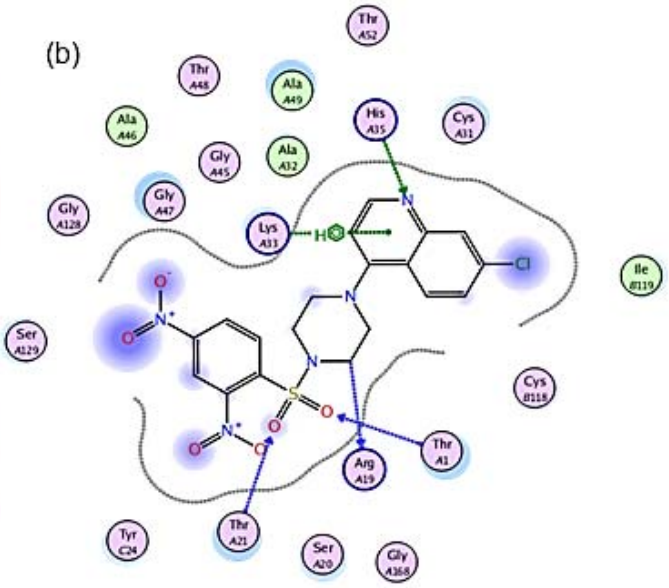

(c)

Ligand	Receptor			Interaction	Distance	E (kcal/mol)
C 18	O	ARG 19	(H)	H-donor	3.09	-1.3
N 16	NE2	HIS 35	(H)	H-acceptor	3.48	-1.3
O 32	N	THR 21	(H)	H-acceptor	3.32	-1.5
O 33	N	THR 1	(H)	H-acceptor	3.73	-0.5
6-ring	CG	LYS 33	(H)	pi-H	3.88	-0.9

B

(a)

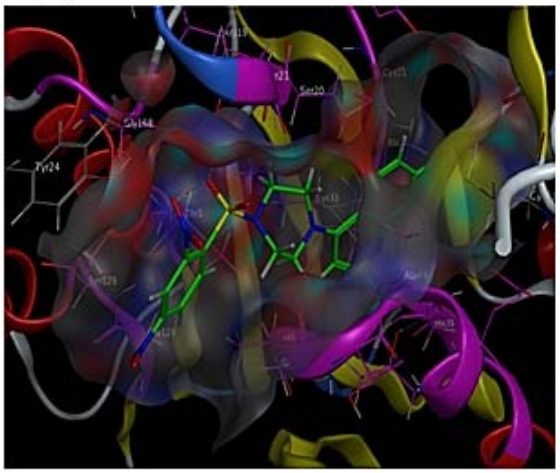

RMSD: 0.9363
S-score: -5.0766

(b)

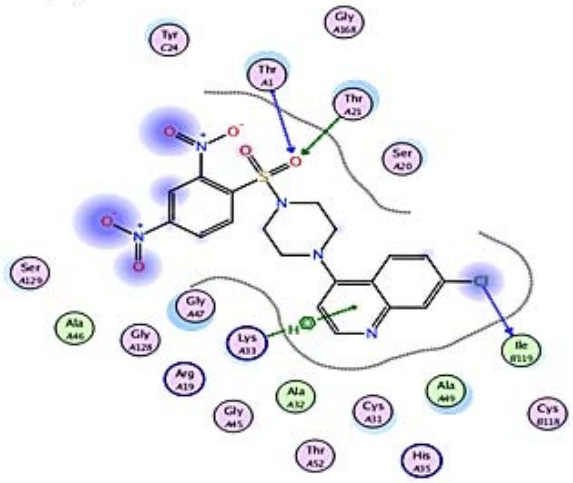

(c)

Ligand	Receptor			Interaction	Distance	E (kcal/mol)
Cl 6	O	ILE 119	(I)	H-donor	3.28	-1.0
O 33	N	THR 1	(H)	H-acceptor	3.71	-0.6
O 33	OG1	THR 21	(H)	H-acceptor	3.00	-0.9
6-ring	CG	LYS 33	(H)	pi-H	3.74	-1.1

Figure 19: Interactions between VR23 and the β2 subunit of 20S proteasome

A and **B**. (**a**) Molecular modelling of VR23 (green molecule) with the β2 subunit (PDB: 2F16.V). (**b**) Ligand interactions between receptor (proteosome) and ligand (VR23) in the F216, V shown in (**a**). The hydrogen bonds formed are shown as arrows. The hydrogen bonds formed between VR23 and the receptor via threonine 21. The arene group of chloroquine is forming pi-bonds (noncovalent binding) with lysine 33 (cation-pi interactions) and alanine 49. Glycine 47 forms hydrogen bond with the C group. RMSD scores are in Å, and S-score are in kcal/mol. (**c**) Summary of ligand interactions, the average distance between the interacting sites, and type of bonds formed by VR23 in the pocket shown in (**a**).

A

(a)

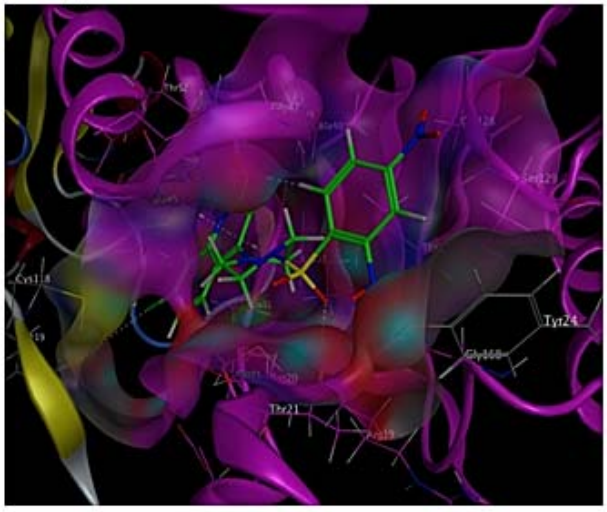

(b)

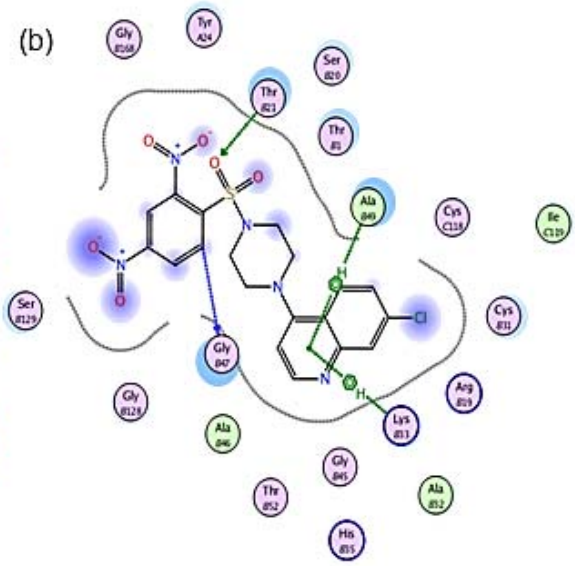

RMSD: 0.0035
S-score: -5.5983

(c)

Ligand		Receptor				Interaction	Distance	E (kcal
C	37	O	GLY	47	(V)	H-donor	3.51	-0.8
O	33	OG1	THR	21	(V)	H-acceptor	2.79	-1.6
6-ring		CG	LYS	33	(V)	pi-H	3.96	-1.0
6-ring		CA	ALA	49	(V)	pi-H	3.72	-0.6

B

(a)

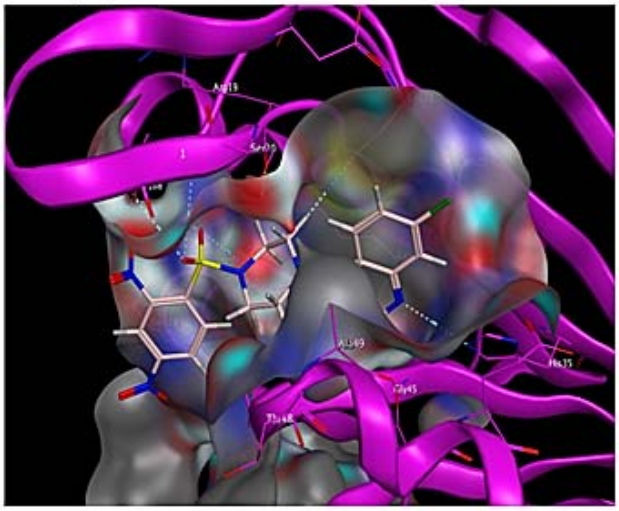

(b)

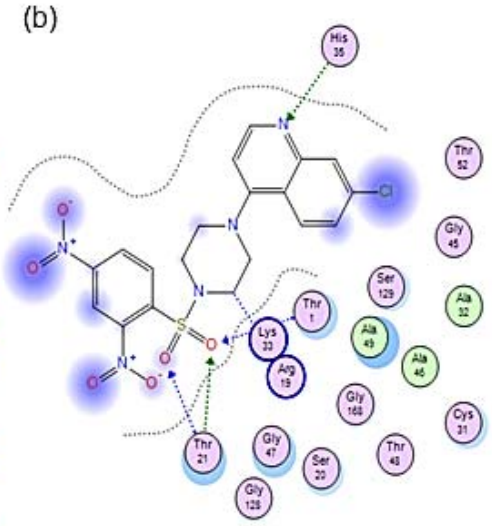

RMSD: 1.1441
S-score: -5.0735

(c)

Ligand		Receptor				Interaction	Distance	E (kcal/mol)
C	18	O	ARG	19	(H)	H-donor	3.09	-1.3
N	16	NE2	HIS	35	(H)	H-acceptor	3.48	-0.9
O	32	N	THR	21	(H)	H-acceptor	3.32	-2.0
O	32	OG1	THR	21	(H)	H-acceptor	2.96	-1.9
O	33	N	THR	1	(H)	H-acceptor	3.73	-3.2
O	33	OG1	THR	1	(H)	H-acceptor	3.21	-1.4
O	33	OG1	THR	21	(H)	H-acceptor	3.44	-0.7

proteolysis (163). VR23 also showed potential hydrogen bond interactions with glycine 47. Some other important interactions in the active site of β2 subunit include the interactions with alanine 49 (pi-H), arginine 45 (H-bond) and histidine 35 (H-bond).

The best fit conformation (pose) was examined manifold to check if there are any other poses with good scores that are also part of pose families (i.e., groups of poses with only minor variations in conformational structure). This further confirmed if the "best fit" pose is "realistic". In MOE software docking, an 'S score' is calculated by considering Van der Waals interaction energy, electrostatic energy (taking place between the ligand and the protein and the solvation energy) and the ligand energy in the complex. VR23 did not show strong interactions/poses with the β1 or β5 subunit (Fig. A10). This docking data further supports the previous *in vitro* data that VR23 very efficiently inhibits trypsin-like proteasome activity but somewhat less efficiently inhibits chymotrypsin-like and not very effectively caspase-like proteasome activity. Even though some interactions may occur between VR23 and β5 subunits (PDB: 2F16. K and Y) (Fig. A10).

3.8 Formation of multiple centrosomes in response to VR23

VR23 induced the formation of multiple spindles in asynchronous HeLa S3 and MCF7 cells (Figs. 9 and 13). To further study the cause of these multiple spindles, asynchronous cells were immunostained with an antibody specific for γ-tubulin, a centrosome marker (164). 20% of asynchronous HeLa S3 and 12% of asynchronous MCF7 cells had >4 centrosomes per cell (Fig. A11).

Figure 20: Cells form multiple centrosomes within 3 h post-G1/S arrest

A. HeLa S3 cells synchronized by double thymidine block were released at time 0 h into complete medium (non-treated) or in the presence of VR23 (20 µM) for 3, 6, 12 and 24 h.
B. Cells were fixed at the end of each timepoint and immunostained with an antibody specific for γ-tubulin (green). DNA was stained with DRAQ5 (blue). Multiple centrosomes were observed at 3 (**b**) and 6 h (**d**) post-G1/S block in VR23-treated cells. Results shown are representative of three independent experiments.
C. Cells with multiple centrosomes were quantified for each timepoint (3 to 24 h) in VR23-treated (20 µM) *vs* non-treated cells. The experiment was repeated three times. An average of twenty different fields/per coverslip/per trial was counted under a confocal microscope.

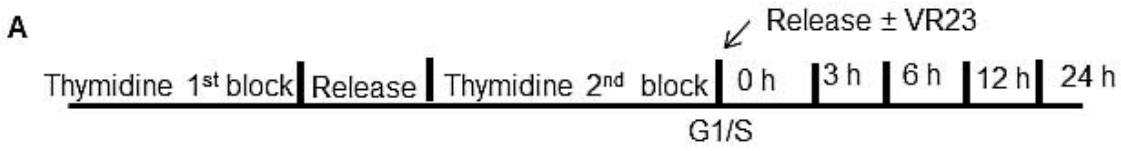
A
Release ± VR23
Thymidine 1st block
Release
Thymidine 2nd block
0 h
3 h
6 h
12 h
24 h
G1/S

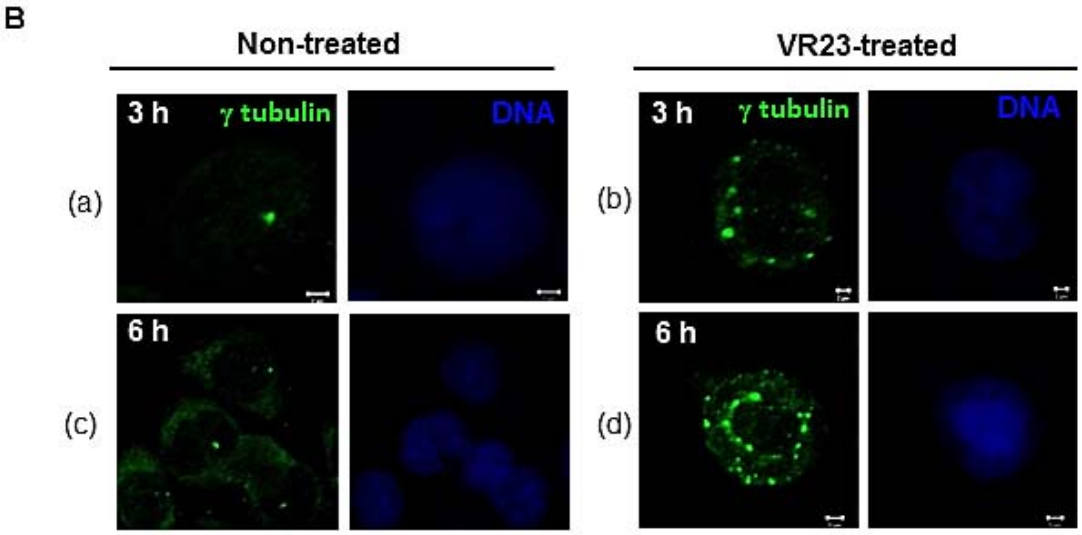
B
Non-treated
VR23-treated
3 h
γ tubulin
DNA
(a)
(b)
6 h
(c)
(d)

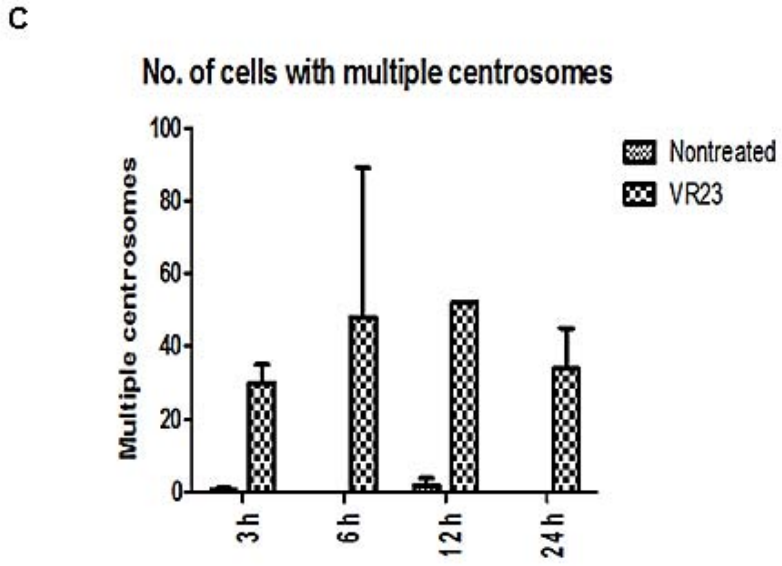
C
No. of cells with multiple centrosomes
Multiple centrosomes
100
80
60
40
20
0
3 h
6 h
12 h
24 h
Nontreated
VR23

To further study how VR23 induces multiple centrosomes, centrosome formation was examined with cells synchronized in G1/S. Since HeLa S3 cells are synchronized very efficiently, they were used for synchronization experiments. In VR23-treated cells synchronized with double thymidine, multiple foci of γ-tubulin, ranging from 5-15 per cell, were observed as early as 3 h post-release in 45-80% of HeLa S3 cells (Fig. 21).

γ-tubulin is also present in PCM (pericentriolar material). Therefore, to determine if these are "true" centrosomes and not fragmentation of either centrosomes or PCM, cells were immunostained with an antibody specific for centriolin as it is localized to mature centrosomes in human cells (165). Centriolin was found to be co-localized with γ-tubulin in VR23-treated cells, showing that these are true and mature centrosomes (Fig. 21).

It was shown previously that Mps1 and hSAS6 can induce the formation of multiple centrosomes. I therefore examined if VR23-induced centrosome amplification is accompanied with an increase in Mps1 or hSAS6. In G1/S synchronized non-treated cells, there was a decrease in Mps1 and hSAS-6 from 3 to 6 h, which correlates with the initiation of centrosome duplication (Fig. 22). The down-regulation of these two proteins also prevents subsequent re-duplication. In contrast, a reverse pattern was observed in VR23-treated cells, in which MpS1 and hSAS-6 levels increased from 3 to 6 h, suggesting a continuous initiation of centrosome synthesis.

The size of the centrosomes in VR23-treated cells was also bigger than those in non-treated cells (Fig. 21). This raises the possibility that other

Figure 21: Centriolin, a mature centrosome marker, and cyclin E are co-localized to centrosomes in VR23-treated cells

HeLa S3 cells synchronized at G1/S were released into cell cycle for 3 h by incubating them in complete medium ± VR23. Cells were fixed and immunostained with antibodies specific for proteins indicated at 3 h post release.
A. Cells were immunostained with antibodies specific for γ-tubulin (green), and centriolin (red), respectively. DNA was stained with DRAQ5 (blue). Unlike non-treated cells, multiple centrosomes were observed in VR23-treated (20 μM) cells and centriolin was co-localized with γ-tubulin.
B. Cyclin E (red) was co-localized with γ-tubulin (green) in VR23-treated cells.
C. Cells were immunostained with antibodies specific for centriolin (green), and cyclin E (red), respectively. DNA was stained with DRAQ5 (blue). Centriolin was co-localized with cyclin E to the centrosomes in VR23-treated cells. The experiment was performed three times, and representative figures are shown. Images were captured in an LSM510 microscope equipped with 488 nm, 546 nm and 633 nm lasers.

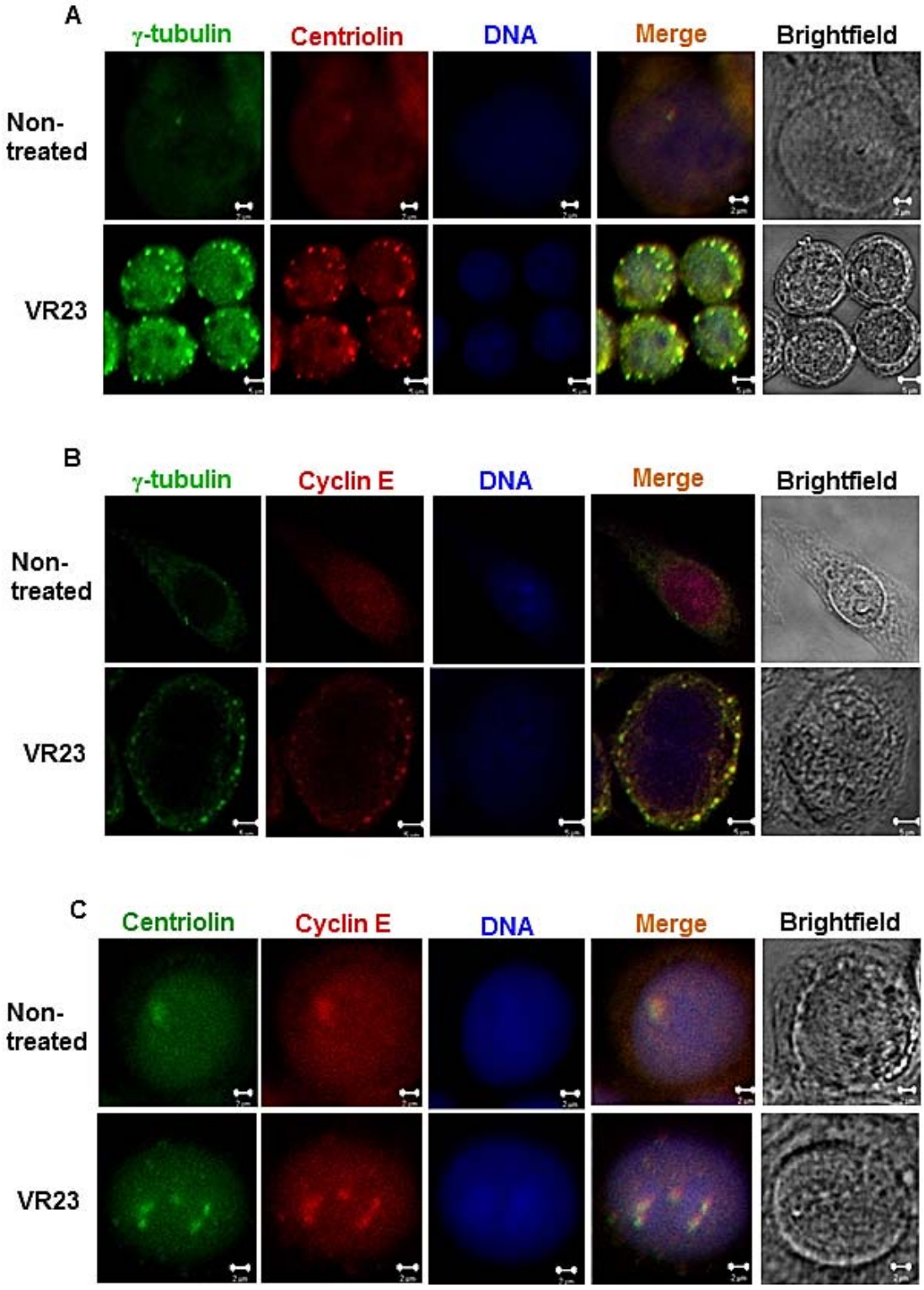
A
γ-tubulin
Centriolin
DNA
Merge
Brightfield
Non-treated
VR23
B
γ-tubulin
Cyclin E
DNA
Merge
Brightfield
Non-treated
VR23
C
Centriolin
Cyclin E
DNA
Merge
Brightfield
Non-treated
VR23

Figure 22: Increase in the levels of centrosomal proteins in VR23-treated cells

A. HeLa S3 cells synchronized by double thymidine block at G1/S were released into the cell cycle ± VR23 (20 μM). Proteins were extracted from non-treated and VR23-treated samples at the indicated timepoints.
B. Mps1 and hSas6 protein levels decrease in non-treated cells as cells progress from G1/S to G2/M (3 to 6 h), these protein levels increase in VR23-treated cells (3 to 6 h). Representative blots are shown (B). Gapdh is shown as loading control. Non is non-treated.

A

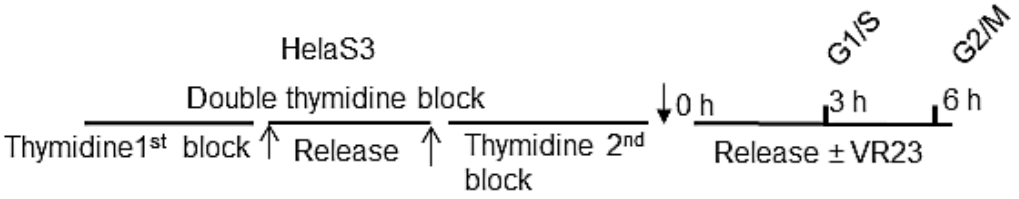
HelaS3
Double thymidine block
Thymidine1st block
Release
Thymidine 2nd block
0 h
Release ± VR23
G1/S
3 h
G2/M
6 h

B

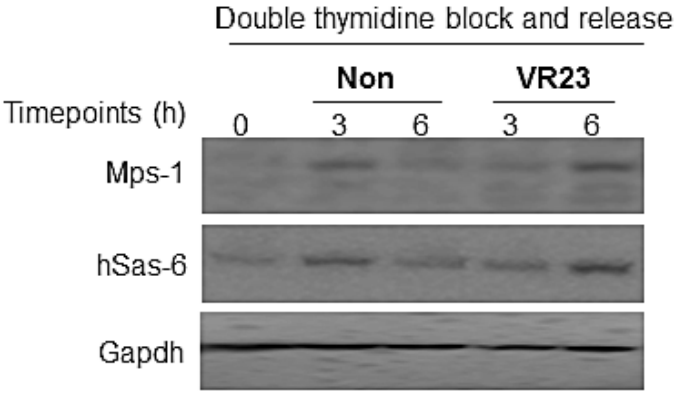
Double thymidine block and release
Non
VR23
Timepoints (h)
0
3
6
3
6
Mps-1
hSas-6
Gapdh

Figure 23: Plk1, cyclin A and hSAS6 accumulate at the centrosomes in VR23-treated cells

HeLa S3 cells synchronized in G1/S were released into the cell cycle for 3 h by adding complete medium ± VR23. At the end of 3 h, cells were fixed and immunostained with antibodies specific for proteins indicated.

A. Cells immunostained with antibodies specific for γ-tubulin (green) and plk1 (red) are shown. DNA was stained with DRAQ5 (blue). Unlike non-treated cells, multiple centrosomes were observed in VR23-treated (20 μM) cells and plk1 was co-localized with γ-tubulin.

B. Cyclin A accumulates on centrosomes in VR23-treated cells. Cells were fixed and immunostained with antibodies specific for γ-tubulin (green) and cyclin A (red). DNA was stained with DRAQ5 (blue). Unlike non-treated cells, multiple centrosomes were observed in VR23-treated (20 μM) cells, and cyclin A was co-localized with γ-tubulin.

C. hSAS6 accumulates on centrosomes in VR23-treated cells. Cells were fixed and immunostained with antibodies specific for γ-tubulin (green) and hSAS6 (red). DNA was stained with DRAQ5 (blue). Unlike non-treated cells, multiple centrosomes were observed in VR23-treated (20 μM) cells, and hSAS6 was co-localized with γ-tubulin. The experiments were repeated three times and representative figures are shown. Images were captured by a LSM510 confocal microscope.

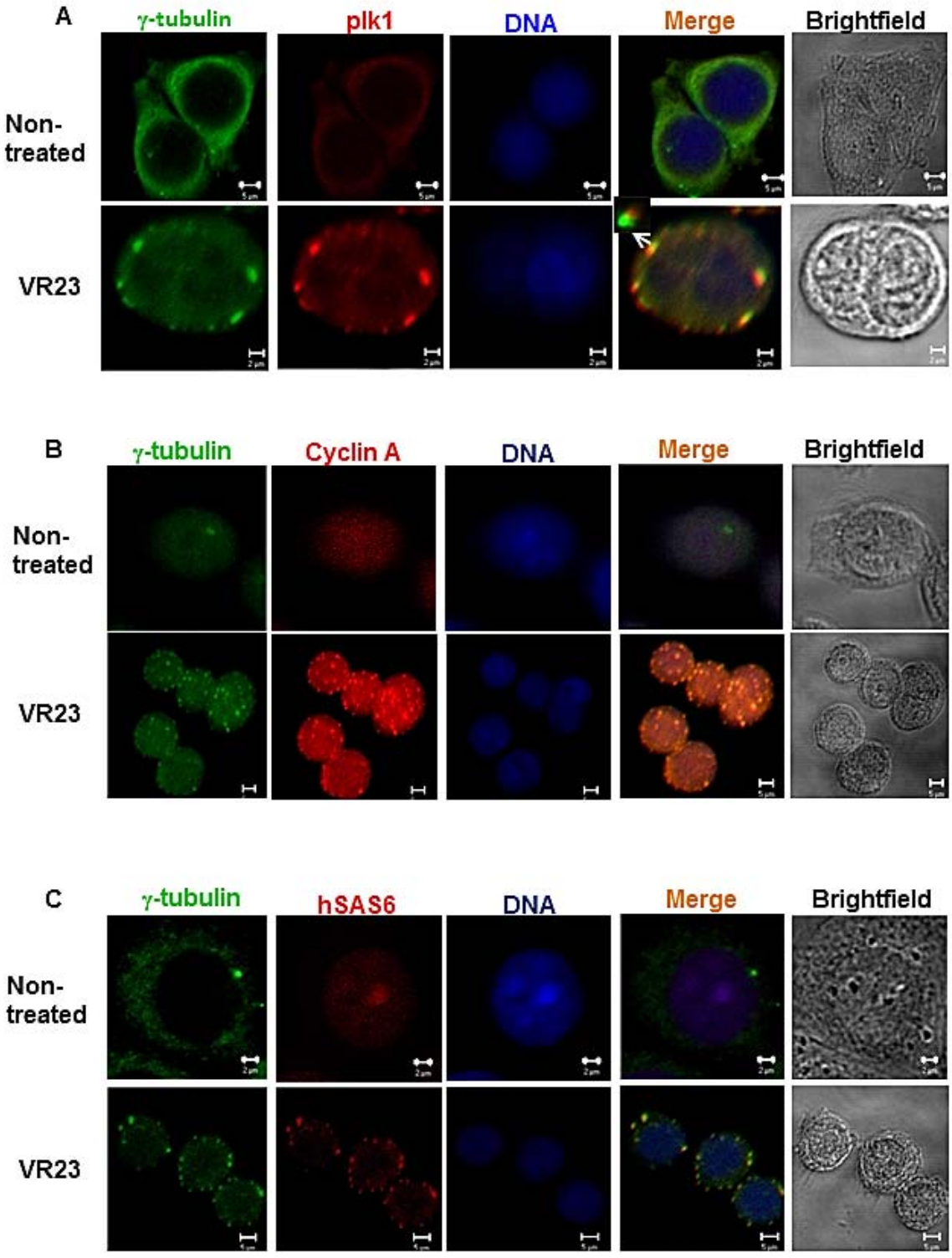
A
γ-tubulin
plk1
DNA
Merge
Brightfield
Non-treated
VR23
B
γ-tubulin
Cyclin A
DNA
Merge
Brightfield
Non-treated
VR23
C
γ-tubulin
hSAS6
DNA
Merge
Brightfield
Non-treated
VR23

centrosomal proteins may be accumulated in PCM. To test this possibility, γ-tubulin was immunostained with antibodies specific for various centrosomal proteins that localize to the centrosome and drive centrosome duplication and maturation. Cyclin E, plk1, centriolin, hSAS6 and cyclin A, which fall in this category, were co-localized with γ-tubulin (Figs. 21 and 23). psmc6, an antibody specific for 26S proteasome subunits, was also co-localized with γ-tubulin (Fig. A12). This data confirms the previous studies that the active proteasomal machinery are present on centrosomes, and centrosomes expand in response to proteasome inhibition (166). The only positive regulator that was not found with the majority of γ-tubulin was plk4. To determine whether centrosomal localization of proteins involved in the centrosome regulation is different between non-treated and VR23-treated cells, co-immunostaining experiments were performed. Cells were synchronized in G1/S and released into complete medium ± VR23. Cells were fixed and immunostained at 0, 1, 2 and 3 h. Multiple γ-tubulin foci appeared by 3 h in treated cells but not in non-treated samples. In some experiments, more than one γ-tubulin foci were seen at 2 h, but it wasn't very reproducible. Therefore, all the subsequent experiments carried out at 3 h post-release from double thymidine block. Plk4 has previously been reported to initiate centrosome duplication, and overexpression of plk4 has been noted to cause centrosome amplification (148). Because of this important role played by plk4 in regulating centrosome biogenesis, further experiments were carried out to examine if plk4 localizes at centrosomes prior to the 3 h post-G1/S. Simultaneously, cyclin E and plk1 localization at centrosomes were also observed to examine differences between non-treated and VR23-treated cells. Cells

synchronized in G1/S by double thymidine block were released into the cell cycle at time 0 h in the presence or absence of VR23. Cells were examined at 0, 1, 2 and 3 h timepoints. Cyclin E was not co-localized to centrosome at 0, 1 or 2 h in both treated and non-treated cells. At 3 h, cyclin E was co-localized with γ-tubulin at all of the centrosomal foci in the VR23-treated cells. Conversely, only a few foci of γ-tubulin (1.7%) were co-localized with cyclin E in non-treated cells (Fig. 24 and Table 5).

In non-treated cells, 44% of γ-tubulin foci were co-immunostained with plk1 (44%) at 3 h; however, co-immunostaining was not observed at 0, 1 or 2 h (Fig. 25). Interestingly, all of γ-tubulin foci in VR23-treated cells were co-immunostained with plk1 at 3 h. However, again, there was no co-immunostaining at 0, 1 or 2 h. 97% of γ-tubulin foci were co-immunostained with plk4 at 0, 1 and 3 h in non-treated cells (Fig. 26). Interestingly, plk4 was localized to centrosomes at 3 h. This pattern was not seen in VR23-treated cells. Plk4 was not co-localized to centrosomes at any of these timepoints in the majority of VR23-treated cells (only 9% of treated cells had one centrosome which co-stained with plk4). The cells were also examined at 6 h post-G1/S to learn if plk4 localizes at centrosomes at a later timepoint. When cells were approaching G2/M at 6 h timepoint, however, plk4 was not localized to centrosomes in VR23-treated cells. In these cells, plk4 was present inside the nucleus, suggesting that cyclin E can initiate centrosome duplication in the presence of VR23 even when plk4 is not localized to centrosomes. Thus, this data obtained from cells treated with VR23 is not consistent with the previous reports that plk4 is the one responsible for initiating centrosome duplication (105).

Some variations were observed in non-treated samples at 2 h where plk4 was found in the nucleus, but not at centrosomes. The variations at 2 h timepoint in this set of experiments were observed mostly in non-treated cells. Plk4 in some experiments was co-immunostained with γ-tubulin at 2 h in some of the non-treated cells. In addition, immunostaining of cyclin E and γ-tubulin was increased at 2 h. However, the general pattern in non-treated cells was that plk4 was mostly co-localized with γ-tubulin in non-treated controls. Plk1 was localized to centrosomes at 3 h in 40% of cases but not at 1 or 2 h in non-treated controls. Cyclin E was not found at centrosomes at 1 or 2 h post-release from G1/S. 1.7% of non-treated cells had cyclin E localized to centrosomes by 3 h. Whereas, in VR23-treated cells, all the foci of γ-tubulin were co-immunostained with cyclin E and plk1 at 3 h, but not at 1 or 2 h (Table 6). Since these centrosomes formed multiple spindle poles, they are apparently functional in forming MTOCs (Microtubule organizing centres).

It was surprizing to observe the absence of plk4 from centrosomes in VR23-treated cells, given its presumably essential role in the initiation of the centrosome synthesis. However, in some cases, a minority of VR23-treated cells (9-11%) with multiple centrosomes (>5 centrosomes per cell), plk4 was co-immunostained with γ-tubulin on one of the centrosomes (Fig. 26). Interestingly, a minority of cells did not form multiple centrosomes in VR23-treated cells that also contain plk4. (Fig. A15).

3.9 *De novo* centrosome amplification in response to VR23 in malignant cells

The multiple centrosomes induced by VR23 were dispersed throughout the cytoplasm and were not in a ‘rosette-like’ pattern as previously observed with plk4

Figure 24: Localization of cyclin E to the centrosomes at different timepoints

A. Localization of cyclin E was observed in cells released into the cell cycle at 0 h ± VR23 after double thymidine block (G1/S synchronization).
B. Cells fixed at 0, 1, 2, and 3 h in the presence of VR23 (20 μM). Non-treated cells were examined at the same timepoints as VR23-treated cells. Cells were immunostained with antibodies specific for γ-tubulin (green) and cyclin E (red). DNA was stained with DRAQ5 (blue). No centrosome amplification was seen at 1 or 2 h in VR23-treated cells, nor the accumulation of cyclin E at early timepoints. The experiment was performed three times in duplicate. Twenty different fields were observed per coverslip, per sample, and representative figures are shown.

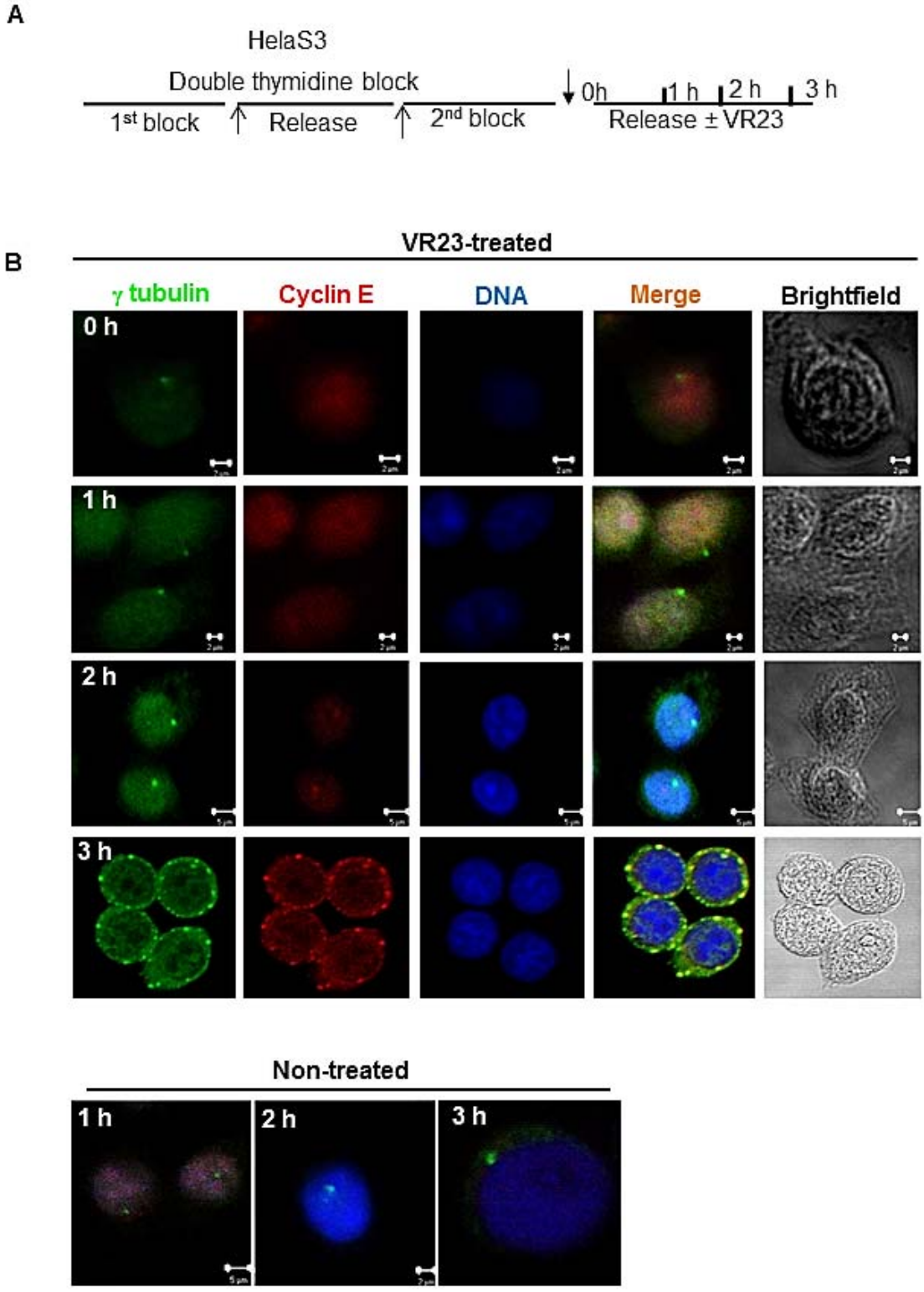
A
HelaS3
Double thymidine block
1st block
Release
2nd block
0h
1 h
2 h
3 h
Release ± VR23
B
VR23-treated
γ tubulin
Cyclin E
DNA
Merge
Brightfield
0 h
1 h
2 h
3 h
Non-treated
1 h
2 h
3 h

Figure 25: Localization of plk1 on centrosomes at different timepoints

A. Localization of plk1 was examined in cells released into the cell cycle ± VR23 after double thymidine block (G1/S synchronization).
B. VR23-treated (20 μM) and non-treated cells were collected at 0, 1, 2, and 3 h. Cells were immunostained with antibodies specific for γ-tubulin (green), and plk1 (red). DNA was stained with DRAQ5 (blue). No centrosome amplification was seen at 1 or 2 h in VR23-treated cells, nor the accumulation of plk1 at early timepoints. The experiment was repeated three times in duplicate. Twenty different fields were observed per coverslip, per sample, and representative figures are shown.

A

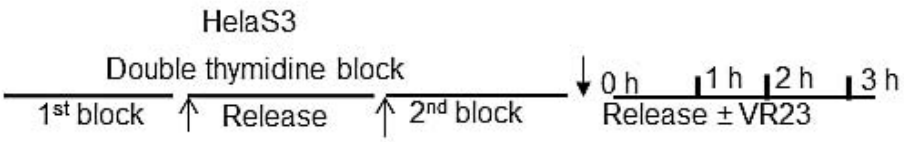
HelaS3
Double thymidine block
1st block
Release
2nd block
0 h
1 h
2 h
3 h
Release ± VR23

B

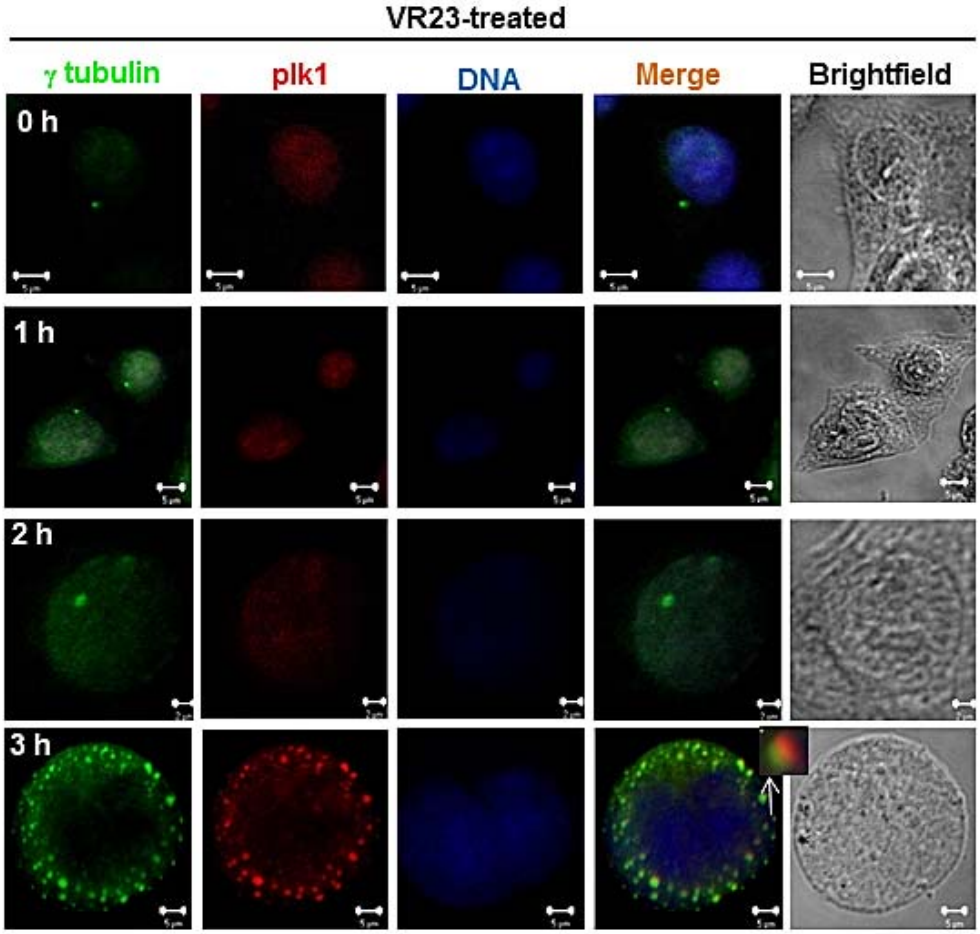
VR23-treated
γ tubulin
plk1
DNA
Merge
Brightfield
0 h
1 h
2 h
3 h

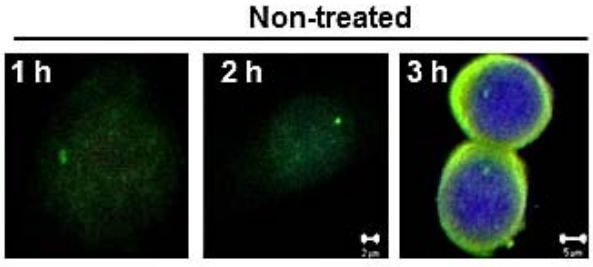
Non-treated
1 h
2 h
3 h

Figure 26: Differential localization of plk4 on centrosomes

Differential localization of plk4 in non-treated and VR23-treated cells was observed in cell released into the cell cycle after double thymidine block.
A. Cells maintained in medium ± VR23 (20 μM) were collected at 0, 1, 2, 3 h.
B. In non-treated cells, plk4 (red) was co-localized with γ-tubulin (green) at 0, 1 and 3 h but not at 2 h. Thus, plk4 localization appears at 1 h and then disappears at 2 h and reappear at 3 h in non-treated cells. In VR23-treated cells, plk4 was not co-localized at centrosomes at 1 or 2 h. At the 3 h timepoint, some of the centrosomes (yellow arrow) were co-localized with γ-tubulin but it was not common (11.3% of cells with multiple centrosomes had one centrosome that was co-localized with plk4). Each VR23-treated cell had more than 5 centrosomes. The experiment was repeated two times in duplicate. Twenty different fields were observed per coverslip per sample, and representative figures are shown.

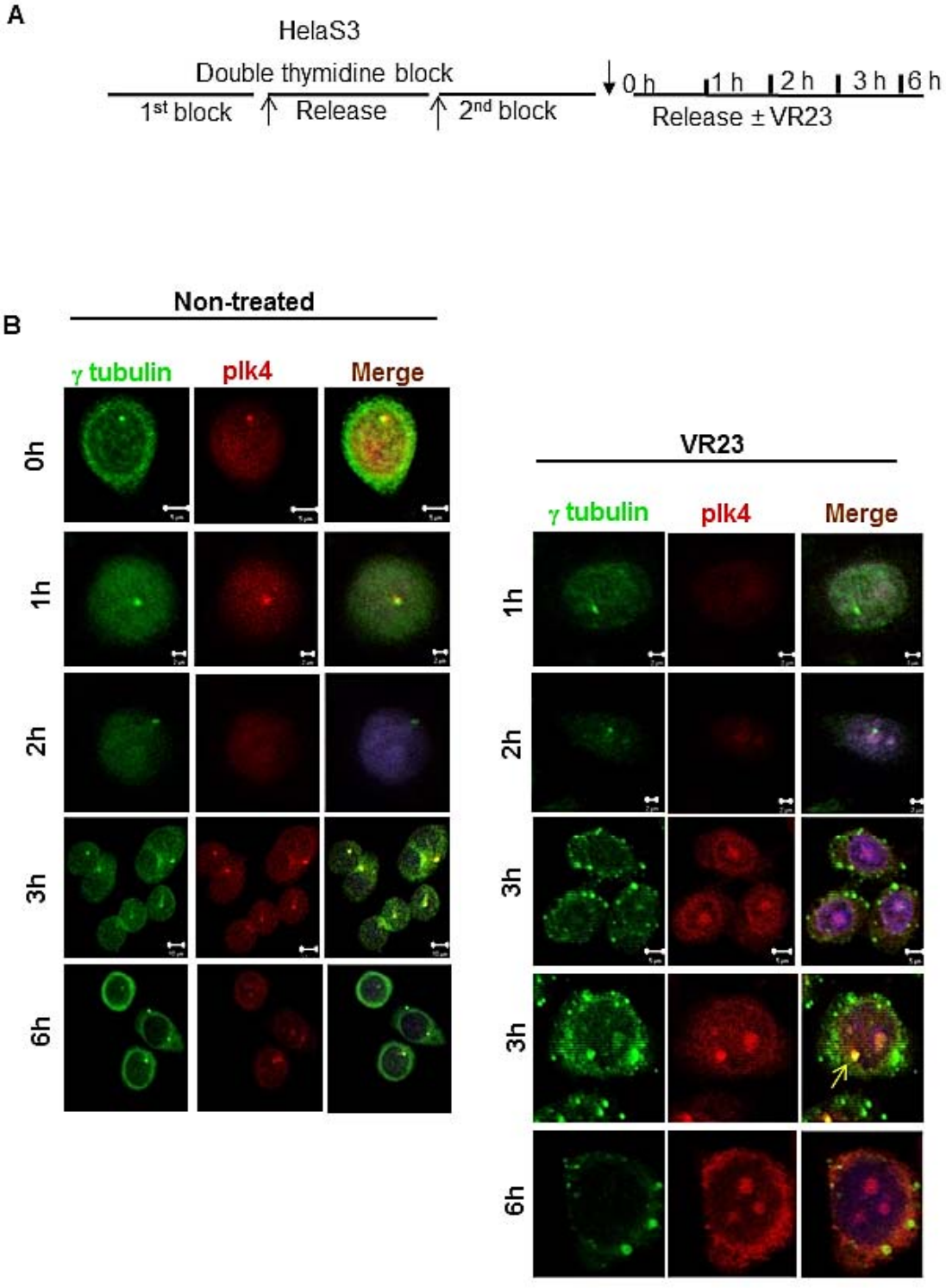
A
HelaS3
Double thymidine block
1st block
Release
2nd block
0 h
1 h
2 h
3 h
6 h
Release ± VR23
B
Non-treated
γ tubulin
plk4
Merge
0h
1h
2h
3h
6h
VR23
γ tubulin
plk4
Merge
1h
2h
3h
3h
6h

Table 5: Co-localization of cyclin E, plk1 and plk4 with γ-tubulin at different timepoints in VR23-treated and non-treated cells

Summary of the co-localization of cyclin E, plk1 and plk4 at centrosomes in the presence or absence of VR23 treatment. Samples were collected at 0, 1, 2, and 3 h post-double thymidine block. “No” indicates no co-localization, and “yes” indicates co-localization with γ-tubulin.

Co-localization with γ-tubulin						
	Cyclin E		plk1		plk4	
0 h	No		No		No	
Sample/ Timepoints	Non-treated	VR23	Non-treated	VR23	Non-treated	VR23
1 h	No	No	No	No	Yes	No
2 h	No	No	No	No	No	No
3 h	co-localized with γ-tubulin in a very few cells (1.7%).	co-localized with multiple γ-tubulin within a cell.	co-localized with γ-tubulin in some cells (44%).	co-localized with multiple γ-tubulin within a cell in all the cells	In most cells, co-localized with γ-tubulin (97.7%).	Not co-localized with γ-tubulin (9% cells show co-staining with γ-tubulin).

overexpression (104). The appearance of >5 mature centrosomes within 3 h suggests that it is a *de novo* amplification. This may be caused by the assembly of centrosomal proteins by the accumulation of centriolar proteins (as a result of inhibition of proteasomes). To systematically examine the role of cyclin E and plk4 in centrosome amplification caused by VR23, the formation of multiple centrosomes was further studied by knocking down cyclin E or plk4 with siRNA, in the presence or absence of VR23.

Centrosome amplification was not observed in cells where cyclin E was knocked down in combination with VR23. In contrast, cells treated with only VR23 showed increased levels of multiple centrosomes (89%) (Fig. 27). Unlike cyclin E knockdown, plk4 knockdown could only partially rescue the multiple centrosome phenotype caused by VR23. However, the cells that formed multiple centrosomes in VR23-treated+plk4 knockdown cells had cyclin E co-localized at the centrosomes, while cells with rescued phenotype did not have cyclin E co-localized with γ-tubulin. Thus, cells formed multiple centrosomes in the absence of plk4 and presence of VR23 if cyclin E was co-localized with γ-tubulin (Fig. 28).

To examine the possibility of cyclin E accumulation at centrosomes in VR23-treated cells is somehow preventing the localization of plk4 at centrosomes, the localization of plk4 was determined in cyclin E ablated cells in the presence of VR23. Plk4 was still not localized to centrosomes in the absence of cyclin E in the majority of cells (Fig. 29). 11.3% of cells with multiple centrosomes had one centrosome containing plk4 in the presence of VR23. When cyclin E was knocked down (in the presence of VR23), this was increased to 18.6%.

Figure 27: Rescue of VR23-mediated multiple centrosomes by the ablation of cyclin E with siRNA

A. Cyclin E was ablated with siRNA in cells that were synchronized in G1/S, followed by release into the cell cycle in the presence or absence of VR23 (20 μM) for 3 h. The knockdown of cyclin E completely suppressed the formation of multiple centrosomes in the presence of VR23. Results shown are representative of three independent experiments.

B. Quantification of cells with multiple centrosomes. The number of cells with multiple centrosomes was counted in each sample. Twenty different fields were counted per coverslip per sample.

C. Western blot of the proteins extracted from different samples shown in **A**. Samples for protein extraction were taken in parallel with the immunostained. Two independent samples for VR23 + cyclin E siRNA are shown to reveal the efficacy of siRNA. (**i**) Non-treated, (**ii**) VR23-treated, (**iii**) VR23 + scrambled siRNA, (**iv**) Non-treated + scrambled siRNA, (**v**) Nontreated + cyclin E siRNA, (**vi** and **vii**) VR23 + Cyclin E siRNA.

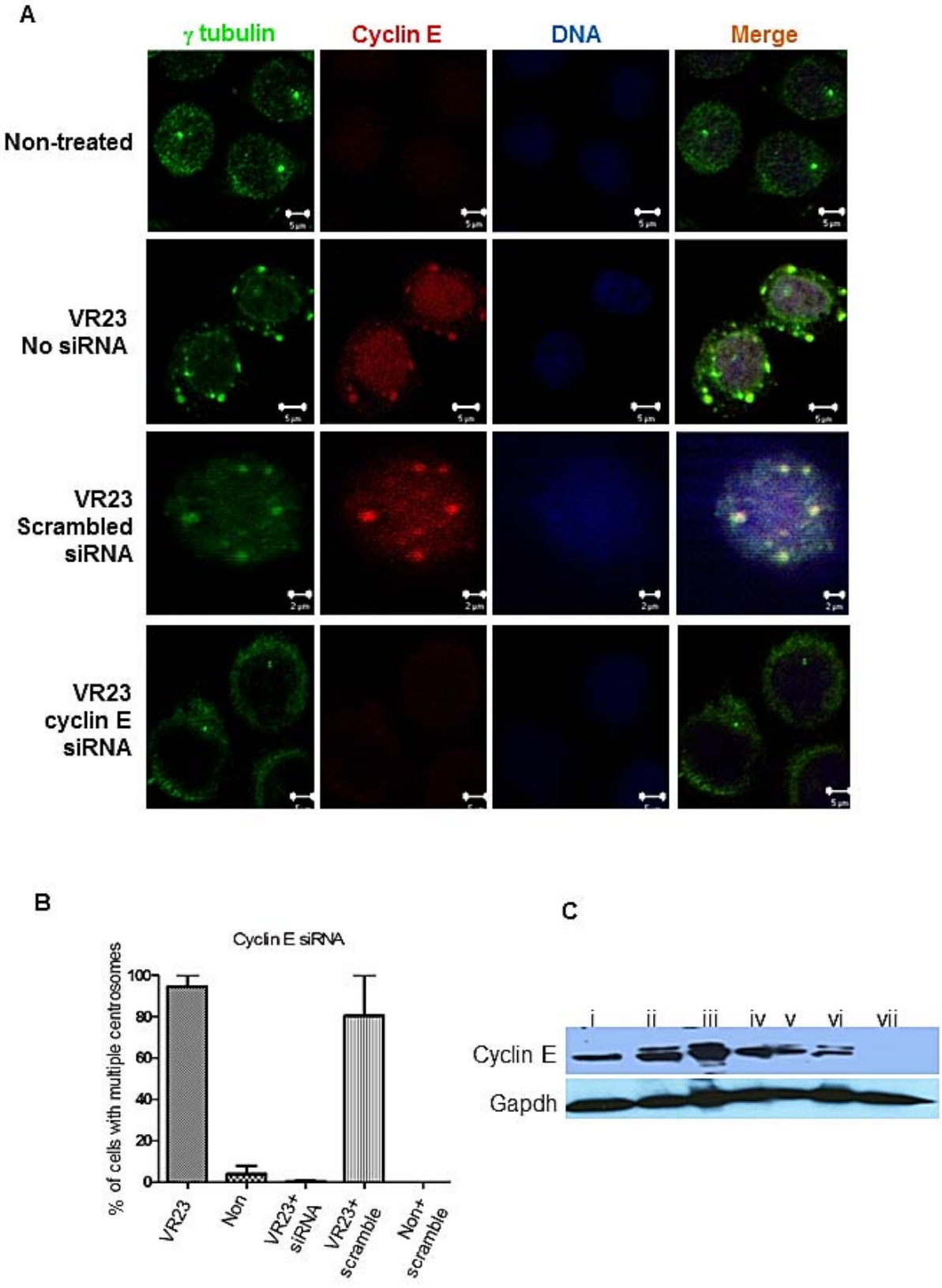
A
γ tubulin
Cyclin E
DNA
Merge
Non-treated
VR23
No siRNA
VR23
Scrambled
siRNA
VR23
cyclin E
siRNA
B
Cyclin E siRNA
% of cells with multiple centrosomes
100
80
60
40
20
0
VR23
Non
VR23+
siRNA
VR23+
scramble
Non+
scramble
C
i
ii
iii
iv
v
vi
vii
Cyclin E
Gapdh

Figure 28: Partial rescue of VR23-mediated centrosome amplification by plk4 knockdown

A. Cyclin E (red) was co-localized with γ-tubulin (green) in plk4 ablated (+VR23) cells. Cells treated with plk4 siRNA were synchronized at G1/S, followed by release into complete medium for 3 h in the presence or absence of VR23. At the end of 3 h, cells were fixed and cyclin E localization was determined with antibodies specific for γ-tubulin and cyclin E. Cyclin E was co-localized with γ-tubulin in VR23-treated plk4 ablated cells, which showed multiple centrosomes. The cells that rescued the multiple centrosome phenotype were negative for cyclin E localization at centrosomes although cyclin E was still present inside the cytoplasm.
B. Quantification of cells that formed multiple centrosomes in plk4 siRNA + VR23 cells. Results are shown from three independent experiments.
C. Western blot of proteins extracted from samples shown in **A**.

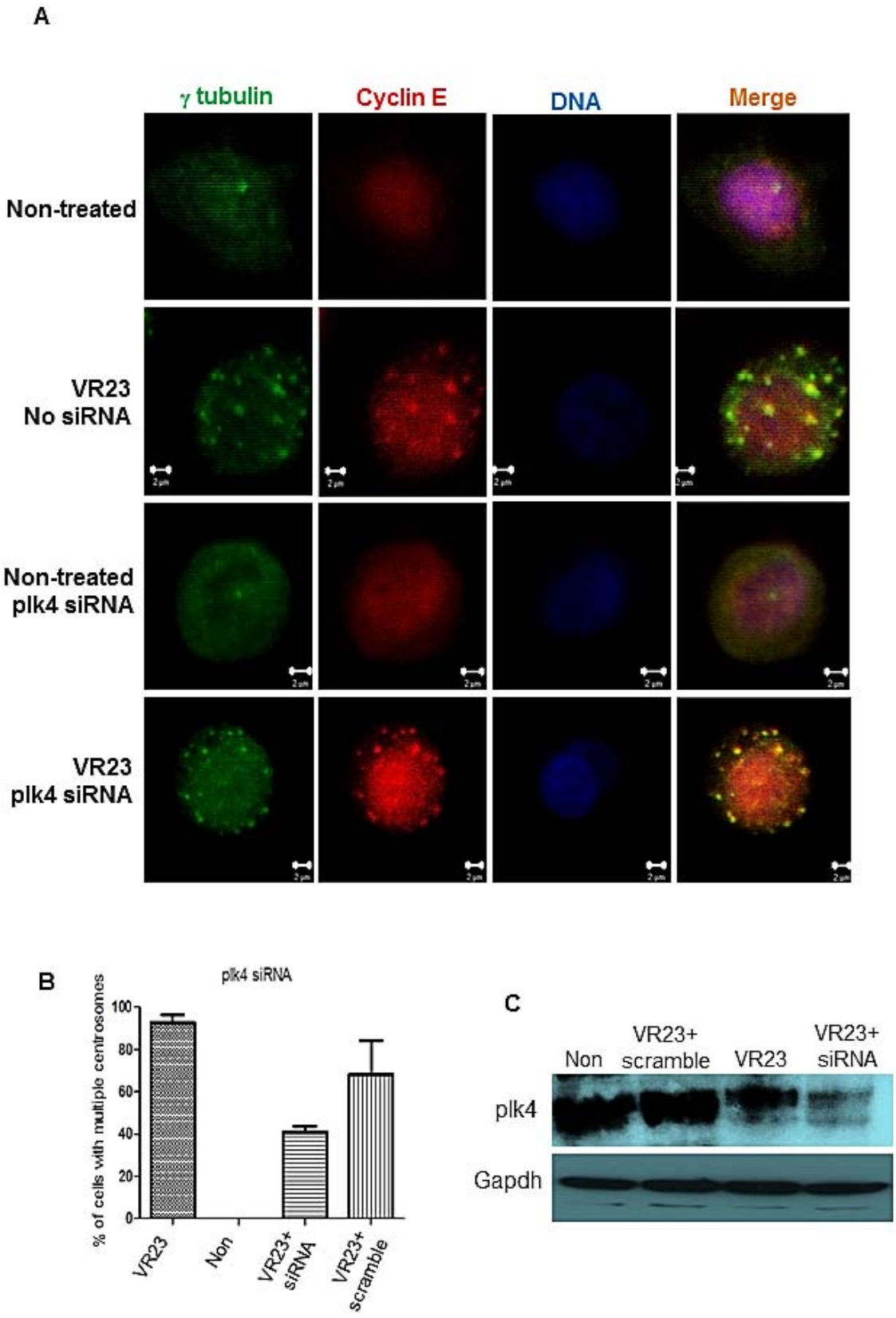
A
γ tubulin
Cyclin E
DNA
Merge
Non-treated
VR23
No siRNA
Non-treated
plk4 siRNA
VR23
plk4 siRNA
B
plk4 siRNA
% of cells with multiple centrosomes
100
80
60
40
20
0
VR23
Non
VR23+
siRNA
VR23+
scramble
C
Non
VR23+
scramble
VR23
VR23+
siRNA
plk4
Gapdh

Figure 29: Plk1 and plk4 do not localize to centrosomes in VR23-treated cells when cyclin E is ablated

A. The localization of plk4 was examined in cells treated with VR23 in conjunction with cyclin E siRNA treatment, Cyclin E was knocked down using siRNA and cells were synchronized in G1/S by double thymidine block, which were then released into the cell cycle for 3 h in the presence or absence of VR23. After 3 h, cells were immunostained with antibodies specific for plk4 (red) and γ-tubulin (green). DNA was stained with DRAQ5 (blue). In VR23-treated cells and VR23 + cyclin E knockdown cells, plk4 does not localize to centrosomes. While only 11.3% of VR23-treated cells had one of their many centrosomes co-immunostained with anti-plk4 antibody. 18.6% of the VR23 + cyclin E siRNA samples had one centrosome, which co-stained with plk4. 'Non' is non-treated. The experiment was performed two times in duplicate, and representative figures are shown. Cells in twenty different fields were counted for each coverslip per sample.
B. Same as in **A**, except immunostaining samples with antibodies specific for γ-tubulin (green), cyclin E (red) and plk1 (blue). As compared to VR23-treated cells, cells knocked down with cyclin E siRNA + VR23 rescued the multiple centrosome phenotype, and these cells do not have plk1 co-localization at γ-tubulin.

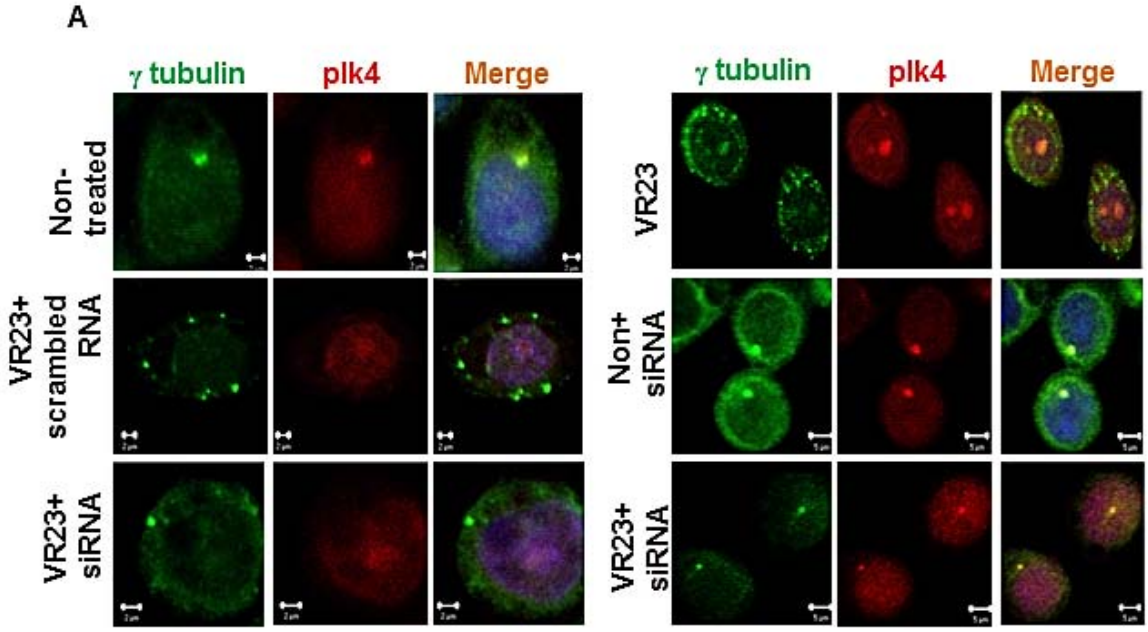
A
γ tubulin
plk4
Merge
Non-treated
VR23+ scrambled RNA
VR23+ siRNA
VR23
Non+ siRNA
VR23+ siRNA

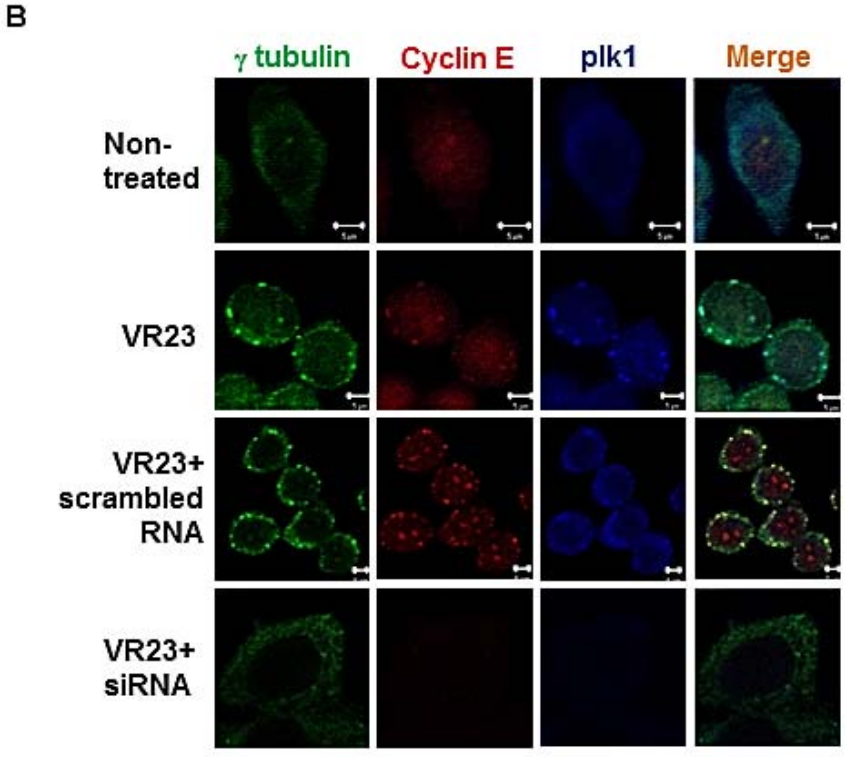
B
γ tubulin
Cyclin E
plk1
Merge
Non-treated
VR23
VR23+ scrambled RNA
VR23+ siRNA

Inhibitors of DNA synthesis such as hydroxyurea and aphidicolin have previously been reported to cause centrosome amplification by uncoupling the cell cycle and centrosome cycles (167, 168). To study if the observed centrosome amplification is not a by-product of the inhibition of DNA synthesis by VR23. Cells were stained with EdU, a thymidine analogue which is incorporated into replicating DNA. EdU labelled DNA in treated samples indicated DNA replication is not inhibited in the presence of VR23 (Fig. 30).

Most of the published data generated using hydroxyurea and aphidicolin as synchronization agents required 16-48 h of drug treatment to observe the multiple centrosomes (167, 168). In contrast, VR23 induces the centrosomes amplification within 3 h, suggesting that its centrosome amplification mechanism is different from these DNA replication inhibitors.

Cdk2 is the activating partner of cyclin E (169). Therefore, in an alternative method to inhibit cyclin E activity, cdk2 was inhibited to examine if it would prevent VR23-induced *de novo* formation of centrosomes. NU6140 (4-[[6-(cyclohexylmethoxy)-1H-purin-2-yl]amino]-N,N-diethylbenzamide) was used because it has been reported to be the most selective inhibitor for cdk2 (170) with an IC_{50} of 0.41 µM for cdk2 and 6.6 µM for cdk1. Three different concentrations of NU6140 were used (0.5, 1.0 and 2.0 µM). The higher concentration (2 µM) did rescue some VR23-treated cells from the multiple centrosome phenotype (Fig. 31). In these samples cyclin E was often not co-localized with γ-tubulin, suggesting that VR23-induced *de novo* centrosome amplification depends on cyclin E accumulation at centrosomes (Fig. 31). In these cells, many ‘small’-sized centrosomes were observed and cyclin E was co-localized only at the ‘large’-sized

Figure 30: Multiple centrosomes induced by VR23 are not caused by the inhibition of DNA replication

A. HeLa S3 cells synchronized at G1/S were released into the cell cycle for 3 h in the presence of EdU (5-ethynyl-2'-deoxyuridine). EdU integrates into replicating DNA allowing detection of newly synthesized DNA. EdU (green) was efficiently incorporated into DNA in the presence of VR23.
B. The number of cells positive for EdU incorporation were counted. 500 cells were counted for each sample. The experiment was performed twice with internal duplicates.

A

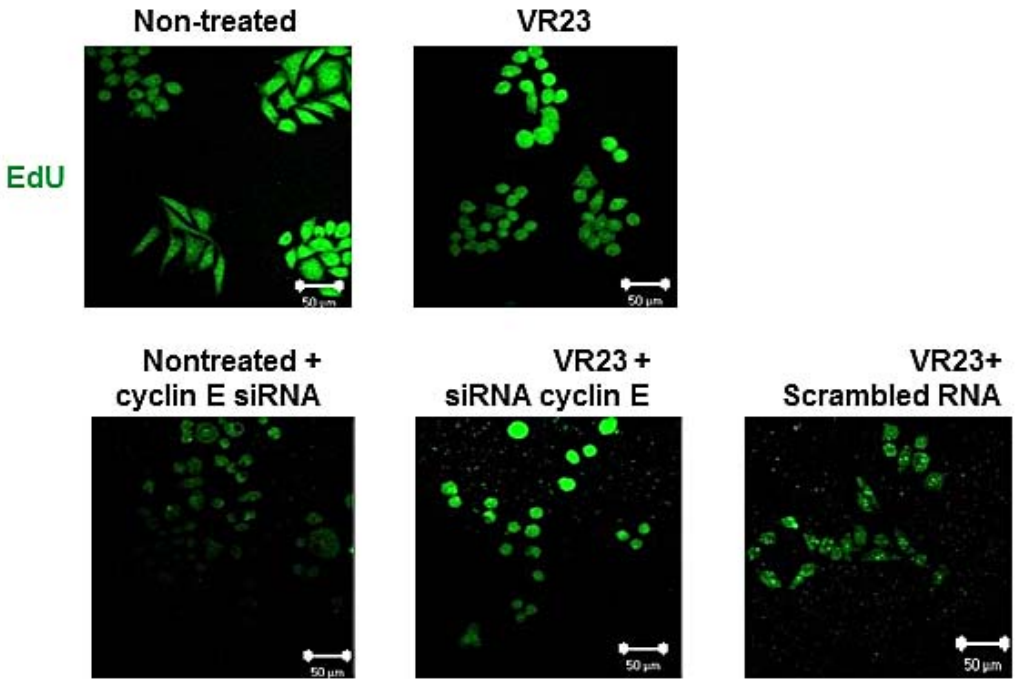

B

Sample	% of cells positive for EdU incorporation
Non-treated	24.3%
VR23	36.7%
Nontreated + cyclin E siRNA	16.5%
VR23 + cyclin E siRNA	22.0%
VR23 + Scrambled RNA	37.2%

Figure 31: Formation of multiple centrosomes upon the inhibition of cdk2 in the presence of VR23

A. Cells synchronized at G1/S by double thymidine block, were released in complete medium ± drug(s) for 3 h. Cdk2 was inhibited by using three different concentrations of NU6140. Although the majority of these cells still formed multiple centrosomes (green) in the presence of VR23 (**e**, **f**), increasing the concentration of NU6140 (2 μM) did reduce number of centrosomes in VR23-treated cells (**g**-**i**). In these cells (11-15%), the number of centrosomes per cell and the size of centrosomes decreased. A decrease in centrosomal localization of cyclin E (red) was also observed. DNA is shown in blue.
(**a**) Non-treated, (**b**) VR23-treated (20 μM), (**c**) NU6140 only (0.5μM), (**d**) NU6140 (1 μM), (**e**) VR23 (20 μM) + NU6140 (0.5 μM), (**f**) VR23 (20 μM) + NU6140 (1μM), and (**g**-**i**) VR23 (20 μM) + NU6140 (2 μM). Yellow arrow (**f**) shows a 'small' sized centrosome with no co-localizaion of cyclin E, and white arrow (**g**) shows localization of cyclin E in nucleus. The experiment was performed three times. Representative pictures are shown.
B. Quantification of VR23-treated cells forming multiple centrosomes in the presence of the cdk2 inhibitor NU6140. This graph summarizes the total number of cells that formed multiple centrosomes.
C. Quantification of the number of cells in the NU6140 (2 μM) + VR23 (20 μM) sample that had a decrease in number (≤5 per cell) and size of centrosomes. 200 cells were counted for each sample in duplicate, repeated three times.

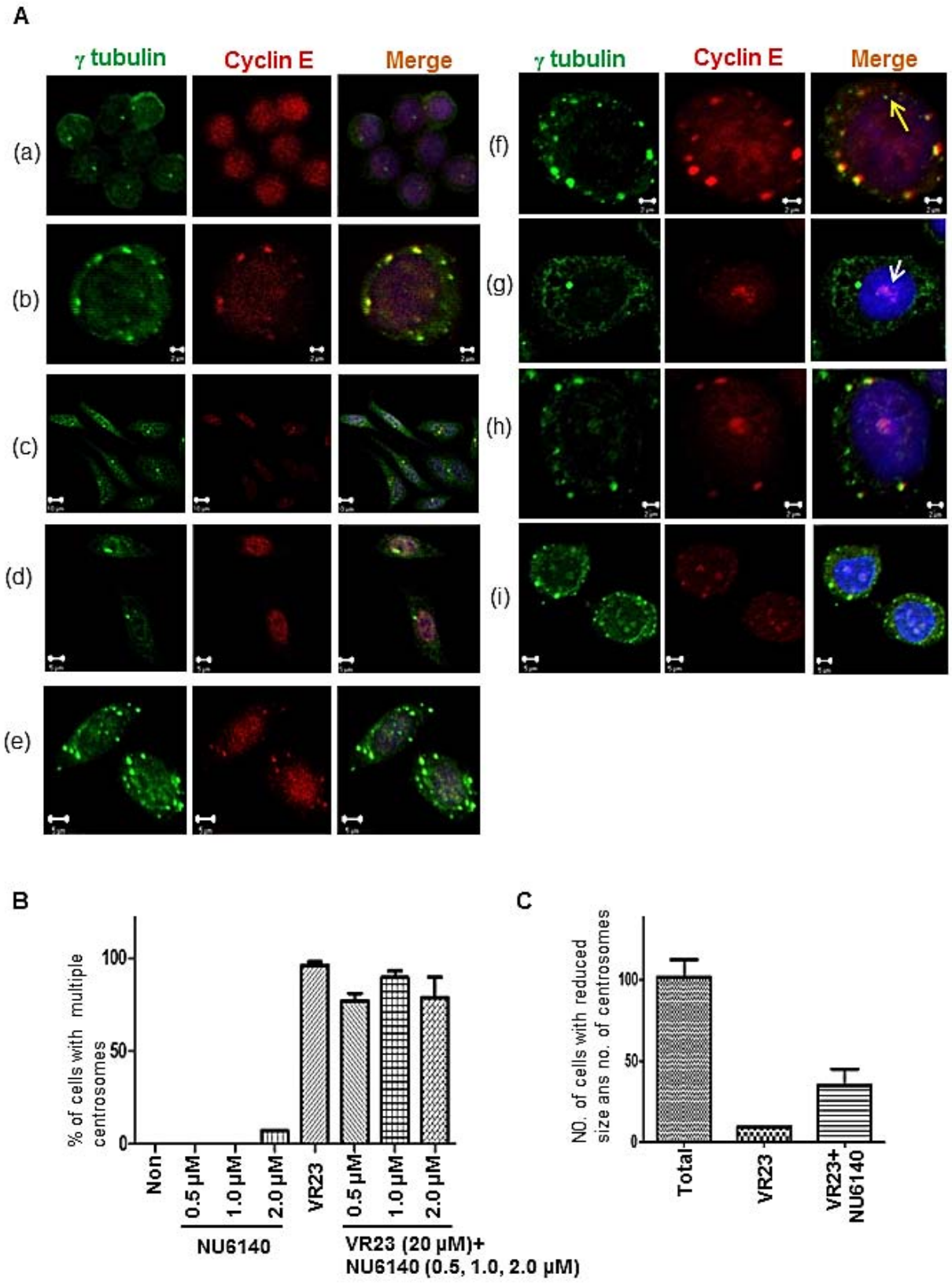
A
γ tubulin
Cyclin E
Merge
(a)
(b)
(c)
(d)
(e)
(f)
(g)
(h)
(i)
B
% of cells with multiple centrosomes
100
50
0
Non
0.5 μM
1.0 μM
2.0 μM
VR23
0.5 μM
1.0 μM
2.0 μM
NU6140
VR23 (20 μM)+
NU6140 (0.5, 1.0, 2.0 μM)
C
NO. of cells with reduced size ans no. of centrosomes
100
50
0
Total
VR23
VR23+
NU6140

centrosomes. Furthermore, cells treated with VR23 + NU6140 (2 μM) had fewer (<5 per cell) centrosomes than observed in VR23-treated cells (Fig. 31). As previously observed, VR23 inhibits proteasome activity and also causes accumulation of ubiquitinated proteins. To test if the presence of excess cyclin E at centrosomes is due to the accumulation of ubiquitinated cyclin E, cells were stained with TUBEs (Tandem ubiquitin binding entities).

TUBEs bind to ubiquitin molecules a 1,000 times more efficient than an anti-ubiquitin antibody. A triple staining of TUBEs, cyclin E and γ-tubulin showed an accumulation of ubiquitinated cyclin E at centrosomes in the presence of VR23 (Fig. 33). This was further examined by immunoprecipitation and Western blotting. The accumulation was observed within 3 h of VR23 treatment (Fig. 32). The experiment was performed by pulling down cyclin E and subsequently blotting with ubiquitin antibody (Fig. 32C). Alternatively, ubiquitin was pulled down and blotted with anti-cyclin E antibody (Fig. 32D).

To further investigate cyclin E localization at centrosomes in the presence of VR23, cells were subjected to immunostaining with antibodies specific for cdk2, cyclin E and γ-tubulin. As expected, cyclin E was co-immunostained with cdk2, and the complex was co-localized with γ-tubulin (Fig. 33). However, cyclin E was also bound to ubiquitin (Fig. 33 and 34).

To determine whether cyclin E was ubiquitinated and at the same time bound to cdk2, cyclin E was immunoprecipitated and blotted with antibodies specific for ubiquitin (Fig. 34) and cdk2. Ubiquitinated cyclin E was bound to cdk2 (Fig. 34B). The inhibition of cdk2 in VR23-treated cells with NU6140 further

Figure 32: Ubiquitinated cyclin E accumulates at centrosomes in the presence of VR23

Cells synchronized by double thymidine block were released into medium ± VR23 for 3 h. After 3 h, cells were either fixed and immunostained with corresponding antibodies or had proteins extracted for immunoprecipitation.
A. Co-immunostaining of cyclin E and ubiquitin was seen in VR23-treated samples. TUBEs-FLR (Tandem ubiquitin binding entities-fluorophore) are shown in green, cyclin E in red, and DNA in blue.
B. Cells were immunostained with TUBEs (green), cyclin E (red) and γ-tubulin (blue). As compared to non-treated cells, VR23-treated cells show the localization of ubiquitinated cyclin E to centrosomes. The experiment was performed three times and representative figures are shown.
C. Cyclin E was immunoprecipitated, followed by protein separation by SDS-PAGE on a 4-6% polyacrylamide gel. Western blot (WB) with an antibody specific for ubiquitin shows the accumulation of ubiquitinated cyclin E in VR23-treated cells.
(**i**) Non-treated, (**ii**) VR23-treated (20 μM), (**iii**) VR23-treated (40 μM), (**iv**) bortezomib® (20 nM), and (**v**) IgG only. The experiment was repeated 3 times and a representative figure is shown. Input is total protein (cyclin E).
D. Ubiquitin proteins were immunoprecipitated with TUBEs, followed by SDS-PAGE on a 4-6% polyacrylamide gel. Western blot carried out with an antibody specific for cyclin E shows accumulation of ubiquitinated cyclin E in VR23-treated cells. (**i**) Non-treated, (**ii**) VR23-treated (20 μM), (**iii**) bortezomib® (20 nM). The experiment was repeated three times and a representative figure is shown. Input is total protein (cyclin E).

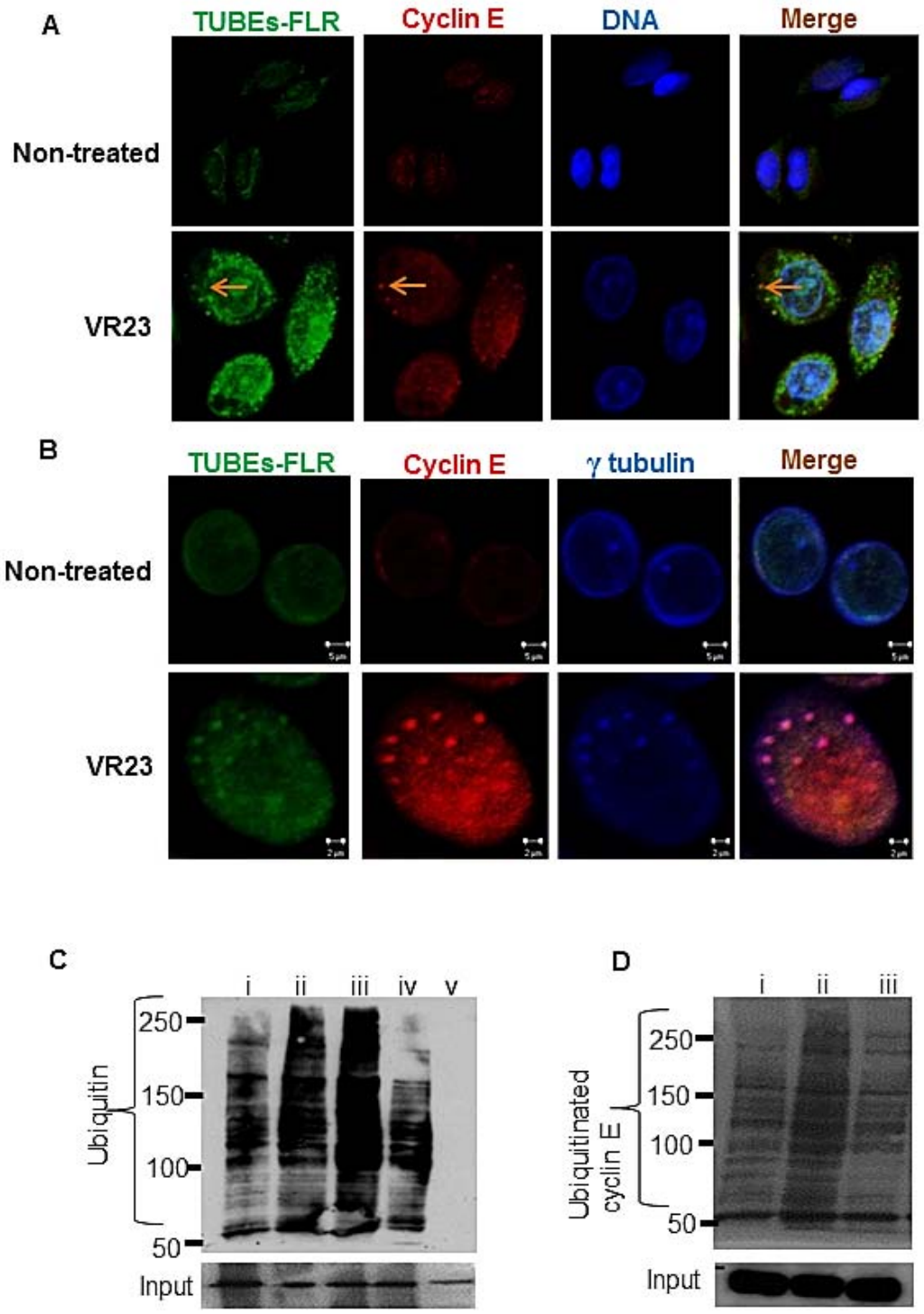
A
TUBEs-FLR
Cyclin E
DNA
Merge
Non-treated
VR23
B
TUBEs-FLR
Cyclin E
γ tubulin
Merge
Non-treated
VR23
C
i
ii
iii
iv
v
250
150
100
50
Ubiquitin
Input
D
i
ii
iii
250
150
100
50
Ubiquitinated cyclin E
Input

Figure 33: Co-localization of cdk2-cyclin E at centrosomes upon the inhibition of cdk2 activity in the presence of VR23

HeLa S3 cells synchronized by double thymidine block were released into the cell cycle for 3 h in the presence or absence of drug(s). At the end of 3 h, cells were fixed and immunostained with antibodies specific for γ-tubulin (green), cyclin E (red) and cdk2 (blue). In the VR23-treated samples, cyclin E and cdk2 are co-localized to the centrosomes (γ-tubulin). VR23 + NU6140 samples showed a decrease in the number of centrosomes with cyclin E localized at γ-tubulin with or without cdk2. The experiment was repeated twice in duplicate.

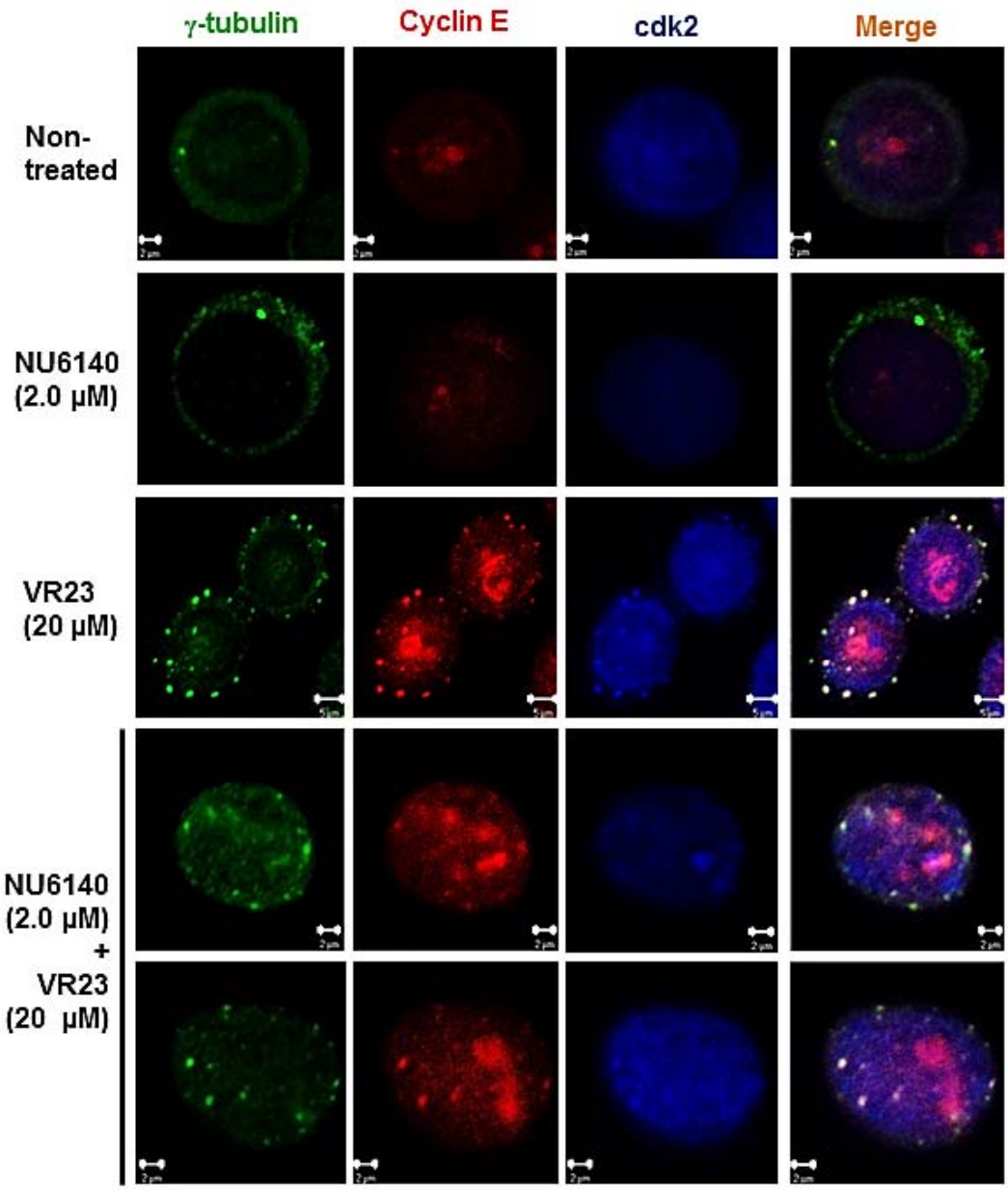
γ-tubulin
Cyclin E
cdk2
Merge
Non-treated
NU6140 (2.0 μM)
VR23 (20 μM)
NU6140 (2.0 μM) + VR23 (20 μM)

increased the accumulation of ubiquitinated cyclin E (Fig. 34C). The quantification of cells with a reduced number and size of centrosomes in NU6140+VR23 is shown in figures 31 and 33.

Microscopic data obtained from triple immunostaining with TUBEs, cyclin E and cdk2, showed that some cyclin E molecules were ubiquitinated while some other cyclin E molecules bound to cdk2. In addition, some cyclin E molecules were co-immunostained both with TUBEs and with cdk2, suggesting that ubiquitinated cyclin E also binds to cdk2 (Fig. 34A). The intensity of staining for TUBEs was very high in VR23-treated cells (Fig. 34A). Therefore, I had to reduce the exposure time to observe the association of cdk2 with ubiquitinated cyclin E. Data from these experiments suggests that ubiquitinated cyclin E localized at the centrosomes and also accumulated in the cytoplasm in VR23-treated cells because of the inhibition of proteasome activity. The excess of cyclin E (Fig. A13) bound to cdk2 at centrosomes may drive the formation of *de novo* centrosomes.

My data is consistent with the notion that cyclin E ubiquitinated but not degraded, resulting in its accumulation at the centrosomes and at discrete sites throughout the cytoplasm. Unbound cyclin E was ubiquitinated but because it has not been degraded it keeps on accumulating at centrosomes and in cytoplasm.

No amplification of centrosomes was found in the MCF10A non-malignant cells under the same treatment conditions (Fig. 36). Similar to non-treated HeLa S3 cells, plk4 was localized to centrosomes in VR23-treated MCF10A cells (Fig. 36C). The subcellular localization of centrosomal proteins in VR23-treated MCF10A cells was similar to that in non-treated HeLa S3 cells. No accumulation of ubiquitinated proteins was found in MCF10A cells either at short-exposure (3 h) or long

Figure 34: Ubiquitinated cyclin E and cdk2-cyclin E accumulates in VR23-treated cells

A. Cells synchronized by double thymidine block were released into complete medium ± drug(s) for 3 h. At the end of 3 h, cells were fixed and stained with TUBEs-FLR (green) and antibodies specific for cyclin E (red) and cdk2 (blue). The localization of cyclin E and cdk2 was observed in VR23-treated and VR23 + NU6140-treated cells. In VR23-treated and NU6140 + VR23-treated samples, cyclin E was co-localized with cdk2. Ubiquitinated (TUBEs) cyclin E also co-localized with cdk2. The increased fluorescence in VR23-treated samples made it difficult to visualize the co-localization with cdk2, therefore signal intensity for 488 nm (TUBEs-green) was reduced. The experiment was repeated two times in duplicate and representative pictures are shown.
B. Cells synchronized by double thymidine block were released into medium ± VR23 for 3 h. At the end of 3 h, cyclin E was immunoprecipitated with an antibody specific for cyclin E, followed by SDS-PAGE on a 4-6% polyacrylamide gel. Western blot carried out with an antibody specific for ubiquitin shows the accumulation of ubiquitinated proteins in VR23-treated cells. Western blot was also carried out with an antibody specific for cdk2. Cyclin E immunoprecipitated from VR23-treated samples is ubiquitinated and bound to cdk2 (sample (**iii**) in the top and bottom blot). (**i**) Non-treated, (**ii**) VR23-treated (20μM), (**iii**) VR23-treated (40μM), (**iv**) IgG only.
D. Accumulation of ubiquitinated cyclin E was considerably increased in cells treated with both a cdk2 inhibitor (NU6140) and VR23 (**iii**), as compared to VR23 alone (**ii**). (**i**) Non-treated, (**ii**) NU6140 (2 μM), (**iii**) VR23 (20 μM), (**iv**) NU6140 (2 μM) + VR23 (20μM). All samples were collected 3 h post-release from G1/S block.

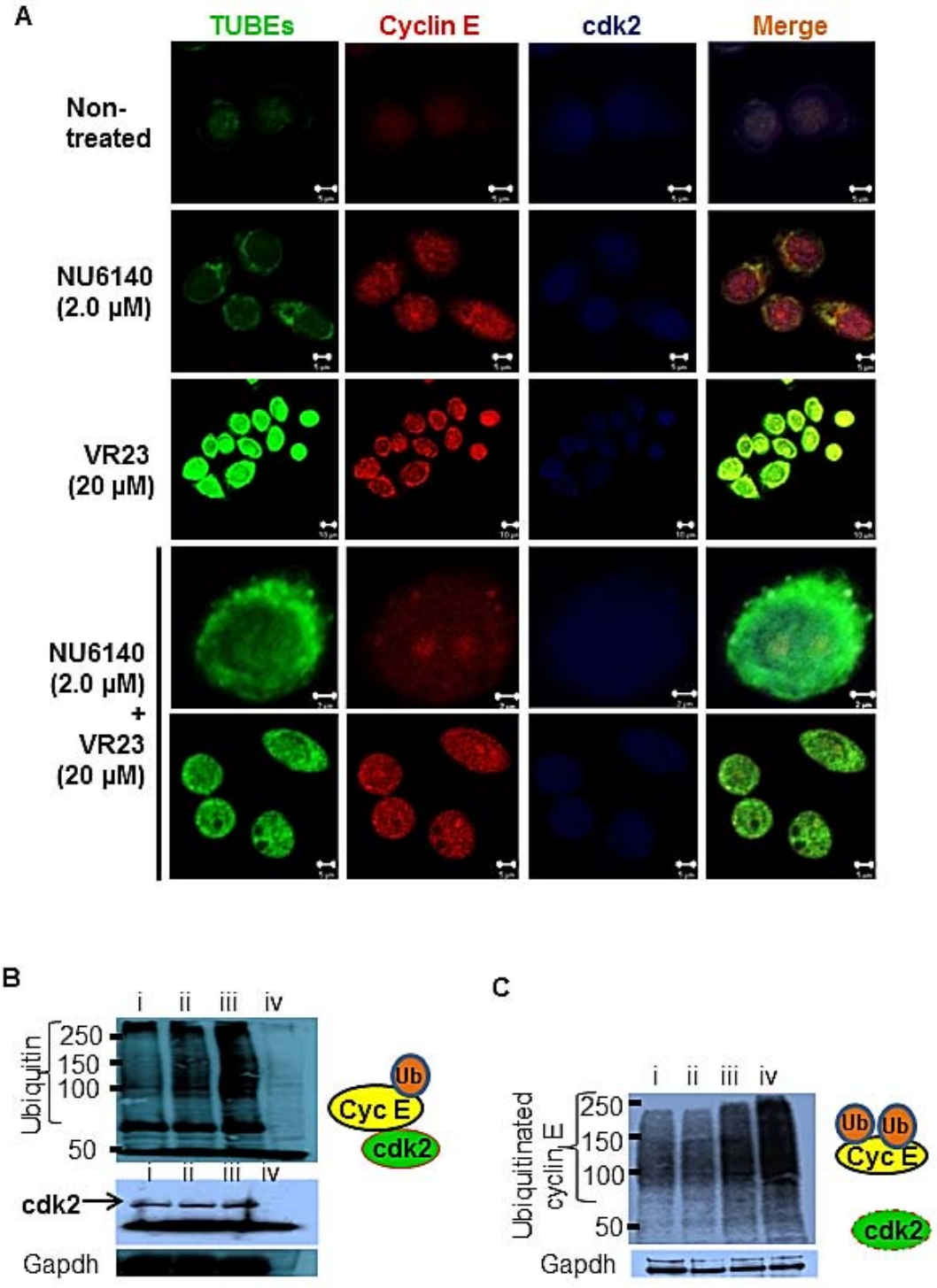
A
TUBEs
Cyclin E
cdk2
Merge
Non-treated
NU6140 (2.0 μM)
VR23 (20 μM)
NU6140 (2.0 μM) + VR23 (20 μM)
B
i ii iii iv
Ubiquitin
250
150
100
50
cdk2
Gapdh
Ub
Cyc E
cdk2
C
i ii iii iv
Ubiquitinated cyclin E
250
150
100
50
Gapdh
Ub
Ub
Cyc E
cdk2

Figure 35: Schematic illustration of multiple centrosome formation in the presence of VR23

Multiple centrosome formation in response to VR23 is largely cyclin E-dependent. (**a**) Multiple centrosomes are formed in the presence of VR23. Cyclin E accumulates at centrosomes and positive regulators of centrosomes also accumulate at centrosomes. (**b**) When cyclin E is knocked down, the multiple centrosome phenotype induced by VR23 is rescued, suggesting that it is not compensated by other proteins such as cyclin A or plk4. (**c**) Partial rescue was seen in plk4 knockdown + VR23 cells. Cells that formed multiple centrosomes in plk4 knockdown + VR23 samples had cyclin E localized at the centrosomes. (**d**) When cdk2 is inhibited with an inhibitor, the majority of cells still formed multiple centrosomes. In these cells, cyclin E was co-stained with ubiquitin, some co-stained with cdk2, while some others co-stained with both cdk2 and ubiquitin.

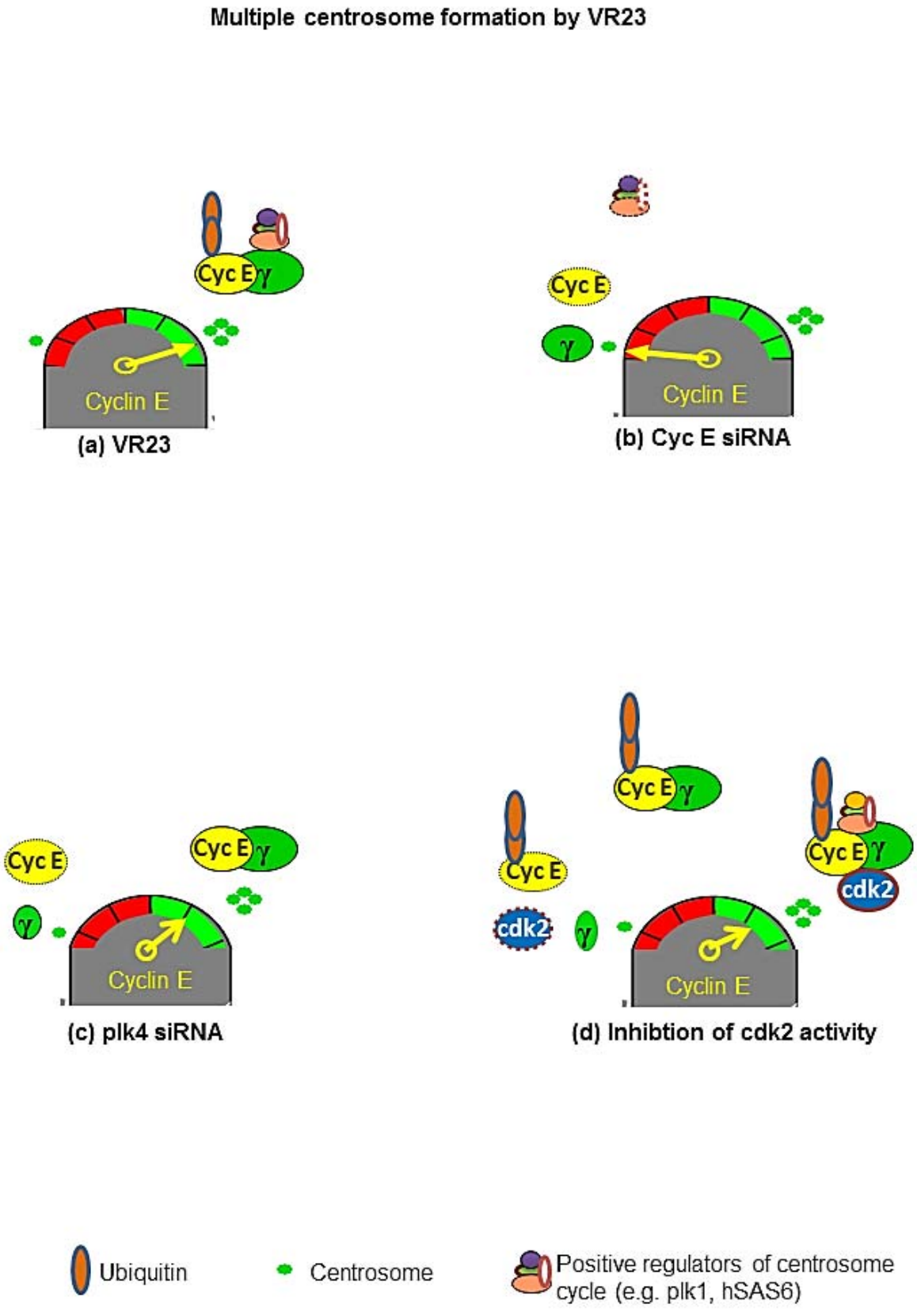
Multiple centrosome formation by VR23
Cyc E
γ
Cyclin E
(a) VR23
Cyc E
γ
Cyclin E
(b) Cyc E siRNA
Cyc E
γ
Cyclin E
(c) plk4 siRNA
Cyc E
γ
Cyc E
cdk2
γ
Cyclin E
(d) Inhibtion of cdk2 activity
Ubiquitin
Centrosome
Positive regulators of centrosome cycle (e.g. plk1, hSAS6)

Figure 36: VR23 treatment does not lead to the formation of multiple centrosomes or accumulation of cyclin E, plk1 or plk4 at centrosomes in the MCF10A non-malignant cells

MCF10A cells synchronized at G1/S were fixed at 3 h post-release from G1/S. Cells were immunostained with antibodies specific for γ-tubulin (green), Cyclin E (**A**), plk1 (**B**) or plk4 (**C**) (red), DNA was stained with DRAQ5 (blue).
A. Unlike the malignant HeLa S3 and MCF7 cells, multiple centrosomes were not observed in VR23-treated MCF10A cells, in which case cyclin E was not co-localized with γ-tubulin.
B. Plk1 was not co-localized with γ-tubulin in VR23-treated cells.
C. Unlike VR23-treated HeLa S3 cells, plk4 co-localizes to centrosomes in the non-malignant MCF10A cells treated with VR23 (**b**). The experiment was performed three times, and representative figures are shown. Images were captured by confocal microscopy.

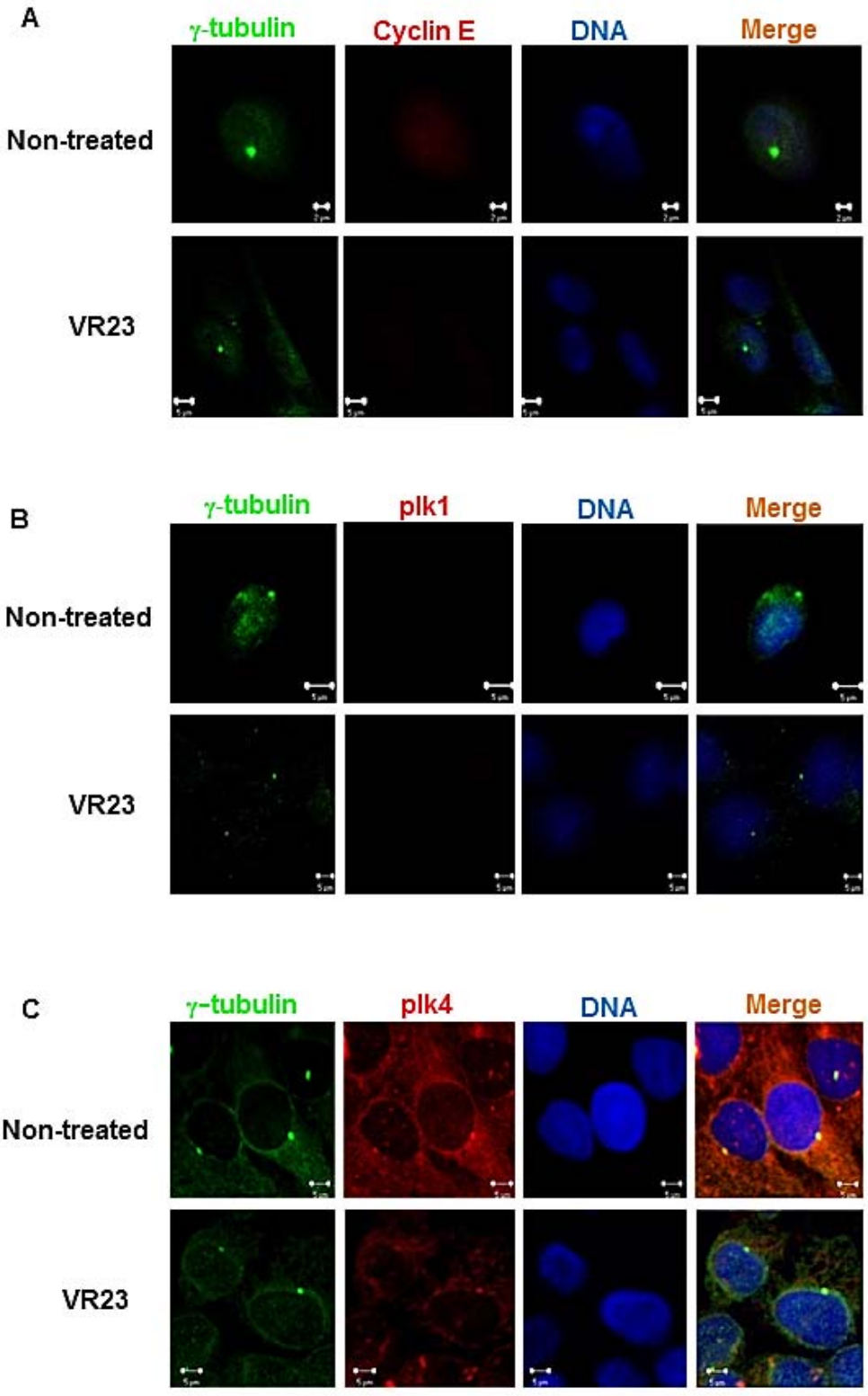
A
γ-tubulin
Cyclin E
DNA
Merge
Non-treated
VR23
B
γ-tubulin
plk1
DNA
Merge
Non-treated
VR23
C
γ-tubulin
plk4
DNA
Merge
Non-treated
VR23

exposure (24 h) to VR23 (Fig. A14). The accumulation of excessive cyclin E was not found in MCF10A non-malignant cells regardless, its ubiquitination status. This provides further evidence in support of cyclin E accumulation at centrosomes in the presence of VR23, driving *de novo* centrosomes formation.

4.0 DISCUSSION

4.1 Identification of VR23, a promising proteasome inhibitor

Screening the library of compounds designed and synthesized in Dr. Hoyun Lee's lab identified VR23, a compound which showed preferential cytotoxicity toward malignant cells. VR23 was initially selected from cytotoxicity assay and was then confirmed for its efficacy by cell survival assays (Fig. 7, Table 3). This compound was selected for further studies as it caused apoptosis in malignant cell lines while showing no cell death in non-malignant cells (Fig. 7). Similarly to CQ, VR23 preferentially kills cancer cells over non-cancer cells. Furthermore, an animal study revealed that VR23 does not have any notable ill-effects to animals. (Determined from animal toxicology and efficacy studies; not described in this thesis). VR23, when combined with other drugs such as paclitaxel, substantially increases the efficacy in selectively killing malignant cells while reducing the toxicity caused by paclitaxel (data from animal work).

The most striking feature of VR23 is that it is a strong inhibitor of trypsin-like activity of the proteasome. Recent efforts to develop specific trypsin-like inhibitors have been met with limited success (171). Current proteasome inhibitors show increased toxicity toward malignant hematologic cells with very limited cytotoxicity toward solid tumors (172). The most important property of VR23 that distinguishes it from existing proteasome inhibitors is that it inhibits solid tumors with high efficacy (data from animal studies). Furthermore, unlike VR23, other reported proteasome inhibitors (e.g., bortezomib® and PR-171) lack specificity toward killing malignant cells over non-malignant cells (172-174). Inhibiting all three sites of the proteasome (β1, β2, and β5) may increase the efficacy in killing cells but it may also lead to undesirable side-effects on non-malignant cells (175). Thus, selective

inhibition of only one specific site at a low dose by VR23 can increase its selectivity toward malignant cells while retaining sufficient anti-tumor activity. Thus, while complete inhibition of proteasomes may increase malignant cell death, but the inhibition of one specific site effectively (in this case, trypsin-like) may improve the therapeutic effect with low side effects.

The experiments presented in this thesis demonstrates that the inhibition of proteasome activity is the key property of VR23 that leads to the accumulation and localization of ubiquitinated cyclin E at the centrosomes and discrete sites in the cytoplasm in malignant cells but not in non-malignant cells.

4.2 VR23 binds primarily to the β2 subunit of proteasomes

Compounds with a high degree of selectivity have been developed for the β5 subunit of proteasomes, whereas the attempts for the selective inhibition of the β2 and β1 subunits have been less successful (171). Among many proteasome inhibitors designed in the recent years, a non-toxic drug primarily site-specific for trypsin-like activity was notably missing. This could be because the chymotrypsin-like site was previously considered as the only site suitable for drug development against proteasomes (175, 176). However, recent data suggests that the trypsin-like site is an important co-target for proteasome targeting drugs. NC-022 has been reported as a site specific inhibitor of trypsin-like activity. However, a toxicity study of NC-022 is currently unavailable (171).

Suppression of the proteolytic activity of the proteasome depends on the N-terminal threonine residue hydroxyl group, as it is responsible for the cleavage of peptides by the nucleophilic attack (177-179). Interestingly, the most energetically

favourable conformation found for VR23 at the β2 subunit was the one where the sulfone group of VR23 would form a hydrogen bond with the N-terminal threonine group (Figs. 18, 19 and, A10).

The tripeptide vinyl sulfone (Z-L_3VS) and related compounds inhibit proteasome activity by a covalent modification of the amino-terminal threonine of the catalytically active β subunit (177, 179-182). Selective covalent binding with the targets is considered highly beneficial because it brings increased biochemical efficiency, as desired inhibition can be achieved at a lower dose. Lower drug doses can avoid off-target effects. Similar to vinyl sulfone proteasome inhibitors, the binding potency of the VR23 depends strongly upon the sulfone group of VR23 (Figs. 18, 19 and A10). However, VR23 displays better characteristics in terms of selectivity and potency compared to the vinyl sulfones. Vinyl sulfones also have very poor cell permeability (171). At a concentration of 1 nM, VR23 specifically and effectively inhibits the activity of trypsin-like proteasome (Fig. 15, and Table 4.). This unique property can be exploited in future to study the role of trypsin-like sites in the protein degradation and other biological processes.

Recent work by the Kisselev's group (182) suggests that the inhibition of trypsin-like sites sensitizes cell death when combined with the inhibitors of chymotrypsin-like activity. With respect to this aspect, VR23 binds to the substrate binding site in β2 and may inhibit β5 activity allosterically (Fig. 17).

4.3 VR23 deregulates the centrosome cycle by stabilizing ubiquitinated cyclin E at centrosomes

VR23 specifically amplifies the centrosomes in cancer cells through the stabilization of ubiquitinated cyclin E in cytoplasm. (Figs. 27 and 32). Multiple centrosomes can be formed by the following mechanisms: cell cycle arrest in S-phase, aborted mitosis, cell fusion and *de novo* formation. The formation of centrosomes from mother centrosomes is known as “template” dependent, whereas the concurrent formation of multiple centrosomes is known as “*de novo*” mechanism (183). HeLa cells have been previously shown to induce centrosome amplification by the *de novo* pathway (184). However, typically the presence of a single centrosome suppresses or inhibits the *de novo* pathway in a cell. Therefore, it was concluded in previous studies that centrosomes have to be removed (by laser microsurgery) to induce *de novo* pathway. In contrast, the mechanism by which *de novo* centrosomes are formed in VR23-treated cells is unique in that multiple centrosomes are synthesized in the presence of pre-existing centrosomes.

Drugs such as hydroxyurea and aphidicolin that inhibit S phase progression can cause multiple centrosomes in cells lacking p53. No arrest or inhibition of DNA replication was seen in VR23-treated cells 3 h post-release from G1/S arrest, the time when centrosome amplification is observed (Figs. 14, 30). This rule out that centrosomes are not amplified simply due to cells being arrested in G1/S (or S) which is the case of cells arrested by hydroxyurea or aphidicolin. VR23 is thus causing the centrosome amplification via a different mechanism. Similarly, abnormal centrosome amplification was still seen when cells in G2/M (i.e., 6 h post-G1/S) were treated with VR23 for 6 h. Since cells in G1/S form multiple centrosomes in the presence of VR23, this rules out abortive mitosis. Thus, multiple centrosomes formed by VR23 are most likely due to *de novo* synthesis.

Furthermore, the formation of more than 5 centrosomes per cell occurred within 3 h in VR23-treated cells. It is difficult to conceive that the formation of multiple centrosomes in such a short time is the result of successive rounds of “template” dependent centrosomes duplication.

The formation of multiple centrosomes was seen in the p53-wild type MCF7 cell line as well as p53-defective HeLa S3 cell line (Figs. 20 and A11). Therefore, it can be inferred that the effect of VR23 is p53-status independent. Knockdown of cyclin E using siRNA in the presence of VR23 prevented the cells from forming multiple centrosomes, indicating that the effect of VR23 is dependent upon cyclin E (Fig. 27). In further support of this, the accumulation of cyclin E was not observed in MCF10A cells, which does not form multiple centrosomes (Figs. 16, 36 and A14). In contrast, HeLa S3 and MCF7 showed significant accumulation of ubiquitinated cyclin E at centrosomes and increased number and size of centrosomes (Figs. 32 and A11).

Although it has been shown previously that proteasome inhibition leads to the accumulation of centrosomal proteins, the effect of proteasome inhibition on the centrosome duplication cycle has not been studied in detail. Therefore, a detailed mechanism characterizing the formation of centrosome amplification by proteasome inhibition remains to be explored.

A study by Duensing, *et al.* (89) reported that the proteasome inhibitor Z-L_3VS caused the formation of multiple centrioles concurrently from a single mother centriole in a “rosette” like arrangement within 48 h. VR23 differs from Z-L_3VS in that it causes the formation of multiple centrosomes within 3 h and the distribution of these centrosomes is random in a cell (Fig. 20). The Z-L_3VS caused the

formation of multiple centrosomes by the overexpression of plk4 and cyclin E. In contrast, plk4 was not found to be overexpressed or co-localized with γ-tubulin in VR23-treated cells (Fig. 28 and A15). The knockdown of cyclin E rescued the centrosome amplification phenotype in 100% of cells. A 37.5% decrease in cells with multiple centrosomes was also observed in plk4 knockdown cells (Fig. 28). However, all the cells in the plk4 knockdown samples that formed multiple centrosomes still had cyclin E co-localized with γ-tubulin. This suggests that if cyclin E is co-localized with γ-tubulin, multiple centrosomes are formed irrespective of the presence of plk4.

The majority of cells showed cyclin E co-localized with γ-tubulin in the plk4 knockdown cells, and these cells formed multiple centrosomes. It still remains to be elucidated why the other half of the population did not show cyclin E co-localization with γ-tubulin and no formation of multiple centrosomes is observed. This could either be because the knockdown of plk4 could be affecting the cell cycle progression of certain populations of cells, and is preventing a cell from reaching a point required for cyclin E-mediated centrosome amplification. Alternatively, plk4 could be working either downstream or in parallel to cyclin E in centrosome biogenesis. However, since plk4 was not found to be co-localized with γ-tubulin in the majority of cells, this latter possibility is unlikely. Another possibility is that plk4 localization is only transient at centrosomes and it could be working upstream of cyclin E and this transient localization escaped its detection in microscopy at fixed timepoints. However, non-treated cells still showed the localization of plk4 at centrosomes at the same timepoints, so the transient localization could not explain the absence of plk4 co-localization with γ-tubulin in the presence of VR23.

Because plk4 was still present in VR23-treated cells, as seen by Western blot (Fig. A15.), its presence in the cell may affect the localization and regulation of other proteins involved in centriole biogenesis for e.g. Cep135 and CPAP.

The constitutive presence of cyclin E at centrosomes in the presence of VR23 may overcome the requirement of localization of plk4 at centrosomes and plk4-dependent *de novo* centrosome amplification. This is further supported by the fact that the minority of cells in the VR23-treated samples where plk4 co-stained with γ-tubulin did not show the formation of multiple centrosomes (Fig. A15). Further study is needed to explain the regulation of plk4 in the presence of excessive cyclin E accumulation at centrosomes.

The activity of cdk2 is very high during G1/S, which drives centrosome amplification. The activity of cyclin E can also be inhibited, in part, by inhibiting its binding partner cdk2 (85, 126). The next question addressed was whether the accumulation of cyclin E alone in cytoplasm can cause centrosome over-amplification, or it is driven by cyclin E acting in complex with cdk2. I therefore investigated the effect of cdk2 inhibition on centrosome amplification. Cdk2 inhibition still allowed for the accumulation of ubiquitinated cyclin E and caused the *de novo* formation of multiple centrosomes in VR23-treated cells (Fig. 31). Using microscopy and immunoprecipitation, it was observed that cdk2-cyclin E complex co-localized to the γ-tubulin sites. Inhibition of cdk2 did rescue some cells from the multiple centrosome phenotype (Figs. 31 and 34), and many cells had several ‘small’-sized centrosomes with no cdk2 localization at smaller sized centrosomes.

When cyclin E dissociates from cdk2, it becomes tagged with ubiquitin marking it for degradation by proteasomes. This is one mechanism how cyclin E

turnover is regulated. The use of the proteasome inhibitor may cause an excess of cyclin E available for cdk2 to bind. Free cyclin E is readily ubiquitinated and localizes to centrosomes and in the cytoplasm. As shown in figure 34, the inhibition of cdk2 increased the accumulation of ubiquitinated cyclin E in the cytoplasm, which was bound to cdk2 (Fig. 34). Thus, the excessive number of cyclin E molecules oversaturates the available cdk2 molecules in the cell. In this case, ubiquitinated/non-ubiquitinated cyclin E molecules may bind to cdk2 or exist as unbound free molecule.

Overexpression of cyclin E in the absence of a functional p53 and p21 can lead to amplification of centrosomes (107). Studies have shown that a loss of cyclin E does not lead to the abrogation of centrosome formation because cyclin A can compensate for the lack of cyclin E in centrosome duplication (93). When cyclin E was knocked down in VR23-treated cells, centrosome amplification was completely inhibited. This suggests that cyclin A is not involved in the VR23-mediated centrosome amplification, even though cyclin A is co-localized with γ-tubulin in VR23-treated cells (Fig 23). This data also raises the possibility that *de novo* centrosome amplification can only be induced by cyclin E accumulation, whereas cyclin A plays only a role in template-dependent duplication of centrosomes. Future study will be needed to shed light on the difference between these two specific mechanisms of centrosome duplication in more detail.

To explain why HeLa S3 cells form an increased number of centrosomes but not MCF10A cells, I found that cyclin E was not co-localized with γ-tubulin in MCF10A cells, unlike in MCF7 and HeLa S3 cells (Figs. 36 and A14). Thus, cells without excessive accumulation of cyclin E did not form multiple centrosomes. My

results are in line with a previous study which reported that the use of proteasome inhibitor did not induce multiple centrosomes in the IMR-90 normal fibroblast cell line (148). Further study on the regulation of cyclin E and proteasome activity is needed to explain this differential phenotype between non-malignant and malignant cells.

The proteasome inhibitor ZL_3-VS causes multiple centrosomes in U2OS cells and, to a lesser extent, in T98G and HeLa. Proteasome inhibitors MG262 and MG132 caused the formation of multiple centrosomes but significantly less than Z-L_3VS. Epoxomycin and lactacystin have not been reported to cause formation of multiple centrosomes. Bortezomib® has also been reported to cause the formation of multiple centrosomes in a small sub-population of cells. These differences could be because of the different mechanisms by which these inhibitors inhibit the proteasome activity, and each of them may have several different off-target effects that are yet to be fully elucidated. For example, MG132 inhibits the centrosome separation by inhibiting separase activity (186), thus, preventing further reduplication of centrosomes. Alternatively, some inhibitors may activate different mechanisms of cell death and cell cycle arrest which could prevent cells from reaching a point required for centrosome amplification.

Genomic instability is a hallmark of cancer cells (185, 186). Given the wide use of proteasome inhibitors at clinics and the development of new inhibitors as a strategy against cancer, it is important to characterize the effects of each proteasome inhibitor on the centrosome cycle to avoid potentially unwanted effects.

4.4 Perspectives

The general aim of this thesis has been to study the property of VR23, a novel compound derived from the CQ pharmacophore. The findings from this work suggests that the strong inhibition of trypsin-like proteasome activity in conjunction with the inhibition of chymotrypsin-like activity may offer better therapeutic effect, compared to the complete inhibition of all three proteasomes activities. The significance of the work described in this thesis is two-fold: firstly, VR23 is a non-toxic and specific inhibitor of trypsin-like proteasome activity with high potency. Cell survival assay suggests that we can use VR23 in combination with other chemotherapeutics to increase specificity and efficacy against malignant cells. Secondly, the VR23 effect on cell cycle and centrosome cycle is studied in detail.

Despite the remarkable efficacy of CQ against malignant cells, several limitations of CQ are noted. Most importantly, it is mostly effective only when used in combination with other chemotherapeutic agents. The data described in this thesis suggest that VR23 has superior anti-cancer properties than its parent molecule. It also highlights the potential of the CQ pharmacophore as a lead in the design of effective and safe anticancer drug. An attempt has been made in the work described in this thesis to characterize the multiple effects of VR23 on cell cycle, abnormal centrosome amplification and chromosome missegregation.

In this work, I have shown that the accumulation of ubiquitinated cyclin E is critical mechanism in inducing *de novo* centrosome amplification. This adds to the previous reports of proteasome inhibitors being able to cause centrosome amplification (148, 150, 187). Given the wide use of proteasome inhibitors at clinics to treat leukemia and multiple myeloma, it’s important to investigate the possibility

of this mechanism potentially leading to genomic instability in cells exposed to proteasome inhibitors, if apoptosis is not activated. I report here, for the first time, that accumulated ubiquitinated cyclin E can synthesize centrosomes *de novo* in the absence of plk4 overexpression.

It has been reported previously that transformed cells are more sensitive to proteasome inhibition than normal cells (175, 188). The observation that the similar doses of VR23 show only a minimal effect in non-malignant cells is a very desirable property for an anti-cancer drug. However, the precise mechanism for this differential response is a subject of further studies. Three possible explanations for this differential response could be: (a) Previously, it has been reported that quiescent cells are not effected by proteasome inhibition, whereas the actively replicating cells are severely affected by proteasome inhibition (188). The high proliferating rate of malignant cells may make them more sensitive to the drug. However, the proliferating rates of MCF10A and 184B5 cells are not significantly different from malignant cells in *in vitro* cell culture conditions. Therefore, this possibility may not be the case of VR23 exposed cells, at least for my experimental conditions. One plausible explanation could be that malignant cells are often aneuploid, and high chromosome numbers may lead to the overproduction of certain proteins. This may cause an overload of protein complexes in malignant cells. Their high dependency on the proteasome system to regulate the degradation/recycling of extra proteins may make malignant cells overly sensitive to even a slight inhibition of proteasome activity. (b) It has been previously reported that a sub-population of lymphoblastoid cells are able to survive in the presence of proteasome inhibition. This survival was not due to multi-

drug resistance or genetic mutations, but these cells could survive by up-regulating protease expression that can compensate for the inhibited proteasomes. It still remains to be explored if MCF10A or VR23-resistant cells such as T98G have similar mechanisms. MCF10A cells did not show any increase in the accumulation of cyclin E either at high concentration of the drug (40 μM) or at long treatment duration (24 h). Perhaps some other proteases may function in these cell lines to compensate for the known proteasome activity in degrading cyclin E. (c) A third possibility is that VR23 may not effectively penetrate through the cell membrane of MCF10A cells. Selective permeability of the cell membrane and the presence of pumps expulsing drugs from the cell have been previously noted reasons for drug resistance in cells (189, 190). Experiments using labeled or tagged VR23 molecules allowing VR23 to be monitored in cells may give the definitive answer in future.

The properties of VR23 provide an extremely promising tool to study biological mechanisms, in addition to its potential as an effective and safe anticancer drug. The findings described in this thesis elucidate a basis for the evaluation of VR23 as an effective and safe anti-cancer agent to be used alone or in combination with existing chemotherapeutic agents.

Figure 37: Proposed model of *de novo* formation of centrosomes by VR23

Inhibition of proteolytic activity by VR23 prevents the cyclical degradation of centrosome regulatory proteins at centrosomes. As a result, proteins (such as cyclin E) accumulate at centrosomes and at discrete sites in the cytoplasm which in turn, attract other centrosomal proteins (plk1, hSAS-6, centriolin). This accrual of proteins leads to formation of *de novo* centrosomes.

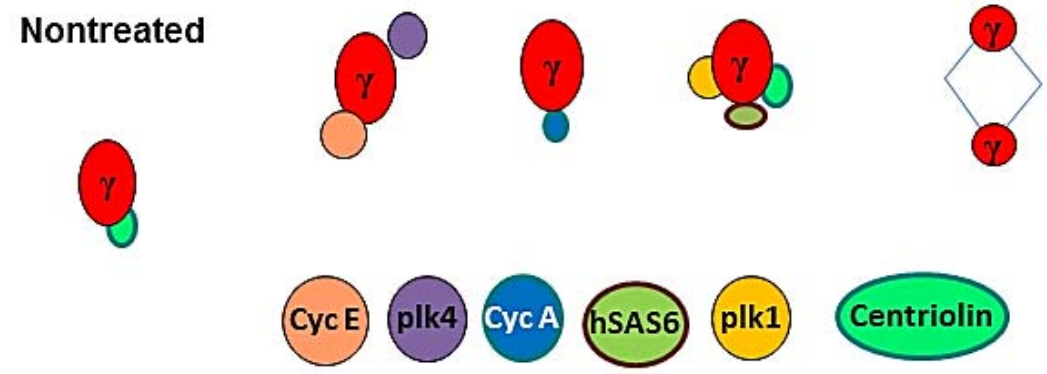

Cell cycle	G1	S	G2	Mitosis

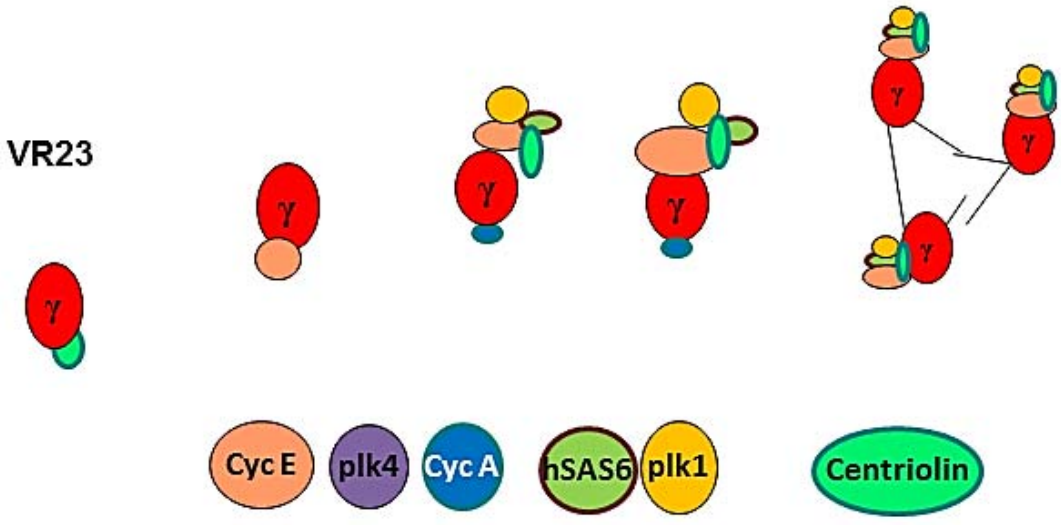

5.0 References

1. Kimura, T., Takabatake, Y., Takahashi, A. & Isaka, Y. Chloroquine in cancer therapy: a double-edged sword of autophagy. Cancer Res. 73, 3–7 (2013).

2. Zhao, H., Cai, Y., Santi, S., Lafrenie, R. & Lee, H. Chloroquine-mediated radiosensitization is due to the destabilization of the lysosomal membrane and subsequent induction of cell death by necrosis. Radiat. Res. 164, 250–257 (2005).

3. Sasaki, K. et al. Chloroquine potentiates the anti-cancer effect of 5-fluorouracil on colon cancer cells. BMC Cancer 10, 370 (2010).

4. Hu, C., Solomon, V. R., Ulibarri, G. & Lee, H. The efficacy and selectivity of tumor cell killing by Akt inhibitors are substantially increased by chloroquine. Bioorganic Med. Chem. 16, 7888–7893 (2008).

5. Vazquez-Martin, A. *et al.* Repositioning chloroquine and metformin to eliminate cancer stem cell traits in pre-malignant lesions. *Drug Resist. Updat.* 14, 212–223 (2011).

6. Cufí, S. *et al.* The anti-malarial chloroquine overcomes primary resistance and restores sensitivity to trastuzumab in HER2-positive breast cancer. *Sci. Rep.* 3, 2469 (2013).

7. Maycotte, P. *et al.* Chloroquine sensitizes breast cancer cells to chemotherapy independent of autophagy. *Autophagy* 8, 200–212 (2012).

8. Carew, J. S. *et al.* Targeting autophagy augments the anticancer activity of the histone deacetylase inhibitor SAHAto overcome Bcr-Abl-mediated drug resistance. *Blood* 110, 313–322 (2007).

9. Firat, E., Weyerbrock, A., Gaedicke, S., Grosu, A. L. & Niedermann, G. Chloroquine or Chloroquine-PI3K/Akt Pathway Inhibitor Combinations Strongly Promote Irradiation-Induced Cell Death in Primary Stem-Like Glioma Cells. *PLoS One* 7, (2012).

10. Wang, Y. *et al.* Chloroquine enhances the cytotoxicity of topotecan by inhibiting autophagy in lung cancer cells. *Chin. J. Cancer* 30, 690–700 (2011).

11. Verschooten, L. *et al.* Autophagy Inhibitor Chloroquine Enhanced the Cell Death Inducing Effect of the Flavonoid Luteolin in Metastatic Squamous Cell Carcinoma Cells. *PLoS One* 7, (2012).

12. Anchoori, R. K. *et al.* Stressing the ubiquitin-proteasome system without 20s proteolytic inhibition Selectively Kills cervical cancer cells. *PLoS One* 6, (2011).

13. Adar, Y. *et al.* Imidazoacridinone-dependent lysosomal photodestruction: a pharmacological Trojan horse approach to eradicate multidrug-resistant cancers. *Cell Death Dis.* 3, e293 (2012).

14. Bellodi, C. *et al.* Targeting autophagy potentiates tyrosine kinase inhibitor-induced cell death in Philadelphia chromosome-positive cells, including primary CML stem cells. *J. Clin. Invest.* 119, 1109–1123 (2009).

15. Liang, X. *et al.* Inhibiting systemic autophagy during interleukin 2 immunotherapy promotes long-term tumor regression. *Cancer Res.* 72, 2791–2801 (2012).

16. Wu, Z. *et al.* Autophagy Blockade Sensitizes Prostate Cancer Cells towards Src Family Kinase Inhibitors. *Genes Cancer* 1, 40–49 (2010).

17. Ghadimi, M. P. *et al.* Targeting the PI3K/mTOR Axis, Alone and in Combination with Autophagy Blockade, for the Treatment of Malignant Peripheral Nerve Sheath Tumors. *Mol. Cancer Ther.* 11, 1758–1769 (2012).

18. Levy, J. M. M. *et al.* Autophagy inhibition improves chemosensitivity in BRAFV600E brain tumors. *Cancer Discov.* 4, 773–780 (2014).

19. Correa, R. J. M. *et al.* Combination of AKT inhibition with autophagy blockade effectively reduces ascites-derived ovarian cancer cell viability. *Carcinogenesis* bgu049– (2014).

20. Solomon, V. R. & Lee, H. Chloroquine and its analogs: A new promise of an old drug for effective and safe cancer therapies. *Eur. J. Pharmacol.* 625, 220–233 (2009).

21. Strekowski, L. et al. Structure-activity relationship analysis of substituted 4-quinolinamines, antagonists of immunostimulatory CpG-oligodeoxynucleotides. Bioorg. Med. Chem. Lett. 9, 1819–1824 (1999).

22. Strekowski, L. et al. Synthesis and activity of substituted 2-phenylquinolin-4-amines, antagonists of immunostimulatory CpG-oligodeoxynucleotides. J. Med. Chem. 46, 1242–1249 (2003).

23. Hu, C., Raja Solomon, V., Cano, P. & Lee, H. A 4-aminoquinoline derivative that markedly sensitizes tumor cell killing by Akt inhibitors with a minimum cytotoxicity to non-cancer cells. Eur. J. Med. Chem. 45, 705–709 (2010).

24. Jiang, N. et al. Design, synthesis and cytotoxicity of novel 2-arylvinyl-4-aminoquinoline derivatives. Chem. Pharm. Bull. (Tokyo). 60, 659–64 (2012).

25. An, Z. Y. et al. Synthesis and evaluation of graveoline and graveolinine derivatives with potent anti-angiogenesis activities. Eur. J. Med. Chem. 45, 3895–3903 (2010).

26. Abouzid, K. & Shouman, S. Design, synthesis and in vitro antitumor activity of 4-aminoquinoline and 4-aminoquinazoline derivatives targeting EGFR tyrosine kinase. Bioorganic Med. Chem. 16, 7543–7551 (2008).

27. Zhang, H., Solomon, V. R., Hu, C., Ulibarri, G. & Lee, H. Synthesis and in vitro cytotoxicity evaluation of 4-aminoquinoline derivatives. *Biomed. Pharmacother.* 62, 65–69 (2008).

28. Kisselev, A. F. et al. The caspase-like sites of proteasomes, their substrate specificity, new inhibitors and substrates, and allosteric interactions with the trypsin-like sites. J. Biol. Chem. 278, 35869–35877 (2003).

29. Kisselev, A. F., Akopian, T. N., Castillo, V. & Goldberg, A. L. Proteasome active sites allosterically regulate each other, suggesting a cyclical bite-chew mechanism for protein breakdown. Mol. Cell 4, 395–402 (1999).

30. Kisselev, a F. & Goldberg, a L. Proteasome inhibitors: from research tools to drug candidates. Chem.Biol. 8, 739–758 (2001).

31. Ruschak, A. M., Slassi, M., Kay, L. E. & Schimmer, A. D. Novel proteasome inhibitors to overcome bortezomib resistance. J. Natl. Cancer Inst. 103, 1007–1017 (2011).

32. Chauhan, D., Hideshima, T. & Anderson, K. C. A novel proteasome inhibitor NPI-0052 as an anticancer therapy. Br. J. Cancer 95, 961–965 (2006).

33. Li, X. et al. Effect of noncompetitive proteasome inhibition on bortezomib resistance. J. Natl. Cancer Inst. 102, 1069–1082 (2010).

34. Jiang, P. D. *et al.* Cell Growth Inhibition, G(2)/M Cell Cycle Arrest, and Apoptosis Induced by Chloroquine in Human Breast Cancer Cell Line Bcap-37. *Cell. Physiol. Biochem.* 22, 431–440 (2008).

35. Bush, K. T., Goldberg, A. L. & Nigam, S. K. Proteasome inhibition leads to a heat-shock response, induction of endoplasmic reticulum chaperones, and thermotolerance. *J. Biol. Chem.* 272, 9086–9092 (1997).

36. Palombella, V. J., Rando, O. J., Goldberg, A. L. & Maniatis, T. The ubiquitin-proteasome pathway is required for processing the NF-kB1 precursor protein and the activation of NF-kB. Cell 78, 773–785 (1994).

37. Alkalay, I. et al. Stimulation-dependent I kappa B alpha phosphorylation marks the NF-kappa B inhibitor for degradation via the ubiquitin-proteasome pathway. Proc. Natl. Acad. Sci. U. S. A. 92, 10599–10603 (1995).

38. Traenckner, E. B., Wilk, S. & Baeuerle, P. A. A proteasome inhibitor prevents activation of NF-kappa B and stabilizes a newly phosphorylated form of I kappa B-alpha that is still bound to NF-kappa B. EMBO J. 13, 5433–5441 (1994).

39. Strauss, S. J. et al. The proteasome inhibitor bortezomib acts independently of p53 and induces cell death via apoptosis and mitotic catastrophe in B-cell lymphoma cell lines. Cancer Res. 67, 2783–2790 (2007).

40. Fleming, J. A. et al. Complementary whole-genome technologies reveal the cellular response to proteasome inhibition by PS-341. Proc. Natl. Acad. Sci. U. S. A. 99, 1461–1466 (2002).

41. Reddy, S. K., Rape, M., Margansky, W. A. & Kirschner, M. W. Ubiquitination by the anaphase-promoting complex drives spindle checkpoint inactivation. Nature 446, 921–925 (2007).

42. Ling, Y.-H., Liebes, L., Zou, Y. & Perez-Soler, R. Reactive oxygen species generation and mitochondrial dysfunction in the apoptotic response to Bortezomib, a novel proteasome inhibitor, in human H460 non-small cell lung cancer cells. J. Biol. Chem. 278, 33714–33723 (2003).

43. Joyce, D. *et al.* NF-kB and cell-cycle regulation: The cyclin connection. *Cytokine Growth Factor Rev.* 12, 73–90 (2001).

44. Montagnoli, A. et al. Ubiquitination of p27 is regulated by Cdk-dependent phosphorylation and trimeric complex formation. Genes Dev. 13, 1181–1189 (1999).

45. Sterz, J. et al. BSc2118 is a novel proteasome inhibitor with activity against multiple myeloma. Eur. J. Haematol. 85, 99–107 (2010).

46. Mi, L., Gan, N. & Chung, F. L. Isothiocyanates inhibit proteasome activity and proliferation of multiple myeloma cells. Carcinogenesis 32, 216–223 (2011).

47. Zhang, W. & Liu, H. T. MAPK signal pathways in the regulation of cell proliferation in mammalian cells. Cell Res. 12, 9–18 (2002).

48. Befani, C. D. et al. Bortezomib represses HIF-1α protein expression and nuclear accumulation by inhibiting both PI3K/Akt/TOR and MAPK pathways in prostate cancer cells. J. Mol. Med. 90, 45–54 (2012).

49. Chen, L. & Madura, K. Increased proteasome activity, ubiquitin-conjugating enzymes, and eEF1A translation factor detected in breast cancer tissue. Cancer Res. 65, 5599–5606 (2005).

50. Kumatori, A. et al. Abnormally high expression of proteasomes in human leukemic cells. Proc. Natl. Acad. Sci. U. S. A. 87, 7071–7075 (1990).

51. Hideshima, T., Richardson, P. G. & Anderson, K. C. Mechanism of Action of Proteasome Inhibitors and Deacetylase Inhibitors and the Biological Basis of Synergy in Multiple Myeloma. Mol. Cancer Ther. 10, 2034–2042 (2011).

52. Hideshima, T. et al. The proteasome inhibitor PS-341 inhibits growth, induces apoptosis, and overcomes drug resistance in human multiple myeloma cells. Cancer Res. 61, 3071–3076 (2001).

53. Masdehors, P., Merle-Béral, H., Magdelénat, H. & Delic, J. Ubiquitin-proteasome system and increased sensitivity of B-CLL lymphocytes to apoptotic death activation. Leuk. Lymphoma 38, 499–504 (2000).

54. Orlowski, R. Z. et al. Tumor growth inhibition induced in a murine model of human Burkitt's lymphoma by a proteasome inhibitor. Cancer Res 58, 4342–4348 (1998).

55. An, B., Goldfarb, R. H., Siman, R. & Dou, Q. P. Novel dipeptidyl proteasome inhibitors overcome Bcl-2 protective function and selectively accumulate the cyclin-dependent kinase inhibitor p27 and induce apoptosis in transformed, but not normal, human fibroblasts. Cell Death Differ. 5, 1062–1075 (1998).

56. Franke, N. E. et al. Impaired bortezomib binding to mutant β5 subunit of the proteasome is the underlying basis for bortezomib resistance in leukemia cells. Leukemia 26, 757–768 (2012).

57. Fuchs, D., Berges, C., Opelz, G., Daniel, V. & Naujokat, C. Increased expression and altered subunit composition of proteasomes induced by continuous proteasome inhibition establish apoptosis resistance and hyperproliferation of Burkitt lymphoma cells. J. Cell. Biochem. 103, 270–283 (2008).

58. Glas, R., Bogyo, M., McMaster, J. S., Gaczynska, M. & Ploegh, H. L. A proteolytic system that compensates for loss of proteasome function. Nature 392, 618–622 (1998).

59. Geier, E. et al. A giant protease with potential to substitute for some functions of the proteasome. Science 283, 978–981 (1999).

60. Chauhan, D. et al. Combination of proteasome inhibitors bortezomib and NPI-0052 trigger in vivo synergistic cytotoxicity in multiple myeloma. Blood 111, 1654–1664 (2008).

61. Kuhn, D. J. et al. Targeted inhibition of the immunoproteasome is a potent strategy against models of multiple myeloma that overcomes resistance to conventional drugs and nonspecific proteasome inhibitors. Blood 113, 4667–4676 (2009).

62. Ling, Y.-H. et al. Mechanisms of proteasome inhibitor PS-341-induced G(2)-M-phase arrest and apoptosis in human non-small cell lung cancer cell lines. Clin. Cancer Res. 9, 1145–1154 (2003).

63. Gavet, O. & Pines, J. Progressive Activation of CyclinB1-Cdk1 Coordinates Entry to Mitosis. Dev. Cell 18, 533–543 (2010).

64. Guardavaccaro, D. & Pagano, M. Stabilizers and Destabilizers Controlling Cell Cycle Oscillators. Mol. Cell 22, 1–4 (2006).

65. Tsai, T. Y.-C. et al. Robust, tunable biological oscillations from interlinked positive and negative feedback loops. Science 321, 126–129 (2008).

66. Gachet, Y., Tournier, S., Millar, J. B. & Hyams, J. S. A MAP kinase-dependent actin checkpoint ensures proper spindle orientation in fission yeast. Nature 412, 352–355 (2001).

67. Deacon, K., Mistry, P., Chernoff, J., Blank, J. L. & Patel, R. p38 Mitogen-activated protein kinase mediates cell death and p21-activated kinase mediates cell survival during chemotherapeutic drug-induced mitotic arrest. Mol. Biol. Cell 14, 2071–2087 (2003).

68. Boutros, R., Dozier, C. & Ducommun, B. The when and wheres of CDC25 phosphatases. Curr. Opin. Cell Biol. 18, 185–191 (2006).

69. Bulavin, D. V., Amundson, S. A. & Fornace, A. J. p38 and Chk1 kinases: Different conductors for the G2/M checkpoint symphony. Curr. Opin. Genet. Dev. 12, 92–97 (2002).

70. Takenaka, K., Moriguchi, T. & Nishida, E. Activation of the protein kinase p38 in the spindle assembly checkpoint and mitotic arrest. Science (80-.). 280, 599–602 (1998).

71. Mikhailov, A., Shinohara, M. & Rieder, C. L. The p38-mediated stress-activated checkpoint. A rapid response system for delaying progression through antephase and entry into mitosis. Cell Cycle 4, 57–62 (2005).

72. Matsusaka, T. & Pines, J. Chfr acts with the p38 stress kinases to block entry to mitosis in mammalian cells. J. Cell Biol. 166, 507–516 (2004).

73. Scolnick, D. M. & Halazonetis, T. D. Chfr defines a mitotic stress checkpoint that delays entry into metaphase. Nature 406, 430–435 (2000).

74. Nigg, E. A. & Raff, J. W. Centrioles, Centrosomes, and Cilia in Health and Disease. Cell 139, 663–678 (2009).

75. Mennella, V., Agard, D. A., Huang, B. & Pelletier, L. Amorphous no more: Subdiffraction view of the pericentriolar material architecture. Trends Cell Biol. 24, 188–197 (2014).

76. Zheng, X. et al. Conserved TCP domain of Sas-4/CPAP is essential for pericentriolar material tethering during centrosome biogenesis. Proc. Natl. Acad. Sci. U. S. A. 1–10 (2014).

77. Fuller, S. D. et al. The core of the mammalian centriole contains gamma-tubulin. Curr. Biol. 5, 1384–1393 (1995).

78. Rapley, J. et al. Coordinate regulation of the mother centriole component nlp by nek2 and plk1 protein kinases. Mol. Cell. Biol. 25, 1309–1324 (2005).

79. Dammermann, A. & Merdes, A. Assembly of centrosomal proteins and microtubule organization depends on PCM-1. J. Cell Biol. 159, 255–266 (2002).

80. Sonnen, K. F., Gabryjonczyk, A.-M., Anselm, E., Stierhof, Y.-D. & Nigg, E. a. Human Cep192 and Cep152 cooperate in Plk4 recruitment and centriole duplication. J. Cell Sci. 126, 3223–33 (2013).

81. Fu, J. & Glover, D. M. Structured illumination of the interface between centriole and peri-centriolar material. Open Biol. 2, 120104–120104 (2012).

82. Lawo, S., Hasegan, M., Gupta, G. D. & Pelletier, L. Subdiffraction imaging of centrosomes reveals higher-order organizational features of pericentriolar material. Nat. Cell Biol. (2012).

83. Mattison, C. P. & Winey, M. The centrosome cycle. *Results Probl. Cell Differ.* 42, 111–146 (2006).

84. Tarapore, P., Okuda, M. & Fukasawa, K. A mammalian in vitro centriole duplication system: evidence for involvement of CDK2/cyclin E and nucleophosmin/B23 in centrosome duplication. Cell Cycle 1, 75–81 (2002).

85. Okuda, M. et al. Nucleophosmin/B23 is a target of CDK2/cyclin E in centrosome duplication. Cell 103, 127–140 (2000).

86. Fukasawa, K. p53, cyclin-dependent kinase and abnormal amplification of centrosomes. Biochim. Biophys. Acta - Rev. Cancer 1786, 15–23 (2008).

87. Habedanck, R., Stierhof, Y.-D., Wilkinson, C. J. & Nigg, E. A. The Polo kinase Plk4 functions in centriole duplication. Nat. Cell Biol. 7, 1140–1146 (2005).

88. Lacey, K. R., Jackson, P. K. & Stearns, T. Cyclin-dependent kinase control of centrosome duplication. Proc. Natl. Acad. Sci. U. S. A. 96, 2817–2822 (1999).

89. Duensing, A. et al. Cyclin-dependent kinase 2 is dispensable for normal centrosome duplication but required for oncogene-induced centrosome overduplication. Oncogene 25, 2943–2949 (2006).

90. Lange, B. M. H. Integration of the centrosome in cell cycle control, stress response and signal transduction pathways. Curr. Opin. Cell Biol. 14, 35–43 (2002).

91. Stucke, V. M., Sillj, H. H. W., Arnaud, L. & Nigg, E. A. Human Mps1 kinase is required for the spindle assembly checkpoint but not for centrosome duplication. EMBO J. 21, 1723–1732 (2002).

92. Kwiatkowski, N. et al. Small-molecule kinase inhibitors provide insight into Mps1 cell cycle function. Nat. Chem. Biol. 6, 359–368 (2010).

93. Meraldi, P., Lukas, J., Fry, A. M., Bartek, J. & Nigg, E. A. Centrosome duplication in mammalian somatic cells requires E2F and Cdk2-cyclin A. Nat. Cell Biol. 1, 88–93 (1999).

94. Hanashiro, K., Kanai, M., Geng, Y., Sicinski, P. & Fukasawa, K. Roles of cyclins A and E in induction of centrosome amplification in p53-compromised cells. Oncogene 27, 5288–5302 (2008).

95. Tang, C.J. C., Fu, R.H., Wu, K.S., Hsu, W.B. & Tang, T. K. CPAP is a cell-cycle regulated protein that controls centriole length. Nat. Cell Biol. 11, 825–831 (2009).

96. Strnad, P. et al. Regulated HsSAS-6 Levels Ensure Formation of a Single Procentriole per Centriole during the Centrosome Duplication Cycle. Dev. Cell 13, 203–213 (2007).

97. Hatch, E. M., Kulukian, A., Holland, A. J., Cleveland, D. W. & Stearns, T. Cep152 interacts with Plk4 and is required for centriole duplication. J. Cell Biol. 191, 721–729 (2010).

98. Tsou, M. F. B. et al. Polo Kinase and Separase Regulate the Mitotic Licensing of Centriole Duplication in Human Cells. Dev. Cell 17, 344–354 (2009).

99. Fry, A. M. The Nek2 protein kinase: a novel regulator of centrosome structure. Oncogene 21, 6184–6194 (2002).

100. Tsou, M. F. B. & Stearns, T. Controlling centrosome number: Licenses and blocks. Curr. Opin. Cell Biol. 18, 74–78 (2006).

101. Tsou, M.-F. B. & Stearns, T. Mechanism limiting centrosome duplication to once per cell cycle. Nature 442, 947–951 (2006).

102. EH Hinchcliffe, G Sluder. Two for two: Cdk2 and its role in centrosome doubling. Oncogene, 21, (6154-6160) (2002).

103. Rogers, G. C., Rusan, N. M., Roberts, D. M., Peifer, M. & Rogers, S. L. The SCF Slimb ubiquitin ligase regulates Plk4/Sak levels to block centriole reduplication. J. Cell Biol. 184, 225–239 (2009).

104. Holland, A. J. et al. The autoregulated instability of Polo-like kinase 4 limits centrosome duplication to once per cell cycle. Genes Dev. 26, 2684–9 (2012).

105. Kleylein-Sohn, J. et al. Plk4-Induced Centriole Biogenesis in Human Cells. Dev. Cell 13, 190–202 (2007).

106. Rodrigues-Martins, A., Riparbelli, M., Callaini, G., Glover, D. M. & Bettencourt-Dias, M. Revisiting the role of the mother centriole in centriole biogenesis. Science 316, 1046–1050 (2007).

107. Fukasawa, K., Choi, T., Kuriyama, R., Rulong, S. & Vande Woude, G. F. Abnormal centrosome amplification in the absence of p53. Science 271, 1744–1747 (1996).

108. Shinmura, K., Bennett, R. A., Tarapore, P. & Fukasawa, K. Direct evidence for the role of centrosomally localized p53 in the regulation of centrosome duplication. Oncogene 26, 2939–2944 (2007).

109. Bennett, R. a, Izumi, H. & Fukasawa, K. Induction of centrosome amplification and chromosome instability in p53-null cells by transient exposure to subtoxic levels of S-phase-targeting anticancer drugs. Oncogene 23, 6823–9 (2004).

110. Balczon, R. et al. Dissociation of centrosome replication events from cycles of DNA synthesis and mitotic division in hydroxyurea-arrested Chinese hamster ovary cells. J. Cell Biol. 130, 105–115 (1995).

111. Meraldi, P. & Nigg, E. a. The centrosome cycle. FEBS Lett. 521, 9–13 (2002).

112. Matsumoto, Y. & Maller, J. L. A centrosomal localization signal in cyclin E required for Cdk2-independent S phase entry. Science 306, 885–888 (2004).

113. Ferguson, R. L. & Maller, J. L. Cyclin E-dependent localization of MCM5 regulates centrosome duplication. J. Cell Sci. 121, 3224–3232 (2008).

114. Ferguson, R. L. & Maller, J. L. Centrosomal Localization of Cyclin E-Cdk2 Is Required for Initiation of DNA Synthesis. Curr. Biol. 20, 856–860 (2010).

115. Freed, E. et al. Components of an SCF ubiquitin ligase localize to the centrosome and regulate the centrosome duplication cycle. Genes Dev. 13, 2242–2257 (1999).

116. Peel, N. Everything in moderation. Worm 2, 1–4 (2013).

117. Wojcik, C. & DeMartino, G. N. Intracellular localization of proteasomes. Int. J. Biochem. Cell Biol. 35, 579–589 (2003).

118. Puklowski, A. et al. The SCF-FBXW5 E3-ubiquitin ligase is regulated by PLK4 and targets HsSAS-6 to control centrosome duplication. Nat. Cell Biol. 13, 1004–1009 (2011).

119. Hinchcliffe, E. H., Li, C., Thompson, E. A., Maller, J. L. & Sluder, G. Requirement of Cdk2-cyclin E activity for repeated centrosome reproduction in Xenopus egg extracts. Science 283, 851–854 (1999).

120. Eckerdt, F., Yamamoto, T. M., Lewellyn, A. L. & Maller, J. L. Identification of a polo-like kinase 4-dependent pathway for de novo centriole formation. Curr. Biol. 21, 428–432 (2011).

121. Mazumder, S., Gong, B. & Almasan, A. Cyclin E induction by genotoxic stress leads to apoptosis of hematopoietic cells. Oncogene 19, 2828–2835 (2000).

122. Hunt, K. K. & Keyomarsi, K. Cyclin E as a prognostic and predictive marker in breast cancer. Semin. Cancer Biol. 15, 319–326 (2005).

123. Loeb, K. R. et al. A mouse model for cyclin E-dependent genetic instability and tumorigenesis. Cancer Cell 8, 35–47 (2005).

124. Won, K. A. & Reed, S. I. Activation of cyclin E/CDK2 is coupled to site-specific autophosphorylation and ubiquitin-dependent degradation of cyclin E. EMBO J. 15, 4182–4193 (1996).

125. Singer, J. D., Gurian-West, M., Clurman, B. & Roberts, J. M. Cullin-3 targets cyclin E for ubiquitination and controls S phase in mammalian cells. Genes Dev. 13, 2375–2387 (1999).

126. Welcker, M. et al. Multisite phosphorylation by Cdk2 and GSK3 controls cyclin E degradation. Mol. Cell 12, 381–392 (2003).

127. Koepp, D. M. et al. Phosphorylation-dependent ubiquitination of cyclin E by the SCFFbw7 ubiquitin ligase. Science 294, 173–177 (2001).

128. Nakayama, K. et al. Targeted disruption of Skp2 results in accumulation of cyclin E and p27(Kip1), polyploidy and centrosome overduplication. EMBO J. 19, 2069–2081 (2000).

129. Clurman, B. E., Sheaff, R. J., Thress, K., Groudine, M. & Roberts, J. M. Turnover of cyclin E by the ubiquitin-proteasome pathway is regulated by cdk2 binding and cyclin phosphorylation. *Genes Dev.* 10, 1979–1990 (1996).

130. Hao, B., Oehlmann, S., Sowa, M. E., Harper, J. W. & Pavletich, N. P. Structure of a Fbw7-Skp1-Cyclin E Complex: Multisite-Phosphorylated Substrate Recognition by SCF Ubiquitin Ligases. Mol. Cell 26, 131–143 (2007).

131. Strohmaier, H. et al. Human F-box protein hCdc4 targets cyclin E for proteolysis and is mutated in a breast cancer cell line. Nature 413, 316–322 (2001).

132. Kramer, A., Maier, B. & Bartek, J. Centrosome clustering and chromosomal (in)stability: A matter of life and death. Mol. Oncol. 5, 324–335 (2011).

133. Sluder, G. & Nordberg, J. J. The good, the bad and the ugly: The practical consequences of centrosome amplification. Curr. Opin. Cell Biol. 16, 49–54 (2004).

134. Nigg, E. A. Origins and consequences of centrosome aberrations in human cancers. Int. J. Cancer 119, 2717–2723 (2006).

135. Kawamura, E. et al. Identification of novel small molecule inhibitors of centrosome clustering in cancer cells. Oncotarget 4, 1763–1776 (2013).

136. Raab, M. S. et al. GF-15, a novel inhibitor of centrosomal clustering, suppresses tumor cell growth in vitro and in vivo. Cancer Res. 72, 5374–85 (2012).

137. Lingle, W. L. et al. Centrosome amplification drives chromosomal instability in breast tumor development. Proc. Natl. Acad. Sci. U. S. A. 99, 1978–1983 (2002).

138. Mikule, K. et al. Loss of centrosome integrity induces p38-p53-p21-dependent G1-S arrest. Nat. Cell Biol. 9, 160–170 (2007).

139. Sato, N. et al. A possible role for centrosome overduplication in radiation-induced cell death. Oncogene 19, 5281–5290 (2000).

140. Milia, J. et al. Farnesylated RhoB inhibits radiation-induced mitotic cell death and controls radiation-induced centrosome overduplication. Cell Death Differ. 12, 492–501 (2005).

141. Saito, T. et al. Centrosome amplification induced by survivin suppression enhances both chromosome instability and radiosensitivity in glioma cells. Br. J. Cancer 98, 345–355 (2008).

142. Karna, P. et al. A novel microtubule-modulating noscapinoid triggers apoptosis by inducing spindle multipolarity via centrosome amplification and declustering. Cell Death Differ. 18, 632–644 (2011).

143. Liang, Y.-X. et al. Mitotic cell death in BEL-7402 cells induced by enediyne antibiotic lidamycin is associated with centrosome overduplication. World J. Gastroenterol. 10, 2632–2636 (2004).

144. Wigley, W. C. et al. Dynamic association of proteasomal machinery with the centrosome. J. Cell Biol. 145, 481–490 (1999).

145. Tarapore, P., Horn, H. F., Tokuyama, Y. & Fukasawa, K. Direct regulation of the centrosome duplication cycle by the p53-p21Waf1/Cip1 pathway. Oncogene 20, 3173–3184 (2001).

146. Didier, C., Merdes, A., Gairin, J.-E. & Jabrane-Ferrat, N. Inhibition of proteasome activity impairs centrosome-dependent microtubule nucleation and organization. Mol. Biol. Cell 19, 1220–1229 (2008).

147. Loncarek, J., Hergert, P., Magidson, V. & Khodjakov, A. Control of daughter centriole formation by the pericentriolar material. Nat. Cell Biol. 10, 322–328 (2008).

148. Duensing, a et al. Centriole overduplication through the concurrent formation of multiple daughter centrioles at single maternal templates. Oncogene 26, 6280–6288 (2007).

149. Hansen, D. V, Hsu, J. Y., Kaiser, B. K., Jackson, P. K. & Eldridge, A. G. Control of the centriole and centrosome cycles by ubiquitination enzymes. Oncogene 21, 6209–21 (2002).

150. Ehrhardt, A. G. & Sluder, G. Spindle pole fragmentation due to proteasome inhibition. J. Cell. Physiol. 204, 808–818 (2005).

151. Franken, N. A. P., Rodermond, H. M., Stap, J., Haveman, J. & van Bree, C. Clonogenic assay of cells in vitro. Nat. Protoc. 1, 2315–2319 (2006).

152. Vichai, V. & Kirtikara, K. Sulforhodamine B colorimetric assay for cytotoxicity screening. Nat. Protoc. 1, 1112–1116 (2006).

153. Dolbeare, F., Gratzner, H., Pallavicini, M. G. & Gray, J. W. Flow cytometric measurement of total DNA content and incorporated bromodeoxyuridine. Proc. Natl. Acad. Sci. U. S. A. 80, 5573–5577 (1983).

154. Nunez, R. DNA measurement and cell cycle analysis by flow cytometry. Curr. Issues Mol. Biol. 3, 67–70 (2001).

155. Salic, A. & Mitchison, T. J. A chemical method for fast and sensitive detection of DNA synthesis in vivo. Proc. Natl. Acad. Sci. U. S. A. 105, 2415–2420 (2008).

156. Lightcap, E. S. et al. Proteasome inhibition measurements: clinical application. Clin. Chem. 46, 673–683 (2000).

157. Li, X. *et al.* Effect of noncompetitive proteasome inhibition on bortezomib resistance. *J. Natl. Cancer Inst.* 102, 1069–1082 (2010).

158. Groll, M., Berkers, C. R., Ploegh, H. L. & Ovaa, H. Crystal structure of the boronic acid-based proteasome inhibitor bortezomib in complex with the yeast 20S proteasome. Structure 14, 451–456 (2006).

159. Porter, L. A. & Donoghue, D. J. Cyclin B1 and CDK1: nuclear localization and upstream regulators. Prog. Cell Cycle Res. 5, 335–347 (2003).

160. Potapova, T. A., Sivakumar, S., Flynn, J. N., Li, R. & Gorbsky, G. J. Mitotic progression becomes irreversible in prometaphase and collapses when Wee1 and Cdc25 are inhibited. Mol. Biol. Cell 22, 1191–1206 (2011).

161. Kurata, S. Selective activation of p38 MAPK cascade and mitotic arrest caused by low level oxidative stress. J. Biol. Chem. 275, 23413–23416 (2000).129.

162. Kazi, A. et al. Discovery of a novel proteasome inhibitor selective for cancer cells over non-transformed cells. Cell Cycle 8, 1940–1951 (2009).

163. Groll, M. & Huber, R. Inhibitors of the eukaryotic 20S proteasome core particle: A structural approach. Biochim. Biophys. Acta - Mol. Cell Res. 1695, 33–44 (2004).

164. Pannu, V. et al. Induction of robust de novo centrosome amplification, high-grade spindle multipolarity and metaphase catastrophe: a novel chemotherapeutic approach. Cell Death Dis. 3, e346 (2012).

165. Gromley, A. et al. A novel human protein of the maternal centriole is required for the final stages of cytokinesis and entry into S phase. J. Cell Biol. 161, 535–545 (2003).

166. Fabunmi, R. P., Wigley, W. C., Thomas, P. J. & DeMartino, G. N. Activity and regulation of the centrosome-associated proteasome. J. Biol. Chem. 275, 409–413 (2000).

167. Lentini, L., Iovino, F., Amato, A. & Di Leonardo, A. Centrosome amplification induced by hydroxyurea leads to aneuploidy in pRB deficient human and mouse fibroblasts. Cancer Letter. 238, 153–160 (2006).

168. Khodjakov, A. et al. De novo formation of centrosomes in vertebrate cells arrested during S phase. J. Cell Biol. 158, 1171–1181 (2002).

169. Tokuyama, Y., Horn, H. F., Kawamura, K., Tarapore, P. & Fukasawa, K. Specific phosphorylation of nucleophosmin on Thr(199) by cyclin-dependent kinase 2-cyclin E and its role in centrosome duplication. J. Biol. Chem. 276, 21529–21537 (2001).

170. Shapiro, G. I. Cyclin-dependent kinase pathways as targets for cancer treatment. *J. Clin. Oncol.* 24, 1770–83 (2006).

171. Mirabella, A. C. *et al.* Specific cell-permeable inhibitor of proteasome trypsin-like sites selectively sensitizes myeloma cells to bortezomib and carfilzomib. *Chem. Biol.* 18, 608–618 (2011).

172. Bilal Piperdi, Yi-He Ling, Leonard Liebes, *et al.* Bortezomib: Understanding the Mechanism of Action. Mol. Cancer. Ther. 10, 2029-2030 (2011).

173. Voortman, J. & Giaccone, G. Severe reversible cardiac failure after bortezomib treatment combined with chemotherapy in a non-small cell lung cancer patient: a case report. BMC Cancer 6, 129 (2006).

174. Voorhees, P. M., Dees, E. C., Neil, B. O. & Orlowski, R. Z. The Proteasome as a Target for Cancer Therapy. 6316–6325 (2003).

175. Parlati, F. *et al.* Carfilzomib can induce tumor cell death through selective inhibition of the chymotrypsin-like activity of the proteasome. *Blood* 114, 3439–3447 (2009).

176. Adams, J. The development of proteasome inhibitors as anticancer drugs. Cancer Cell 5, 417–421 (2004).

177. Fenteany, G. et al. Inhibition of proteasome activities and subunit-specific amino-terminal threonine modification by lactacystin. Science 268, 726–731 (1995).

178. Bogyo, M., Shin, S., McMaster, J. S. & Ploegh, H. L. Substrate binding and sequence preference of the proteasome revealed by active-site-directed affinity probes. Chem. Biol. 5, 307–320 (1998).

179. Zhang, S. et al. Covalent complexes of proteasome model with peptide aldehyde inhibitors MG132 and MG101: Docking and molecular dynamics study. J. Mol. Model. 15, 1481–1490 (2009).

180. Bogyo, M. et al. Covalent modification of the active site threonine of proteasomal beta subunits and the Escherichia coli homolog HslV by a new class of inhibitors. Proc. Natl. Acad. Sci. U. S. A. 94, 6629–6634 (1997).

181. Johnson, D. S., Weerapana, E. & Cravatt, B. F. Strategies for discovering and derisking covalent, irreversible enzyme inhibitors. Future Med. Chem. 2, 949–964 (2010).

182. Kisselev, A. F., Callard, A. & Goldberg, A. L. Importance of the different proteolytic sites of the proteasome and the efficacy of inhibitors varies with the protein substrate. J. Biol. Chem. 281, 8582–90 (2006).

183. Peel, N., Stevens, N. R., Basto, R. & Raff, J. W. Overexpressing Centriole-Replication Proteins In Vivo Induces Centriole Overduplication and De Novo Formation. Curr. Biol. 17, 834–843 (2007).

184. La Terra, S. et al. The de novo centriole assembly pathway in HeLa cells: cell cycle progression and centriole assembly/maturation. J. Cell Biol. 168, 713–722 (2005).

185. Negrini, S., Gorgoulis, V. G. & Halazonetis, T. D. Genomic instability--an evolving hallmark of cancer. Nat. Rev. Mol. Cell Biol. 11, 220–228 (2010).

186. Hanahan, D. & Weinberg, R. A. Hallmarks of cancer: The next generation. Cell 144, 646–674 (2011).

187. Mailhes, J. B., Hilliard, C., Lowery, M. & London, S. N. MG-132, an inhibitor of proteasomes and calpains, induced inhibition of oocyte maturation and aneuploidy in mouse oocytes. Cell Chromosome 1, 2 (2002).

188. Legesse-Miller, a. et al. Quiescent fibroblasts are protected from proteasome inhibition-mediated toxicity. Mol. Biol. Cell 23, 3566–3581 (2012).

189. Persidis, A. Cancer multidrug resistance. *Nat. Biotechnol.* 17, 94–95 (1999).

190. Shedden, K., Xie, X. T., Chandaroy, P., Chang, Y. T. & Rosania, G. R. Expulsion of small molecules in vesicles shed by cancer cells: Association with gene expression and chemosensitivity profiles. *Cancer Res.* 63, 4331–4337 (2003).

185. Cokic, V. P., Beleslin-Cokic, B. B., Noguchi, C. T. & Schechter, A. N. Hydroxyurea increases eNOS protein levels through inhibition of proteasome activity. Nitric Oxide - Biol. Chem. 16, 371–378 (2007).

188. Swords, R. et al. Cdc7 kinase - A new target for drug development. Eur. J. Cancer 46, 33–40 (2010).

189. Malumbres, M., Pevarello, P., Barbacid, M. & Bischoff, J. R. CDK inhibitors in cancer therapy: what is next? Trends Pharmacol. Sci. 29, 16–21 (2008).

190. Schmidt, M. & Bastians, H. Mitotic drug targets and the development of novel anti-mitotic anticancer drugs. Drug Resist. Updat. 10, 162–181 (2007).

6.0 Appendix

HeLa S3 double thymidine block and release 3 h +VR23

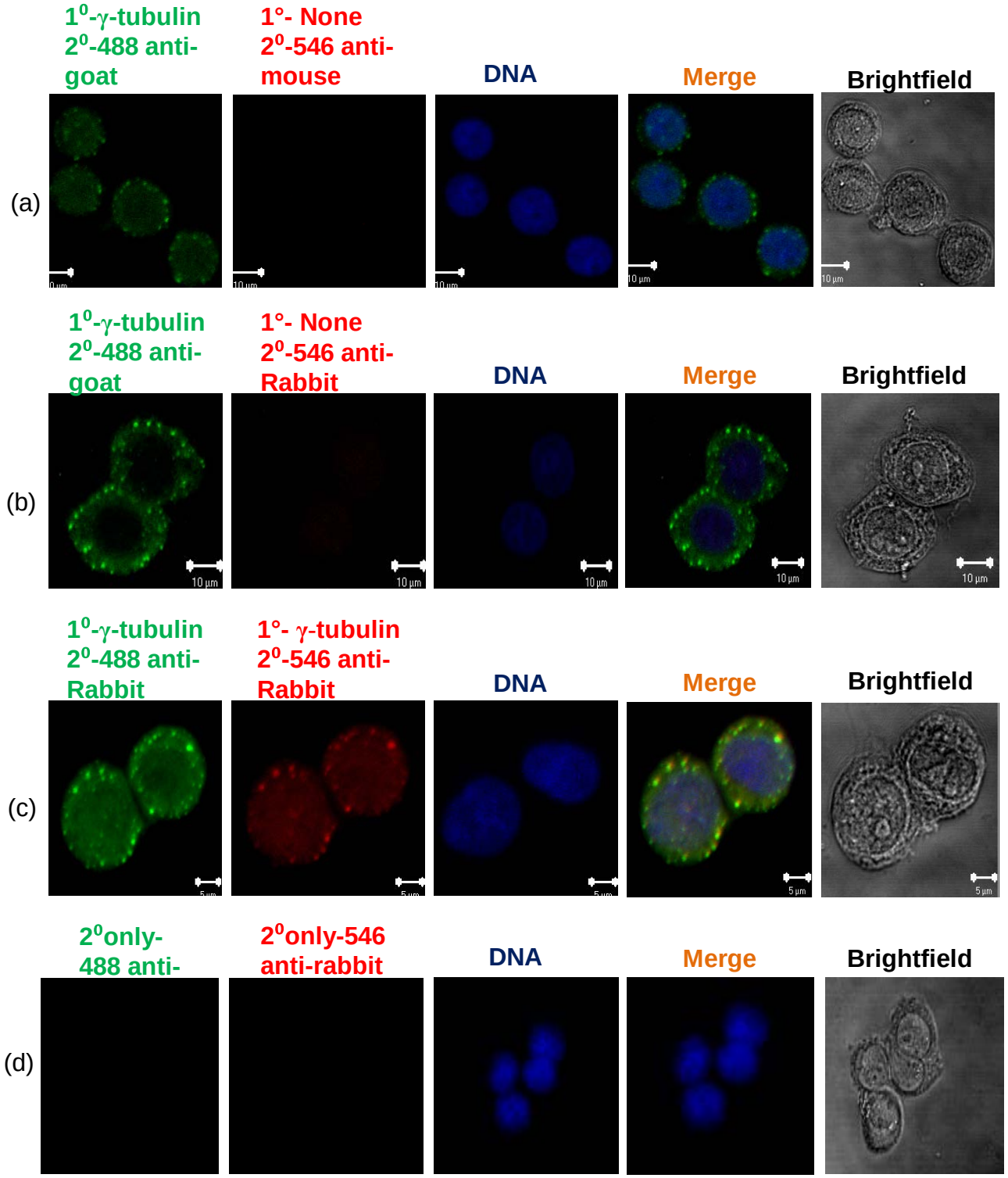

Figure A1. Optimization of confocal microscopy experiments

HeLa S3 cells in G1/S were treated with VR23 for 3 h. Cells were stained with different combinations of primary (1°) and secondary (2°) antibodies. Images were captured with all channels open with the identical settings used for all the experiments in the thesis. The results show the stringent settings and filters used and that each fluorophore recognize the intended target with no bleed through into other channels when captured simultaneously.

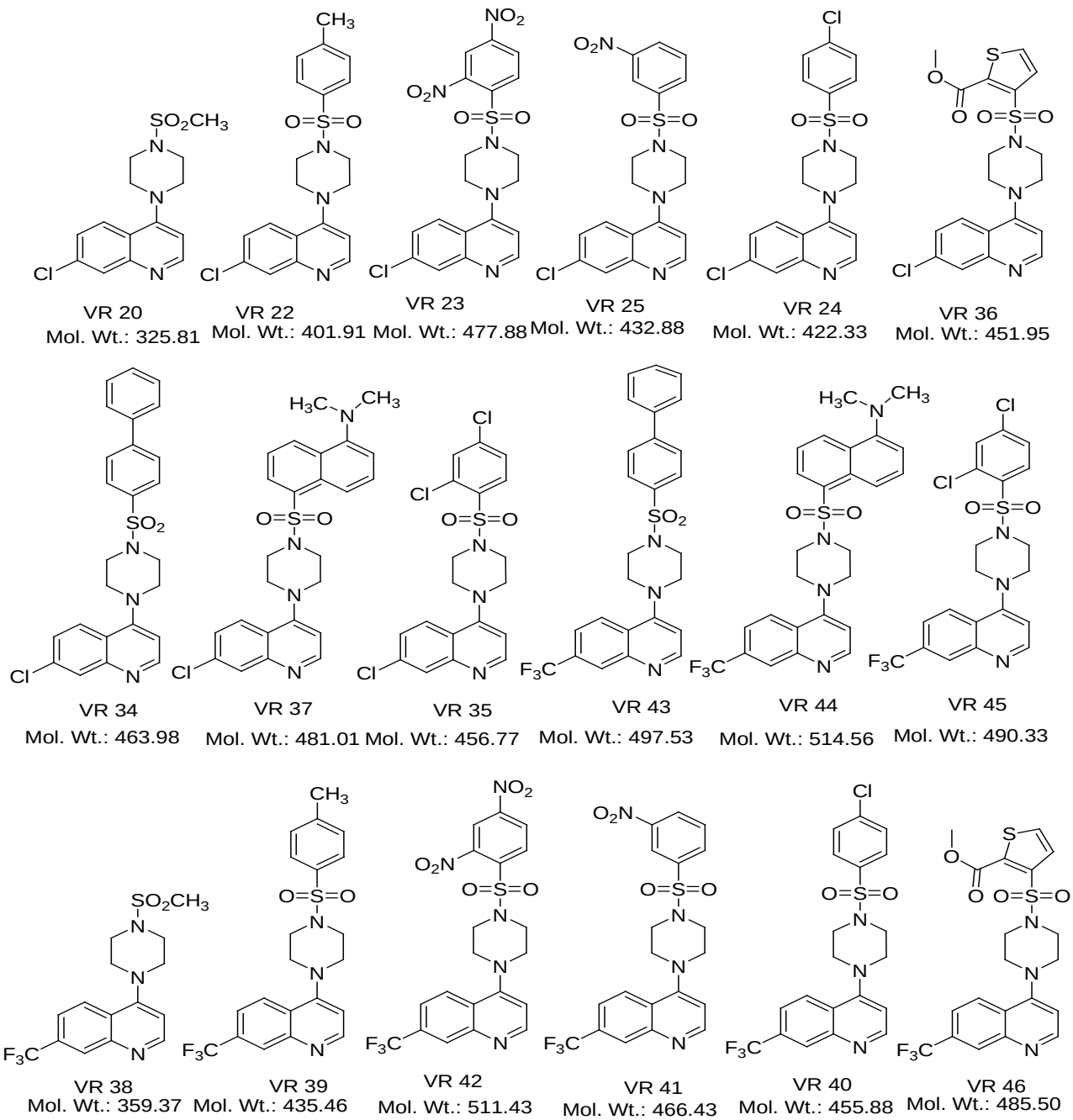

Figure A2: Structures of 4-aminoquinoline propyl sulfonamide derivatives designed and synthesized in Lee lab (Figure obtained from Dr. V.R. Solomon)

Code	MB231	MB468	MCF7	184B5
VR-20	40.36	30.15	22.37	15.19
VR-22	77.16	18.25	9.23	6.36
VR-23	3.2	0.7	1.5	8.99
VR-24	20.25	16.03	7.56	1.98
VR-25	74.70	5.13	14.78	3.32
VR-34	29.35	28.75	63.96	47.46
VR-35	10.32	1.63	60.59	2.37
VR-36	40.12	35.06	42.68	1.48
VR-37	85.04	27.47	22.30	28.25
VR-38	28.58	44.41	25.64	93.93
VR-39	20.20	4.75	20.51	9.09
VR-40	61.44	4.91	27.36	21.80
VR-41	9.44	19.15	24.32	37.78
VR-42	32.19	18.55	10.84	7.73
VR-43	42.70	33.56	20.77	2.95
VR-44	21.96	23.56	22.85	1.98
VR-45	20.27	22.35	66.70	20.44
VR-46	44.74	3.91	5.97	5.88
CQ	22.52	28.58	38.44	76.13

Table A1: IC_{50} (µM) of 4-aminoquinoline propyl sulfonamide derivatives on different cell lines

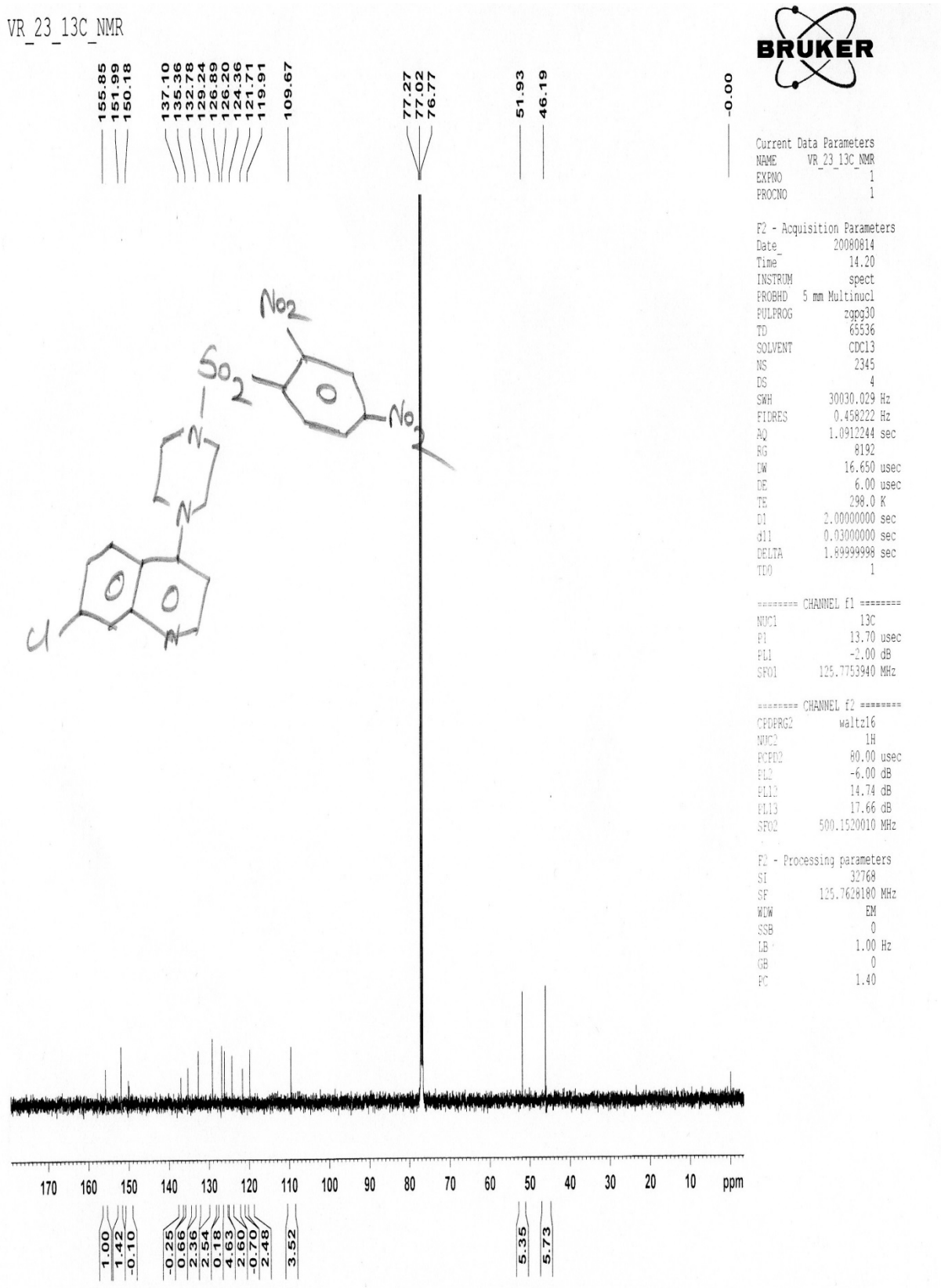

Figure A3: NMR profile of VR23

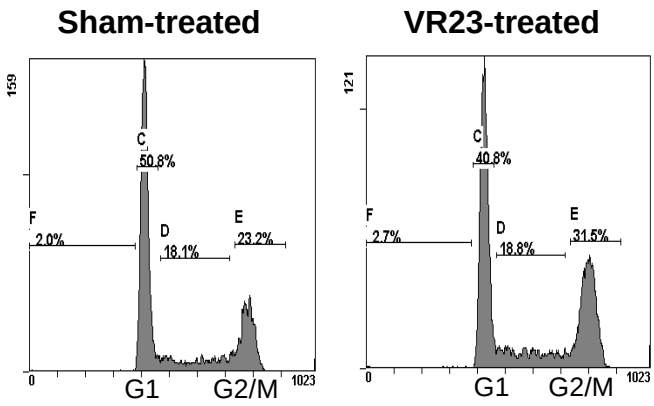

Figure A4. Increase in G2/M population in VR23-treated asynchronous HeLa S3 cells

FACS profile of asynchronous HeLa S3 cells treated with 5 µM of VR23 show an increase in G2/M cell population 12 h post- treatment.

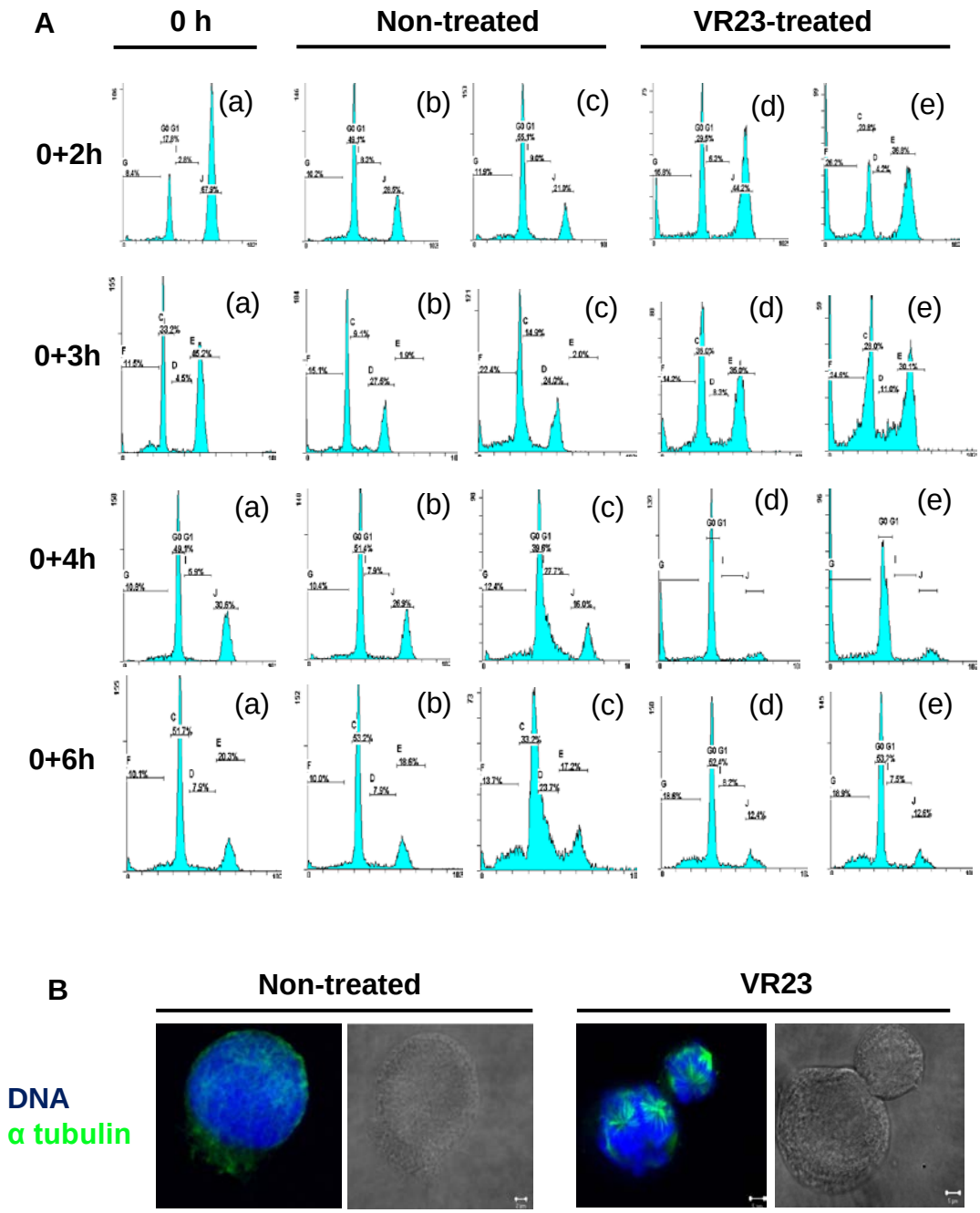

Figure A5. Progression of cells through the cell cycle is impeded in the presence of VR23

A. Cells synchronized in mitosis (0 h) were released into complete medium for 2, 3, 4, or 6 h. At the end of each timepoint VR23 was added and cell cycle progression was observed at +2 h (**b** and **d**), +4 h (**c** and **e**). As compared to nontreated cells (**b** and **c**) VR23 treated cells (**d** and **c**) remain arrested at each timepoint (compare (d) with panel (b) and eventually underwent apoptosis compare panel (e) with panel (c).

B. Morphology of Non-treated and VR23-treated cells corresponding to FACS profile shown in A (0+ 2 h) (**c** and **e**).

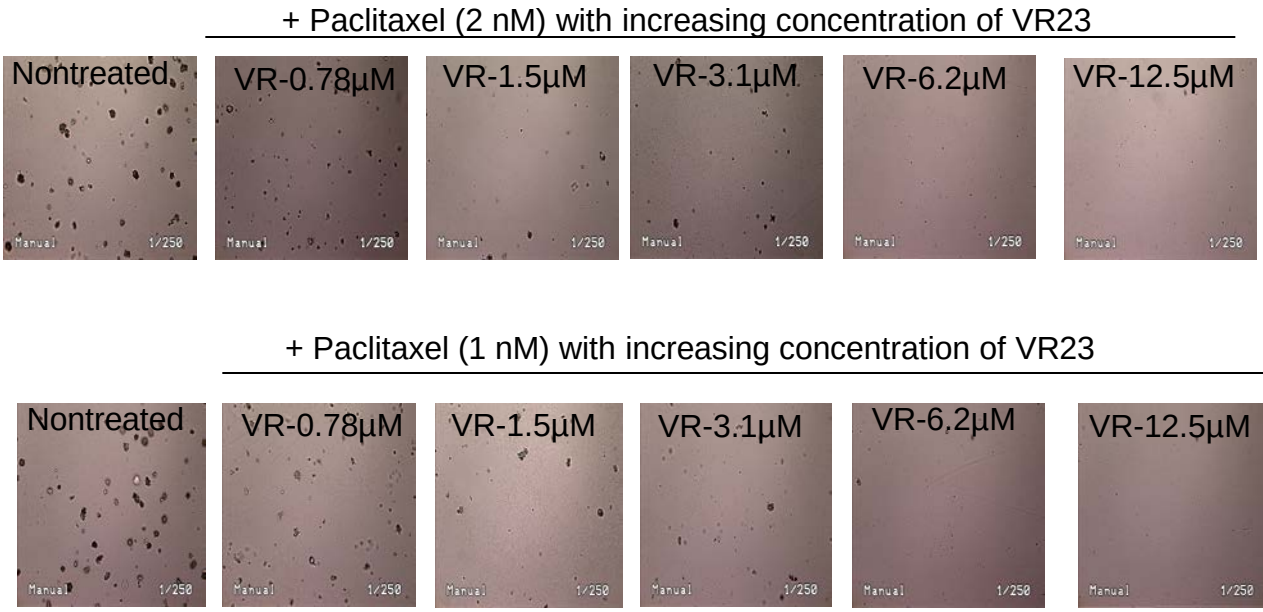

Treatments (MCF7 breast cancer cells)	Survival (% of the control)
Percentage of survival in 1 nm of Paclitaxel alone	35.8%
Percentage of survival in 1.5 µM of VR23 alone	50.3%
Percentage of survival in 1 nm of paclitaxel in combination with 1.5 µM of VR23	21.9%
Percentage of survival in 2 nm of Paclitaxel alone	9.5%
Percentage of survival in 1.5 µM of VR23 alone	50.3%
Percentage of survival in 2 nm of paclitaxel in combination with 1.5 µM of VR23	3.0%

Figure A6. VR23 sensitizes paclitaxel mediated cell killing
Combination of paclitaxel and VR23 effectively inhibits the colony formation in MCF7 cells. Figure shows colonies in clonogenic assay of MCF7 cells. Top panel shows combined treatment of paclitaxel (2 nM) in combination with increasing conc. of VR23 and bottom panel shows combination of paclitaxel (1 nM) with increasing conc. of VR23. Number of colonies were counted. Table shows average no. of colony cell survival in each sample.

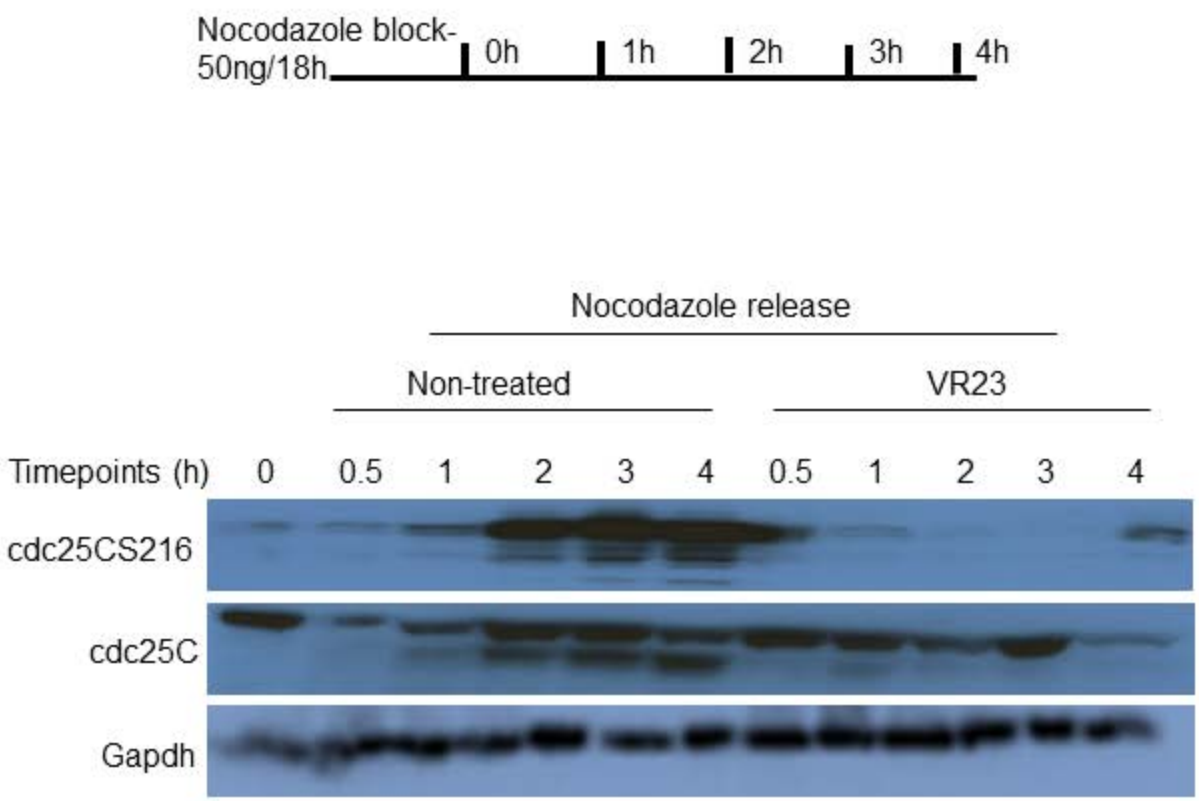

Figure A7. Cdc25C is not phosphorylated at S216 (inhibitory phosphorylation) in VR23-treated mitotic cells

Western blot from proteins extracted from treated and nontreated cells at different timepoints. (0.5 - 4 h). Cells were synchronized by nocodazole (5 ng/ml) and released in complete medium with or without drug. Proteins were extracted and an equal amount of proteins was loaded. Representative blots are shown.

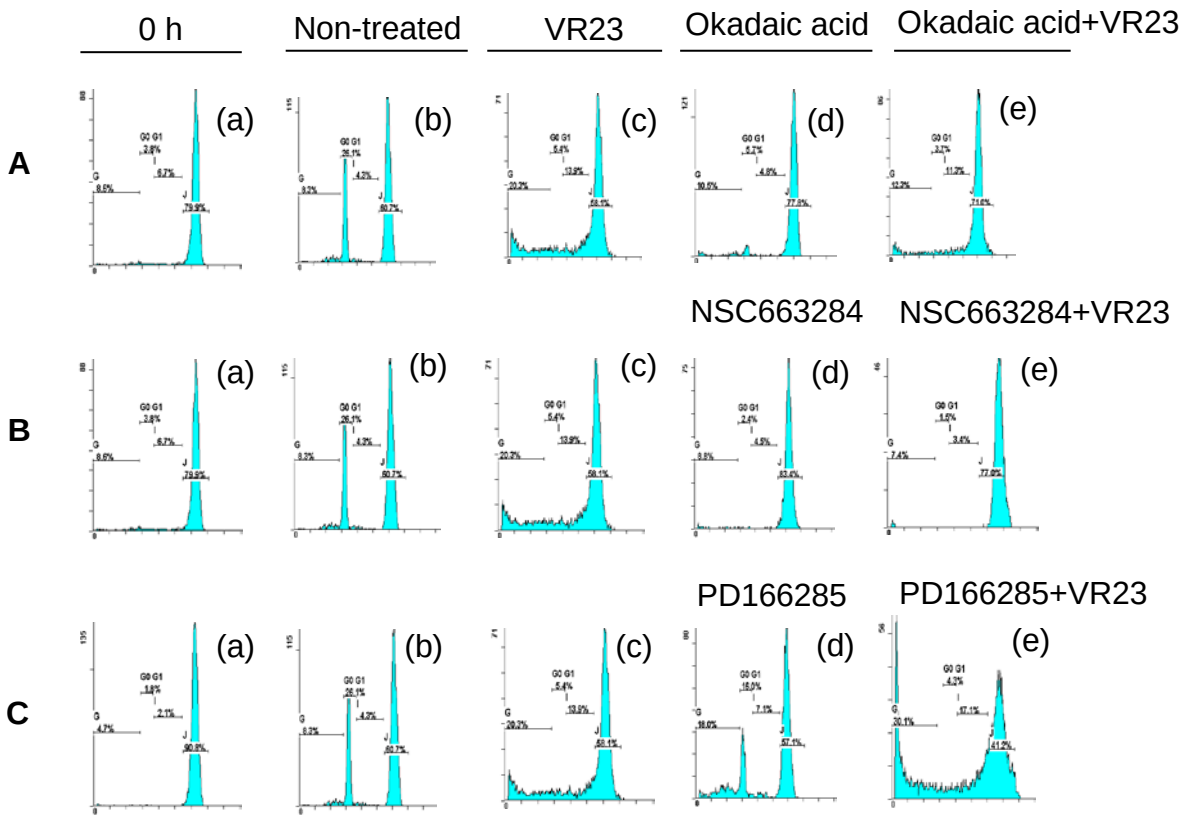

Figure A8. Phosphatase and kinase inhibitors could not rescue cells from VR23 – induced mitotic arrest

Cells synchronized in prophase were released in cell cycle for 4 h with or without drugs. (**a**) Cells synchronized in prophase - 0 h, (**b**) Non-treated, (**c**) VR23-treated, (**d**) PP2A inhibitor (1 µM) in **A**, cdc25C inhibitor (25 µM) in **B** and wee1 inhibitor (0.5 µM) in **C**, (**e**) VR23 (5 µM + phosphatase or kinase inhibitors). Inhibition of PP2A, cdc25C or wee1 in VR23-treated cells did not rescue cells from mitotic arrest.

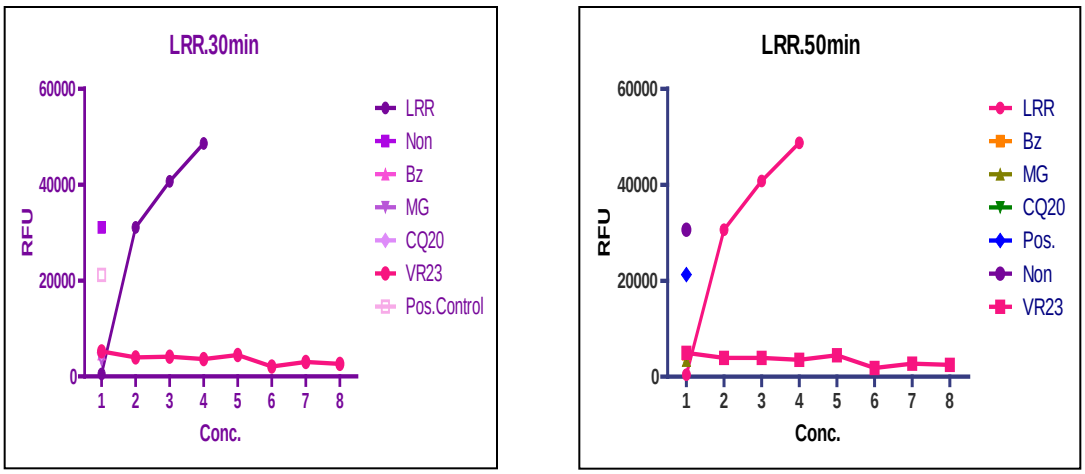

Figure A9. Measurement of trypsin-like activity

Different concentrations of VR23 were added. Points 1-8 on the X-axis of graph corresponds to 0.1, 0 .25, 0.5, 1.0, 2.0, 5.0, 10, 20 (µM) conc. of VR23.

In the same graph different conc. of substrate (25, 50 and 100 µM) conc. was also used on a set of nontreated samples (circles). An increase in fluorescence was observed with increased conc. of substrate. 25 µM of substrate was used for the assay in nontreated, VR23, Bortezomib (100 nM), MG132 (20 µM) and Chloroquine (20 µM) samples. Pos. control is the extracts from jurkat cells with increased proteasome activity.

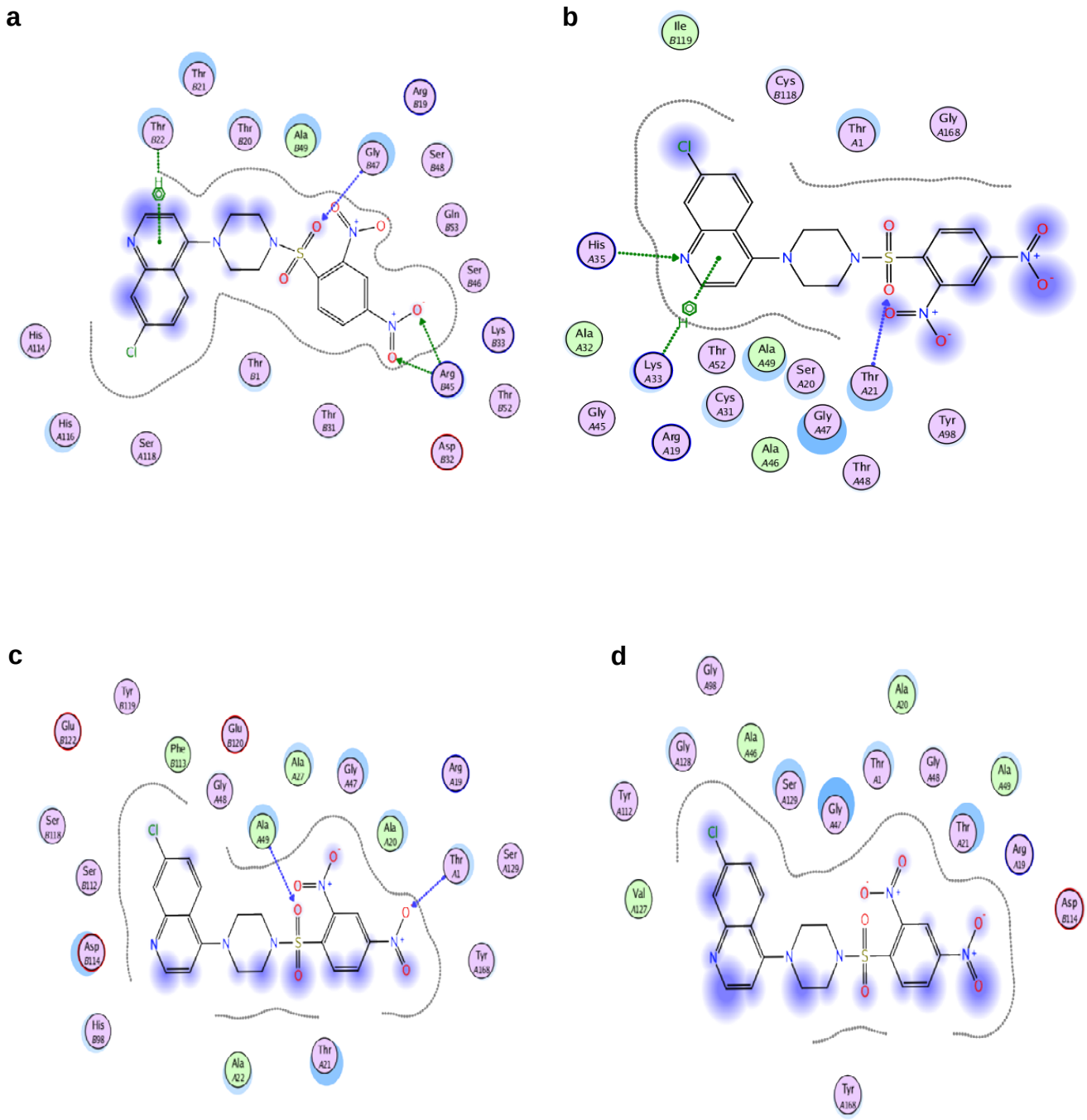

Figure A10. Molecular modelling of VR23 to the β subunit of 20S proteasomes. Panels (**a**, **b**) shows interactions formed by VR23 in two different pockets of β2 subunit of 20S proteasomes (2F16, H). **(c, d)** shows interactions formed by VR23 in the cavity of β5 subunit of 20S proteasomes. (**c**) 2F16, Y corresponding to β5 and (**d**) 2F16, K coresponding to β5 subunit.

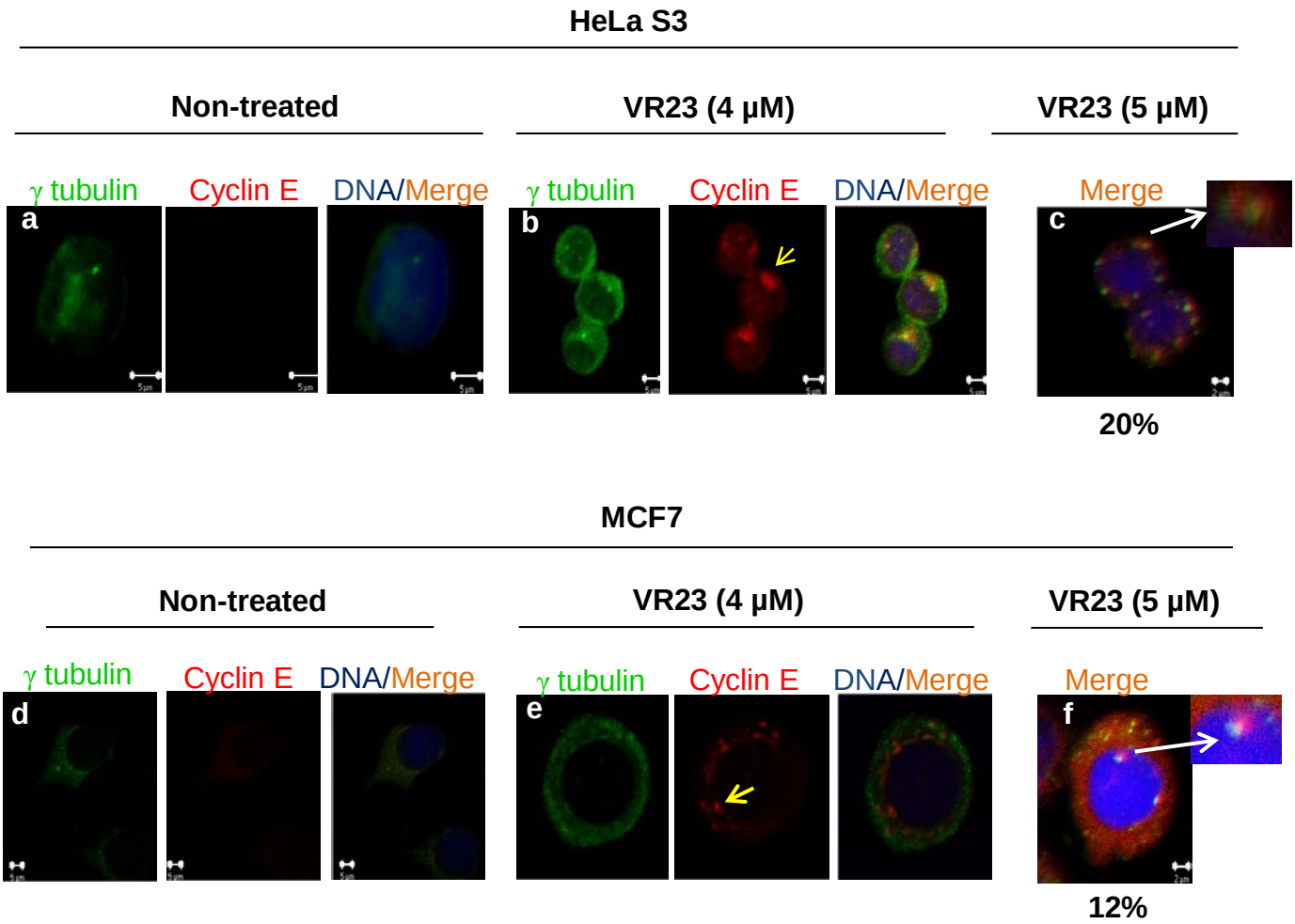

Appendix A11. VR23 induced multiple centrosomes in asynchronous HeLa S3 and MCF7 cells

VR23 induced the formation of multiple centrosomes in asynchronous HeLa S3 and MCF7 cells. HeLa S3 and MCF7 cells were treated with VR23 for 24 h at 4 (**b** and **e**) and 5 μM concentrations (**c** and **f**). Multiple foci of γ-tubulin (green panels) were observed. Red panels represent cyclin E. At lower concentration (4 μM), increased foci of cyclin E was also observed (b, yellow arrow). At higher a concentration (5 μM), multiple centrosomes were observed (panels **c** and **f**). 20% of asynchronous HeLa S3 cells had ≥4 centrosome per cell, 12% of MCF7 cells had ≥4 centrosome per cell, results shown are representative of three independent experiments per cell line.

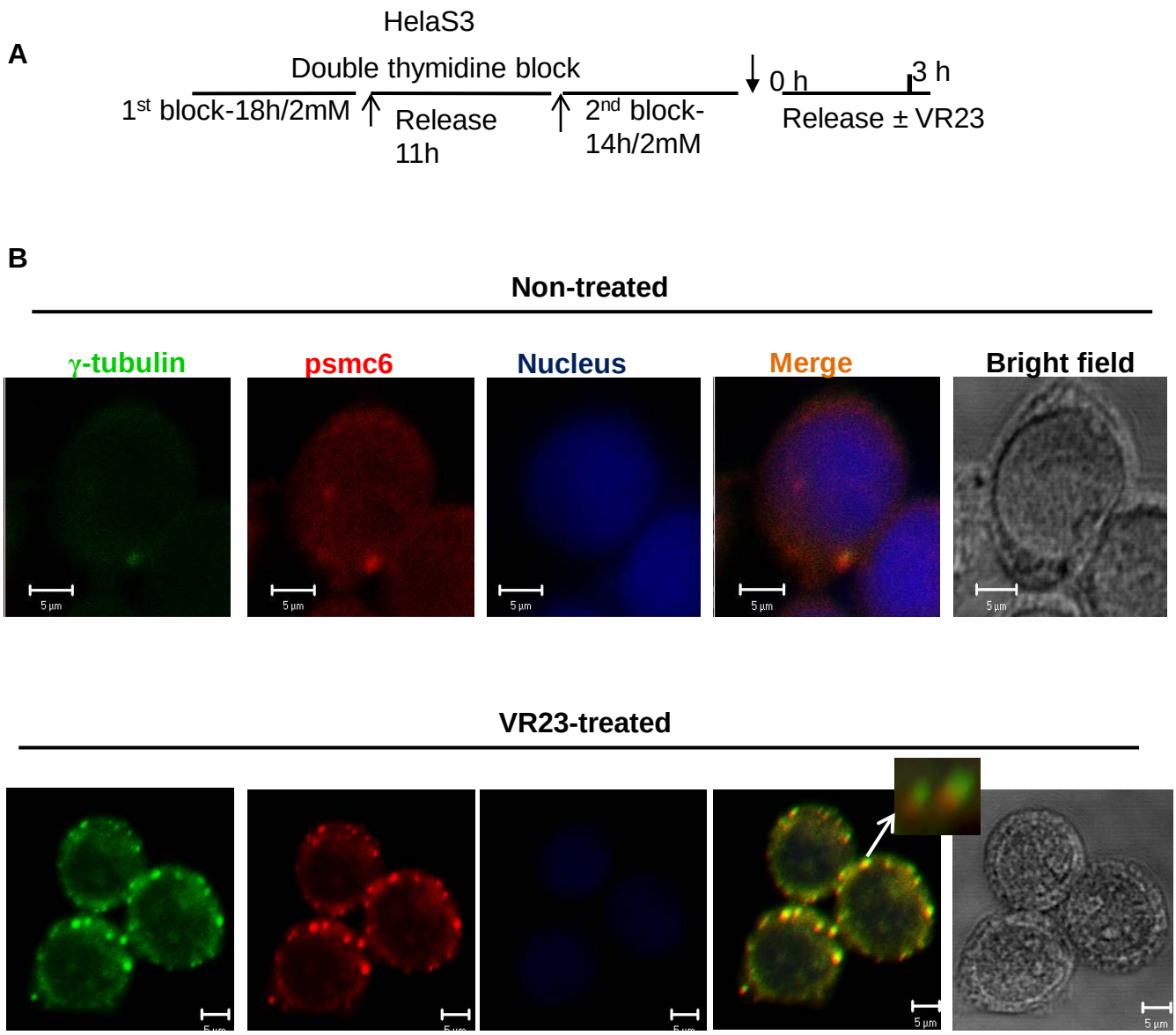

Figure A12. 26S proteasomes subunit is assembled on centrosomes
HeLa S3 cells synchronized in G1/S were released in complete medium for 3 h ± VR23 (20 µM) (A). After 3 h, cells were fixed and stained with antibodies corresponding to γ-tubulin (green panels), psmc6 (red panels) and DRAQ5 for DNA (blue panels). psmc6 is a marker for 26S proteasomes (corresponds to regulatory subunit ATPase 6). psmc6 was found to be co-localized with γ-tubulin suggesting that proteasomes assemble on centrosomes. The experiment was repeated twice and representative figures are shown.

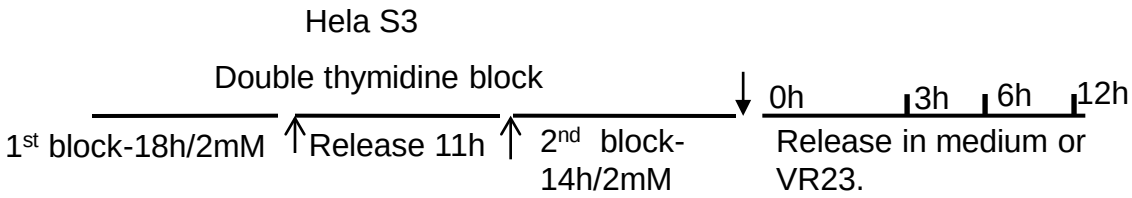

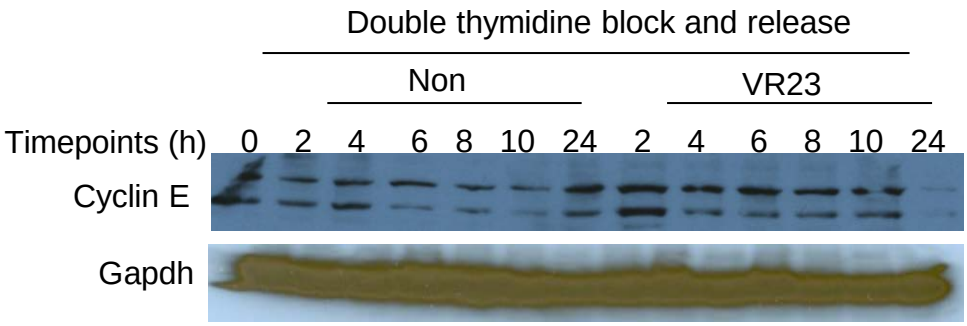

Figure A13. VR23 prevented the timely degradation of cyclin E in G1/S cells
The figure shows the western blot of protein samples extracted from cells treated with VR23 or left non-treated. Cyclin E levels decrease at 6-8 h when majority of cells are in G2/M whereas in VR23-treated cells, levels of cyclin E remain high (2 h timepoint). Gapdh is shown as loading control.

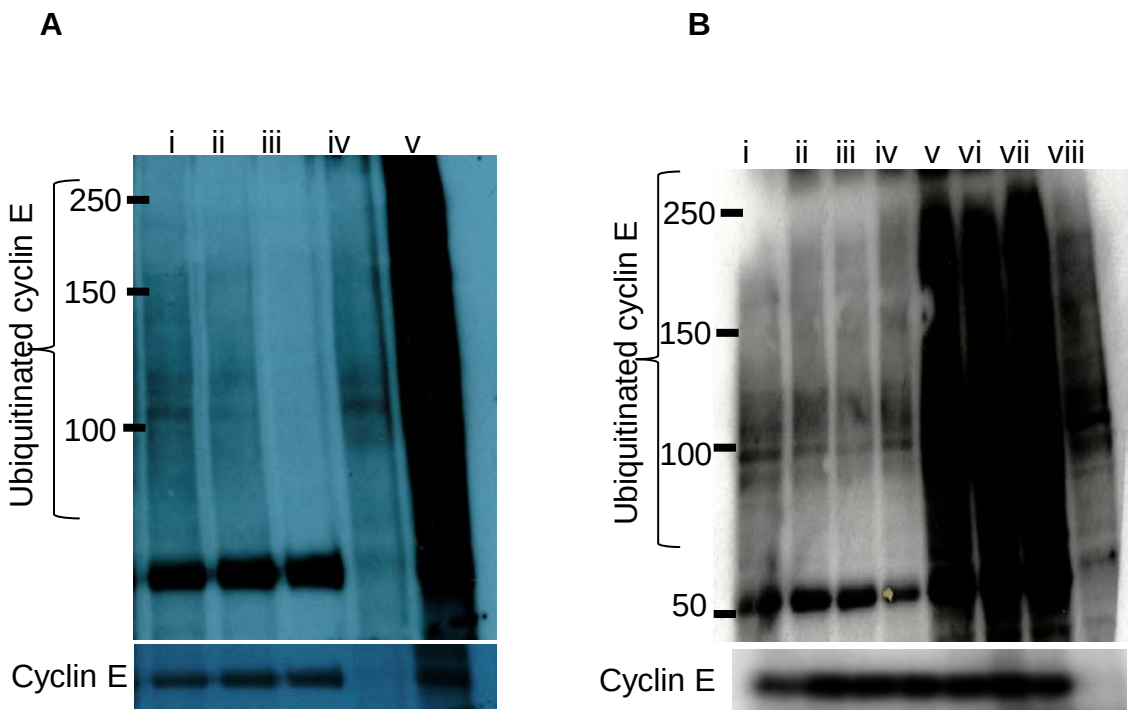

Figure A14. Ubiquitinated cyclin E does not accumulate in VR23-treated MCF10A non-malignant cells 24 h-post treatment

A. Asynchronous MCF10A cells were treated with drugs for 24 h. After 24 h cyclin E was immunoprecipitated (IP) followed by Western blot (WB) with ubiquitin antibody. Accumulation of ubiquitinated cyclin E was observed in bortezomib® treated cells (Bz. 100 nM) but not in VR23-treated cells (20 and 40 µM). (**i**) Non-treated, (**ii**) VR23- 20µM, (**iii**) VR23- 40µM, (**iv**) IgG beads only, (**v**) Bortezomib (100 nM).

B. MCF10A cells synchronized in G1/S were released into cell cycle for 3 h with or without drugs. No accumulation of ubiquitinated cyclin E was observed in VR23-treated cells. (**i**) Non-treated, (**ii**, **iii** and **iv**) VR23- 10, 20 and 40 µM (**v**, **vi**, **vii**). Bortezomib®- 10, 20 and 100 nM respectively, (**viii**) IgG beads only.

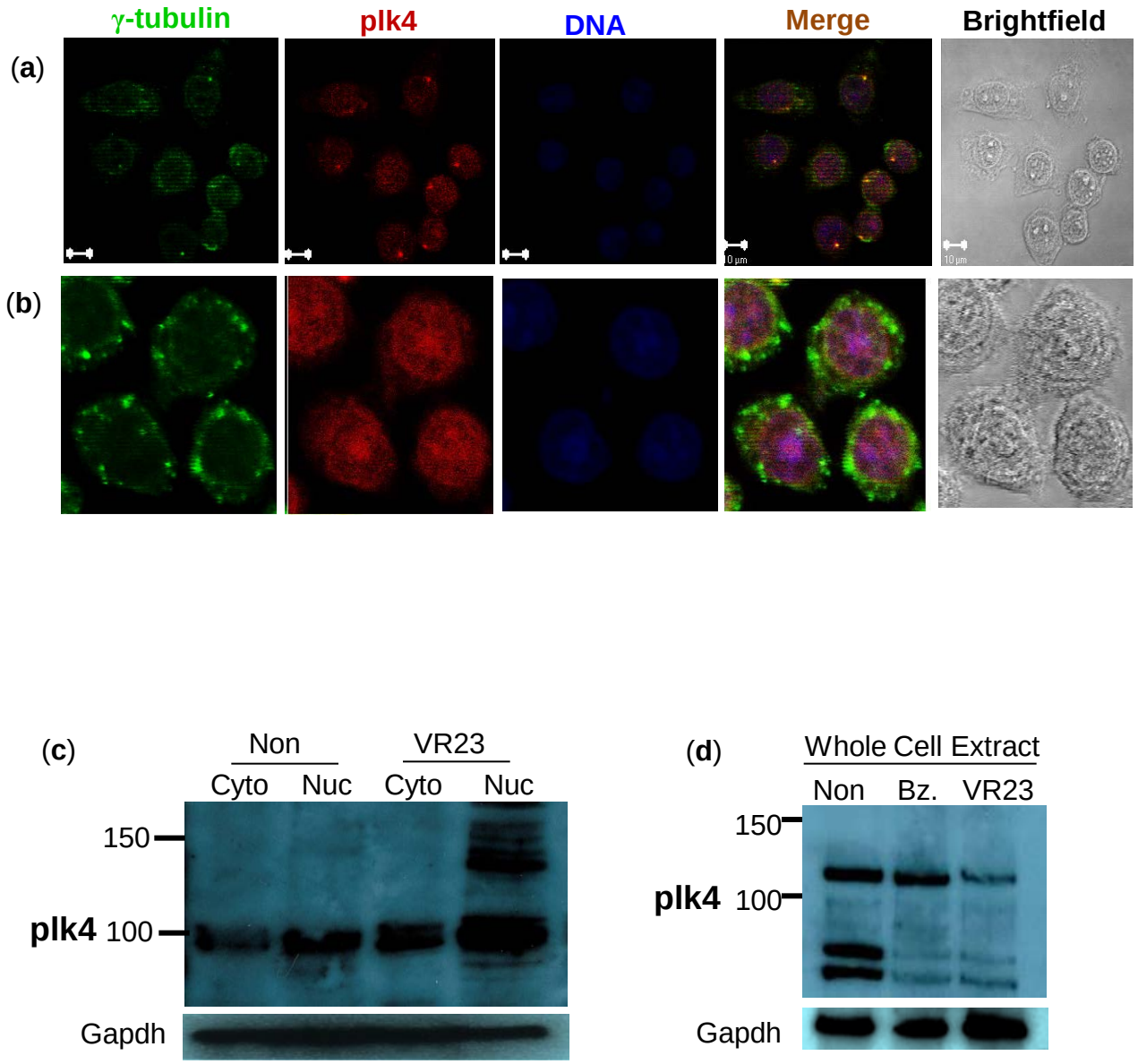

Figure A15. Differential localization of plk4 in VR23-treated cells
The minority of HeLa S3 cells that did not form multiple centrosomes in response to plk4 localized at centrosomes (**a**). In contrast the majority of cells that formed multiple centrosomes in the presence of VR23 did not show co-localization of plk4 at γ-tubulin (**b**). HeLa S3 cells were synchronized by double thymidine bock and released into medium containing VR23 (20 µM) for 3 h. (**c**) shows Western blot from lysates prepared from VR23-treated and non-treated (Non) HeLa S3 cells. Nuclear (Nuc) and cytoplasmic (Cyto) fractions were extracted separately. An increase in the plk4 protein levels were observed in nuclear extracts of VR23. (d) shows the protein samples from whole cell lysates from non-treated (Non), Bortezomib® (Bz. 100 nM) and VR23 (20 µM)-treated samples. Gapdh is the loading control. The band of 110Kd is the reported size of plk4 antibody.

α-tubulin	sc-5286
BUBR1	sc-47744
BUBR1	sc-16195
cdc6	sc-56273
cdk1	sc-137034
cdk2	sc-6248
cdk2 (T14Y15)	sc-28435-R
cdk2 T160	Sc-101656
Centriolin	sc36552
Cyclin A	sc-271682
Cyclin B	sc-7393
Cyclin E	sc-198
Cyclin F	sc-952
Karyopherin	sc-6918
Mcm4	sc-22779
MASTL	sc-243417
Mps1(TTK)	sc-540
NFkB(p65)	sc-8008
PARP-1 (cleaved)	sc-56196
plk	sc-17783
SPAG5 (astrin)	sc-100885
Sas-6	sc81431
SAK (plk4)	sc98929
γ-tubulin	sc7396

cdc25AS124	ab63391
cdc27	ab64878
cdc20	ab18217
cdc25A S124	ab63391
cdc25C	ab13145
cdc25CS216	ab32051
Centrin1	ab11257
Emi1	ab129905
MAP126 (astrin)	ab56724
Orc1	ab85830
PSMC6	ab22639
Proteasome (αβ)	ab22673
plk1	ab17057
Securin	ab3305
wee1	ab2315
γH2A.x S139	ab11174

p38 α(total)	Invitrogen33-1300
p38 α(Y180/Y182)	Invitrogen36-8500
Ubiquitin	Invitrogen13-1600
p-chk1	Cell Sig.#2349P

Table A2. List of primary antibodies used in the experiments
sc- santa cruz and ab- abcam